Variability in the Pinna Motions of Hipposiderid Bats, *Hipposideros Pratti*

Peiwen Qiu

Thesis submitted to the Faculty of the
Virginia Polytechnic Institute and State University
in partial fulfillment of the requirements for the degree of

Master of Science
in
Mechanical Engineering

Rolf Müller, Chair
Alexander Leonessa
Vassilis Kekatos

December 12, 2019
Blacksburg, Virginia

Keywords: Bat biosonar, pinna motions, dynamic sensing, sensory information encoding

Variability in the Pinna Motions of Hipposiderid Bats, *Hipposideros Pratti*

Peiwen Qiu

(ABSTRACT)

Bats are known for their highly capable biosonar systems which make them be able to navigate and forage in dense vegetation. Their biosonar system consists of one emitter (nose or mouth) and two receivers (ears). Some bat species, e.g. in the rhinolophid and hipposiderid families, have complicated pinna motion patterns. It has been shown that these pinna motion patterns fall into two distinct categories: rigid motions and non-rigid motions. In the current work, the pinna of Pratt's leaf-nosed bat (*Hipposideros pratti*) was used as a biological model system to understand how a sensor could benefit from variability. Hence, the variability in the rigid pinna motions and in the non-rigid pinna motions has been investigated by tracking a dense set of landmarks on the pinna surface with stereo vision. Axis-angle representations have shown that the rigid pinna motions exhibited a large continuous variation with rotation axes covering 180° in azimuth and elevation. Distributions of clusters of the landmarks on the pinna surface have shown that the non-rigid pinna motions fall into at least two subgroups. Besides, the acoustic impact of the rigid pinna motions have been investigated using a biomimetic pinna. Normalized mutual information between the acoustic inputs with different rotation axes has shown that different rotation axes can provide at least 50% new sensory information. These results demonstrate that the variability in the pinna motions is an interesting concept for sensor, and how the bats approach that needs to be further investigated.

Variability in the Pinna Motions of Hipposiderid Bats, *Hipposideros Pratti*

Peiwen Qiu

(GENERAL AUDIENCE ABSTRACT)

Sensors have been developed for a long time, and they can be used to detect the environments and then deliver the required sensing information. There are many different types of sensors, such as vision-based sensors (infrared camera and laser scanner) and sound-based sensors (sonar and radar). Ultrasonic transducers are one of the sound-based sensors, and they are more stable and reliable in environments where smoke or steam is present. Similar to human-made ultrasonic transducers, bats have developed highly capable biosonar systems that consist of one ultrasonic emitter (nose or mouth) and two ultrasonic receivers (ears), and these biosonar systems enable them to fly and hunt in cluttered environments. Some bats, e.g. rhinolophid and hipposiderid bats, have dynamic noseleaves (elaborate baffle shapes surrounding the nostrils) and pinna (outer ear), and these could enhance the sensing abilities of bats. Hence, the purpose of this thesis has been to investigate this variability to improve the human-made sensors by focusing on the dynamic pinna of the bats. It has been shown that bats have two distinct categories of pinna motions: rigid motions which change only the orientation of the pinna, and non-rigid motions which change also the shape of the pinna. However, the variability within the rigid and non-rigid pinna motions has received little attention. Therefore, the present work has investigated the variability in the rigid pinna motions and in the non-rigid pinna motions. Landmark points were placed on the pinna of certain bats and the pinna motions were tracked by high-speed video cameras. The rigid pinna motions exhibit a large continuous variation in where the pinna is orientated during rotation. Distributions of clusters of the landmarks on the pinna have shown that the non-

rigid pinna motions fall into at least two subgroups. The acoustic impacts of the rigid pinna motions have been studied by a biomimetic pinna which reproduced the observed range of the rigid pinna motions. Ultrasonic signals mimicking the bats were emitted to be received by the biomimetic pinna. Based on these signals, it has been shown that different rotation axes and even small changes can provide over 50% new sensory information. These findings give engineers a potential way to improve the human-made sensors.

Dedication

This thesis is dedicated to myself and to my parents Qinzhong Qiu and Dihua Yao.

Acknowledgments

I would like to thank my advisor Dr. Rolf Mueller for his comments and suggestions on my research and for all the technical knowledge that he taught me. I am extremely grateful to him for his patience in discussing the research with me. I really appreciate his excellent guidance throughout my masters. It is my great honor to have him as my advisor.

I would like to thank all my committee members, Dr. Vasileios Kekatos and Dr. Alexander Leonessa, for serving on my Master's Advisory Committee and for their help on putting effort and support on my thesis. It is my great honor to work with all committees during the completion of my masters.

I am extremely grateful to my lab-mates Jia Guo for developing the semiautomatic point picking method and Ruihao Wang for helping with design and assembling the rigid pinna motion reproducing setup.

I also want to thank my parents for their love, encouragement and support during my life. They encourage and support me whatever the choices I make and whenever I face challenges.

Contents

List of Figures **xii**

List of Tables **xxi**

1 Introduction **1**

1.1 Background 1

1.2 Objective 4

1.3 Organization 6

2 Review of Literature **7**

2.1 Biological context 7

2.2 Pinna dynamics 9

2.3 Biomimetic reproductions 11

3 Variability in the rigid pinna motions **15**

3.1 Title 15

3.2 Abstract 15

3.3 Introduction 16

3.4 Methods 19

3.4.1 Motion kinematics . . . 19
3.4.2 Acoustic Impact of pinna motion variability . . . 26
3.5 Results . . . 32
3.6 Discussion . . . 39
3.7 Acknowledgements . . . 41

4 Variability in the non-rigid pinna motions **42**
4.1 Introduction . . . 42
4.2 Methods . . . 42
4.3 Results . . . 46
4.4 Discussion . . . 50

5 Conclusions **51**
5.1 Summary of research achievements . . . 51
5.2 Significance . . . 52
5.3 Suggestions for future work . . . 53

Bibliography **56**

Appendices **71**

Appendix A Rigid pinna motion parameters **72**

Appendix B Additional mutual information results **78**

B.1 Reference rotation axis (-60 °, -60 °) 79

B.2 Reference rotation axis (-30 °, -60 °) 79

B.3 Reference rotation axis (0 °, -60 °) 80

B.4 Reference rotation axis (30 °, -60 °) 80

B.5 Reference rotation axis (60 °, -60 °) 81

B.6 Reference rotation axis (-60 °, -30 °) 81

B.7 Reference rotation axis (-30 °, -30 °) 82

B.8 Reference rotation axis (0 °, -30 °) 82

B.9 Reference rotation axis (30 °, -30 °) 83

B.10 Reference rotation axis (60 °, -30 °) 83

B.11 Reference rotation axis (-60 °, 0 °) 84

B.12 Reference rotation axis (-30 °, 0 °) 84

B.13 Reference rotation axis (30 °, 0 °) 85

B.14 Reference rotation axis (60 °, 0 °) 85

B.15 Reference rotation axis (-60 °, 30 °) 86

B.16 Reference rotation axis (-30 °, 30 °) 86

B.17 Reference rotation axis (0 °, 30 °) 87

B.18 Reference rotation axis (30 °, 30 °) 87

B.19 Reference rotation axis (60 °, 30 °) 88

B.20 Reference rotation axis (-60 °, 60 °) 88

B.21 Reference rotation axis (-30 °, 60 °) 89

B.22 Reference rotation axis (0 °, 60 °) 89

B.23 Reference rotation axis (30 °, 60 °) 90

B.24 Reference rotation axis (60 °, 60 °) 90

Appendix C Non-rigid pinna motion parameters **91**

Appendix D Additional clustering results **92**

D.1 Pinna motion sample 1 92

D.2 Pinna motion sample 2 93

D.3 Pinna motion sample 3 93

D.4 Pinna motion sample 4 94

D.5 Pinna motion sample 5 94

D.6 Pinna motion sample 6 95

D.7 Pinna motion sample 7 95

D.8 Pinna motion sample 8 96

Appendix E Additional distances between clusters results **97**

E.1 Distribution of clusters for non-rigid pinna motion samples from 1 to 7 . . . 97

E.2 Pinna motion sample 1 98

E.3 Pinna motion sample 2 98

E.4 Pinna motion sample 3 99
E.5 Pinna motion sample 4 99
E.6 Pinna motion sample 5 100
E.7 Pinna motion sample 6 100
E.8 Pinna motion sample 7 101
E.9 Distribution of clusters for non-rigid pinna motion samples from 8 to 9 . . . 101
E.10 Pinna motion sample 8 102
E.11 Pinna motion sample 9 102

Appendix F Program sources **103**

F.1 Rigid pinna motion analysis 103
F.1.1 Axis-angle representation 103
F.1.2 Normalized mutual information 111
F.2 Non-rigid pinna motion analysis 115
F.2.1 Spectral clustering 115
F.2.2 Euclidean distance 118

List of Figures

3.1 Experimental setup for collection of the pinna kinematics: a) frontal view of the setup with high-speed video cameras and lights, b) schematic top view of the setup including the bat platform. 20

3.2 Example of verification of rigid motions: a) landmarks on the anterior rim and posterior rim of the pinna that were used to verify the rigid motion, b) trajectories of two points on the pinna rim, one on the anterior rim (point 3) and another on the posterior rim (point 13). The distances between the points at each time step (video frame) are indicated by gray lines. For each sequence, the shortest and the longest distances between the points were identified and the difference between them was used to verify the rigid motions. 22

3.3 Pinna-centered coordinate system for determining rotation axis and angle: reference coordinate system derived from the landmark points on the pinna tip (A), and on the anterior (B) and posterior (C) rim of the pinna. 23

3.4 Rigid pinna rotation simulation: a) evenly distributed points on a sphere with a radius that matches that of a spherical fit to the landmark points on a real bat pinna, b) landmark points on the model pinna selected from the points in (a). 25

3.5 Rigid pinna rotation simulation: trajectories of the model landmark points that correspond to a total rotation of 45°. 25

3.6 Pinna morphology of Pratt's leaf-nosed bat (*Hipposideros pratti*): a) bat pinna geometry reconstructed from a microCT scan, b) biomimetic pinna made of silicone. 27

3.7 Experimental setup for acoustic characterization of the rigid pinna motions: A pan-tilt unit and an additional stepper motor were used to create vertical and horizontal rotation axes that intersect in the bottom of the pinna. . . . 29

3.8 Block diagram of the experimental setup for acoustic characterization of the rigid pinna motions 30

3.9 Estimation errors for the rotation parameters as a function of the level of perturbation noise that was added to the landmark positions: a) rotation angle magnitudes, b) azimuth values of the rotation axes, c) elevation values of the rotation axes. For each condition, 50 trials were evaluated. The boxes span the range between first and third quartile. The horizontal line within the box indicates the median and the whiskers indicate the minimum and maximum values. 32

3.10 Verification of rigid motions: a) landmarks on the anterior rim and posterior rim of the pinna that were used to verify the rigid motion, b) matrix of maximum changes in the pairwise distances across all time steps between the pinna rim points shown in (a). 33

3.11 Verification of rigid motions: distribution of the maximum values in the matrix of maximum changes in the pairwise distances for 100 selected pinna motions. 33

3.12 Variability in the rotation angle magnitudes across the analyzed set of rigid pinna motion sequences (n=100). 35

3.13 Variability in the orientations of the pinna rotation axes: a) map showing the axis orientations and the respective rotation angles (color scale), b) histogram estimate of the distribution of the azimuth values of the axis orientations, c) histogram estimate of the distribution of the elevation values of the axis orientations (n=100). 36

3.14 Example of pulse envelopes recorded during rigid pinna rotations with different rotation axes: a) for pulses with a single sine carrier. b) for pulses with a frequency-modulated carrier. Labels (M°,N°) denote azimuth and elevation of the respective rotation axis direction. 37

3.15 Normalized mutual information between the pulse envelopes collected with 110 different pinna rotation axes: a) for pulses with a sine carrier (CF), b) for pulses with a frequency-modulated carrier. For each graph, the different rotation axes positions studied are shown on both axes, so that each cell in the matrix shown represents the mutual information between the signals associated with the respective rotation axes orientations. 38

3.16 Example of normalized mutual information between the pulse envelopes of a reference rotation axis and all other rotation axes in sample: a) for pulses with a single sine carrier. b) for pulses with a frequency-modulated carrier. In each graph, the star marks the reference rotation axis and the dots mark the rotation axes that were used for comparison. The color value of the lines between the reference and the other rotation axes denotes the normalized mutual information between the pulse envelopes between these two orientations of the rotation axis. 38

4.1 Example of a non-rigid motion sequence of a pinna (with landmarks on the surface): a) pinna geometry prior to the start of the non-rigid motion, b) pinna geometry after the non-rigid motion is complete. 44

4.2 Comparison between K-means and spectral clustering algorithms using test data: a) for test data using K-means algorithm, b) for test data using spectral clustering algorithm. 45

4.3 Verification of non-rigid motions: a) landmarks on the anterior rim and posterior rim of the pinna that were used to verify the non-rigid motion, b) matrix of maximum changes in the pairwise distances across all time steps between the pinna rim points shown in (a). 46

4.4 Normalized mean values of Euclidean distances within clusters of 10 non-rigid pinna motion sequences. 47

4.5 Example of spectral clustering results of non-rigid pinna motions with number of clusters equaling 5: a) for pinna motion sample 1, b) for pinna motion sample 2. Dots are the points marked on the pinna. Different colors denote different clusters. The maroon lines are the boundaries between the clusters. (a) and (b) are similar. 48

4.6 Example of spectral clustering results of non-rigid pinna motions with number of clusters equaling 6: a) for pinna motion sample 1, b) for pinna motion sample 2. Dots are the points marked on the pinna. Different colors denote different clusters. The maroon lines are the boundaries between the clusters. (a) and (b) are different. 48

4.7 Example of matrix of Euclidean distances between clusters for non-rigid pinna motion with number of clusters equaling 5: a) matrix of Euclidean distance between clusters, b) distribution of different clusters on the pinna. 49

4.8 Example of matrix of Euclidean distances between clusters for non-rigid pinna motion with number of clusters equaling 6: a) matrix of Euclidean distance between clusters, b) distribution of different clusters on the pinna. 49

B.1 Normalized mutual information between reference rotation axis (-60 °, -60 °) and all the other rotation axes 79

B.2 Normalized mutual information between reference rotation axis (-30 °, -60 °) and all the other rotation axes 79

B.3 Normalized mutual information between reference rotation axis (0 °, -60 °) and all the other rotation axes 80

B.4 Normalized mutual information between reference rotation axis (30 °, -60 °) and all the other rotation axes 80

B.5 Normalized mutual information between reference rotation axis (60 °, -60 °) and all the other rotation axes 81

B.6 Normalized mutual information between reference rotation axis (-60 °, -30 °) and all the other rotation axes 81

B.7 Normalized mutual information between reference rotation axis (-30 °, -30 °) and all the other rotation axes 82

B.8 Normalized mutual information between reference rotation axis (0 °, -30 °) and all the other rotation axes 82

B.9 Normalized mutual information between reference rotation axis (30 °, -30 °) and all the other rotation axes 83

B.10 Normalized mutual information between reference rotation axis (60 °, -30 °) and all the other rotation axes 83

B.11 Normalized mutual information between reference rotation axis (-60 °, 0 °) and all the other rotation axes 84

B.12 Normalized mutual information between reference rotation axis (-30 °, 0 °) and all the other rotation axes 84

B.13 Normalized mutual information between reference rotation axis (30 °, 0 °) and all the other rotation axes 85

B.14 Normalized mutual information between reference rotation axis (60 °, 0 °) and all the other rotation axes 85

B.15 Normalized mutual information between reference rotation axis (-60 °, 30 °) and all the other rotation axes 86

B.16 Normalized mutual information between reference rotation axis (-30 °, 30 °) and all the other rotation axes 86

B.17 Normalized mutual information between reference rotation axis (0 °, 30 °) and all the other rotation axes 87

B.18 Normalized mutual information between reference rotation axis (30 °, 30 °) and all the other rotation axes 87

B.19 Normalized mutual information between reference rotation axis (60 °, 30 °) and all the other rotation axes 88

B.20 Normalized mutual information between reference rotation axis (-60 °, 60 °) and all the other rotation axes 88

B.21 Normalized mutual information between reference rotation axis (-30 °, 60 °) and all the other rotation axes 89

B.22 Normalized mutual information between reference rotation axis (0 °, 60 °) and all the other rotation axes 89

B.23 Normalized mutual information between reference rotation axis (30 °, 60 °) and all the other rotation axes 90

B.24 Normalized mutual information between reference rotation axis (60 °, 60 °) and all the other rotation axes 90

D.1 Spectral clustering results of pinna motion sample 1: a) number of clusters is 5, b) number of clusters is 6. Dots are the points marked on the pinna. Different colors denote different clusters. The maroon lines are the boundaries between the clusters. 92

D.2 Spectral clustering results of pinna motion sample 2: a) number of clusters is 5, b) number of clusters is 6. Dots are the points marked on the pinna. Different colors denote different clusters. The maroon lines are the boundaries between the clusters. 93

D.3 Spectral clustering results of pinna motion sample 3: a) number of clusters is 5, b) number of clusters is 6. Dots are the points marked on the pinna. Different colors denote different clusters. The maroon lines are the boundaries between the clusters. 93

D.4 Spectral clustering results of pinna motion sample 4: a) number of clusters is 5, b) number of clusters is 6. Dots are the points marked on the pinna. Different colors denote different clusters. The maroon lines are the boundaries between the clusters. 94

D.5 Spectral clustering results of pinna motion sample 5: a) number of clusters is 5, b) number of clusters is 6. Dots are the points marked on the pinna. Different colors denote different clusters. The maroon lines are the boundaries between the clusters. 94

D.6 Spectral clustering results of pinna motion sample 6: a) number of clusters is 5, b) number of clusters is 6. Dots are the points marked on the pinna. Different colors denote different clusters. The maroon lines are the boundaries between the clusters. 95

D.7 Spectral clustering results of pinna motion sample 7: a) number of clusters is 5, b) number of clusters is 6. Dots are the points marked on the pinna. Different colors denote different clusters. The maroon lines are the boundaries between the clusters. 95

D.8 Spectral clustering results of pinna motion sample 8: a) number of clusters is 5, b) number of clusters is 6. Dots are the points marked on the pinna. Different colors denote different clusters. The maroon lines are the boundaries between the clusters. 96

E.1 Distribution of clusters on the pinna surface for non-rigid pinna motion samples from 1 to 7: a) number of clusters is 5, b) number of clusters is 6. . . . 97

E.2 Matrix of Euclidean distances between clusters for non-rigid pinna motion sample 1: a) number of clusters is 5, b) number of clusters is 6. 98

E.3 Matrix of Euclidean distances between clusters for non-rigid pinna motion sample 2: a) number of clusters is 5, b) number of clusters is 6. 98

E.4 Matrix of Euclidean distances between clusters for non-rigid pinna motion sample 3: a) number of clusters is 5, b) number of clusters is 6. 99

E.5 Matrix of Euclidean distances between clusters for non-rigid pinna motion sample 4: a) number of clusters is 5, b) number of clusters is 6. 99

E.6 Matrix of Euclidean distances between clusters for non-rigid pinna motion sample 5: a) number of clusters is 5, b) number of clusters is 6. 100

E.7 Matrix of Euclidean distances between clusters for non-rigid pinna motion sample 6: a) number of clusters is 5, b) number of clusters is 6. 100

E.8 Matrix of Euclidean distances between clusters for non-rigid pinna motion sample 7: a) number of clusters is 5, b) number of clusters is 6. 101

E.9 Distribution of clusters on the pinna surface for non-rigid pinna motion samples from 8 to 9: a) number of clusters is 5, b) number of clusters is 6. . . . 101

E.10 Matrix of Euclidean distances between clusters for non-rigid pinna motion sample 8: a) number of clusters is 5, b) number of clusters is 6. 102

E.11 Matrix of Euclidean distances between clusters for non-rigid pinna motion sample 9: a) number of clusters is 5, b) number of clusters is 6. 102

List of Tables

3.1 Mean silhouette value of the clustering results of 100 rigid rotation axes (azimuth [α], elevation [β]) and 100 rigid pinna motions (azimuth [α], elevation [β], angle [θ]). 34

3.2 Statistical characteristics of the distributions for the values of rotation angle magnitudes, azimuths and elevations of rotation axes over the 100 analyzed rigid pinna motions. 35

4.1 Summary of the non-rigid pinna motion data set acquired from three different individuals of Pratt's leaf-nosed bat (*Hipposideros pratti*). 43

A.1 Parameters of the selected rigid pinna motion sequences of *Hipposideros pratti*. (Seq #: sequence number; NP: number of points marked on the pinna surface; T: motion time (ms); L: moving distance of pinna tip (mm); MD: maximum deformation (mm); θ: rotation angle (°); α: azimuth of rotation axis (°); β: elevation of rotation axis (°)) 72

C.1 Parameters of the selected non-rigid pinna motion sequences of *Hipposideros pratti*. (Seq #: sequence number; NP: number of points marked on the pinna surface; T: motion time (ms); L: moving distance of pinna tip (mm); MD: maximum deformation (mm)) 91

List of Abbreviations

α	azimuth of rotation axis (°)
β	elevation of rotation axis (°)
Δ	Euclidean distance per time step ($^{\text{mm}}/_{\text{step}}$)
θ	rotation angle (°)
n_s	number of time steps which is equal to (number of frames - 1)
3D	three-dimensional
CF	constant frequency
Daq	data acquisition
DC	direct current
FIR	finite impulse response
FM	frequency modulated
HEALPix	Hierarchical Equal Area isoLatitude Pixelisation
L	moving distance of pinna tip (mm)
LED	light emitting diode
MD	maximum deformation (mm)
NMI	normalized mutual information

NP number of points marked on the pinna surface

PLA polylactic acid

Seq # sequence number of selected rigid motion

SVD singular value decomposition

T motion time (ms)

Chapter 1

Introduction

1.1 Background

Evolution has created some particularly capable sensory systems in animals where a specific sensory capability is highly relevant to the animal's fitness. In contrast, humans are more generalist where no single sense has been extremely developed. For example, wild turkeys have monocular periscopic vision with a field of view of 270° while humans have binocular vision with a field of view of 160° [3, 13]. Dogs are at least 100 times better at noticing the existence of an odor compared to humans because they have 220 million to 2 billion olfactory neurons in the olfactory epithelium in comparison to the presence of 2–5 million olfactory neurons in humans [66, 104]. Barn owls have excellent directional hearing that can locate the sound source three times more accurate in elevation than humans do [47].

One example of these specialized sensory systems is biosonar. Biosonar systems can be found in three groups of animals: bats [4, 44], birds [46, 49] and toothed whales [57, 60]. Within these animals, bats and birds use in-air biosonar whereas toothed whales use underwater biosonar. They use their biosonar systems to locate and identify objects during their navigation and foraging. The biosonar system can be active and passive. With the active biosonar system, animals emit sound signals out to the environment and then listen to the echos of these signals returning from the surrounding objects. With the passive biosonar system, animals just listen to the sounds generated by a foreign source (i.e., to detect and locate the

prey by listening to the prey's wing beat).

Bats are an attractive group for scientists to research within the animals using biosonar systems because of capability and easy of access. Compared to other echolocation animals, bats rank highly on several measures of ecological and evolutionary success. Firstly, bats are the second most species-rich order of mammals after rodents (order Rodentia) [50]. With over 1200 species, they account for more than 20% species of mammals [110]. Secondly, bats are distributed across almost the entire landmass of the earth including the forests, bush and deserts, only leaving out the polar ice caps and some small remote islands [71, 82]. Thirdly, bats have exploited diverse food sources such as flying insects, crawling arthropods, fish, lizards, birds, rodents, other bats, nectar and pollen, fruit, and blood [76]. Finally, bats can be locally and regionally abundant, with some species being extremely common over large areas and forming large aggregations [39, 71]. These are the measures for success for bats, and biosonar together with flight can be hypothesized to be two key factors in their success [111].

Bat's biosonar system has evolved for more than 50 million years [112, 113]. However, technical sonar has only been discovered for around 100 years [12]. The technical sonar systems can be used to improve sensing capabilities and expand sensing range for humans. Like the bats, technical sonar systems can be grouped as passive sonar system and active sonar system based on whether they listen to the sound produced by themselves or other sources [96]. However, both for the bats and the technical sonar systems, passive does not mean that no action is taken on the receiving side (i.e., scanning). Active sonar system, which is similar to the bat biosonar system, is widely used in engineering applications. For example, the fishing boats contain the active sonar system to scan and detect the cluster of fish [61]. The small drones carry the active sonar system to detect and avoid obstacles during their autonomous navigation in cluttered natural environments [21, 30]. Compared to other

sensor systems (i.e., camera system and laser scanners), the ultrasonic sonar system performs better if smoke, steam or other optically obstructive gases are present in the environment. The small drones use in-air sonar system which is the same as bats but they use more ultrasonic transmitters and receivers compared to bat's one transmitter and two receivers. Although with more transmitters and receivers, the resolution and accuracy of the small drones are still not as good as bats [23]. In addition to the resolution and accuracy, there still remains many other challenges, e.g. size, weight, power requirements, and time-delay. Hence, the problem of designing a capable, accurate and efficient technical sensor system is yet to be solved.

A major difference between the biosonar and the technical sonar is their beamwidth. Bats have wide beams although they are small. For technical sonars, they are always designed to make narrow beams and that is why they are big. Despite having the wide beam, the bats still outperform the technical sonar. Hence, bat's biosonar has been studied as a potential model for the development of the technical sonar systems. Bat biosonar system contains one transmitter and two receivers positioned slightly apart. On the transmitter side, some bats (e.g., Rhinolophidae, Hipposideridae and Phyllostomidae) emit sound through nostrils and the others (e.g., Vespertilionidae, Molossidae and Emballonuridae) emit sound through mouth [88]. The noseleaf in nasal emitting bats and the mouth and lips in oral emitting bats have acoustical influences to the patterns of sound emission [2, 34, 108]. On the receiver side, the external ear (pinna) plays an important role as a component of the echo receiver in bat biosonar system. Some bats have the static pinna and the others have the dynamic pinna [83]. Within the families of nasal emitting bats, Rhinolophidae and Hipposideridae also have the dynamic pinna that can cause complicated pinna motion patterns [99, 100]. These pinna motion patterns are correlated with pulse emissions and have a functional relevance for echo reception [83, 95]. For example, the pinna motion patterns can add the sensory

information of the received echoes such as changing the geometry of the beampattern [22] and causing Doppler shift [126].

Because bat biosonar systems are better than technical sonar (i.e. higher capability, less elements, and smaller size), engineers have tried to reproduce it. Several biomimetic sonar heads inspired by bats have been achieved and developed since 1990s, and they can reproduce the echolocation system of bats at a functional level. For the sonar heads being achieved earlier, they consist of three Polaroid electrostatic transducers that configure as a center transmitter flanked by two receivers [55, 122]. The transmitter and the receivers can rotate to focus on an object that produces echoes [55, 122]. Then, the simple artificial pinna shapes which use the basic geometry of an obliquely truncated horn were mounted on two receivers [70, 90]. After that, the deformation of the artificial pinna, which was made of rubber sheet, was achieved [75]. The simple artificial noseleaf, which was also made of rubber sheet and can deform, was added on the sonar head [8]. Until now, this biomimetic sonar head was further improved by adding nostrils and ear canals, and the artificial noseleaf and pinna, which were made of silicone based on the scanned model of bat, both can deform [9]. However, the rotation of the pinna has not been implemented on this sonar head.

1.2 Objective

Bats are a good model system for the development of technical sonar systems because they have developed a highly capable biosonar system during their evolution [31, 35, 79]. The dynamic pinna is the focus of this thesis. The dynamic pinna works as a dynamic reflective baffle to enhance the receiving ability of the biosonar system. It has been previously demonstrated that horseshoe bats and old world leaf-nosed bats have two distinct categories of pinna motion patterns: rigid motion which changes only the pinna orientation and non-rigid

motion which changes also the pinna shape [127]. However, the functional relevance between the acoustic and the pinna motions within each pinna motion category still remains unclear. In order to learn the relevance between the acoustic and the pinna motions, the variability within rigid pinna motions and non-rigid pinna motions needs to be characterized first.

To learn the variability of the rigid pinna motions, Pratt's leaf-nosed bats (*Hipposideros pratti*) have been used as experimental subjects to collect the pinna motions. Three-dimensional trajectory data of a dense set of landmarks marked on the pinna surface has been captured using stereo vision. Different rigid pinna motion sequences were selected based on the deformation. The rotation axes and angles were used as motion features to represent the rigid pinna motions.

After exploring the variability of the rigid pinna motions, a biomimetic pinna was used to reproduce the rigid pinna motions to investigate the acoustic impact. The ultrasonic signals were emitted by an ultrasonic transducer which faced to the biomimetic pinna. The signals affected by the dynamic pinna were received by the microphone, which was mounted behind the ear canal. To figure out the differences of the received signals in rotation axes, the envelopes of the signals were picked up and compared by the normalized mutual information.

Because the non-rigid pinna motions are much more complicated than the rigid pinna motions, only the pilot research about the variability of the non-rigid pinna motions has been done. Non-rigid pinna motion sequences were selected and the variability was investigated by clustering the motion sequences into different categories based on the distributions of clusters of the landmark points on the pinna surface.

1.3 Organization

The thesis is organized as follows:

Chapter 1: gives a basic introduction to this thesis, including background and objectives.

Chapter 2: reviews the literature related to this thesis and describes the state of the art.

Chapter 3: characterizes the variability in the rigid pinna motions of Pratt's leaf-nosed bats and their acoustic impacts, including methods and results.

Chapter 4: shows the pilot research about the variability in the non-rigid pinna motions of Pratt's leaf-nosed bats, including methods and results.

Chapter 5: presents the summary of the research achievements, the significance of the present work, and the suggestions for future work.

Chapter 2

Review of Literature

2.1 Biological context

Old World leaf-nosed bats (family Hipposideridae) and horseshoe bats (family Rhinolophidae) are two closely related bat families [110] and they are noted for their highly efficient biosonar systems. They can hunt and navigate in structure-rich natural environments [32, 80]. During their navigation and hunting, they use their biosonar systems to recognize if there is a target, to locate where the target is, to classify different targets, and to discriminate the expected target among a range of other targets [43, 78, 85]. Biosonar systems have to recover information about the environment after a reduction from four dimensions (three spatial dimensions, as well as time) to one dimension (time signal) [68].

In order to support such complicated behaviors, the biosonar system must be able to provide the sufficient information. At present, prey detection is the best understood of these behaviors and has produced evidence for adaptive mechanisms in hipposiderid and rhinolophid bat biosonar. Hipposiderid and rhinolophid bats emit a long narrowband constant frequency (CF) pure tone followed by a short broadband frequency modulated (FM) part, which start at high frequency and sweep downward to progressively lower frequency [28]. This special signal design has been adapted for the detection of Doppler shifts that are induced by the wing beat of the prey (e.g., a moth or a beetle) among all the echoes from potential prey and reflecting facets belonging to the dense vegetation. Detecting the small frequency shifts in

these narrow-band signal requires a high frequency resolution that is achieved through specializations in the inner ear (cochlea) [51, 56], its innervation [6], as well as in the brain [105].

In addition to their specialized signal design, hipposiderid and rhinolophid bats have adapted complex and dynamic emitters and receivers. An information-theoretic analysis has shown that these dynamic shape changes of emitter and receiver add sensory information, increase the number of resolvable directions of sound incidence, and improve the accuracy of direction finding [69]. On the emitter side, both hipposiderid and rhinolophid bats, which emit their biosonar pulses nasally, have elaborate baffle shapes surrounding their nostrils (noseleaf) [29, 130, 131]. Noseleaves in rhinolophid bats consist of three parts: anterior leaf, sella, and lancet [67]. Besides these geometric shape features, dynamic noseleaf motions have been observed in rhinolophid bats. The anterior leaf dynamically changes its shape in tight temporal synchronization with the emission of the biosonar pulses [16] and the lancet can also be moved during the emission of biosonar pulses [36]. Similar to the situation in the rhinolophid bats, noseleaves in hipposiderid bats consist of anterior leaf, posterior leaf, coronet, and two nostril flaps [24, 125]. The noseleaf motion patterns observed in hipposiderid bats include the closing motion (the size of the noseleaf aperture was reduced by bending the anterior and posterior leaves towards the nostrils) and the opening motion (reverse to the closing motion) [129]. On the receiver side, there are also potential relationships between form and function. For example, it has been found that the length of the ear is negatively correlated to the frequency of the echolocation calls [40, 83]. Beyond the ear size, the outer ears (pinna) of hipposiderid and rhinolophid bats have complex shape features such as antitragus, lateral pinna rim incision, vertical pinna surface ridge, and periodic washboard ripple patterns [64, 72]. However, these shape features have not been so well understood yet. In addition to the static features, the pinna have the dynamic motions like the noseleaves as described in the next section.

2.2 Pinna dynamics

Conspicuous pinna movements are an integral part of biosonar behaviors in horseshoe bats and Old World leaf-nosed bats [126]. The pinna movements were first described by Schneider in 1960 for rhinolophid bats and in 1961 for hipposiderid bats [99, 100]. Schneider found that the bats made rapidly repeated motions where the left pinna and the right pinna always moved in opposite direction. The greatest activity of the external ears occurred when the bat was alert and was emitting numerous pulses of orientation sound [99, 100]. The pinna movements are enabled by specialized muscular actuation mechanisms [94, 99, 100]. The pinna motions involved variable complex turning components and changes in shape of the pinna as well as movements of the head which was determined from a film recordings taken at 1000 to 1500 frames per second [94]. Recently, it has been found that the complicated pinna motions fall into two discrete categories: In "rigid rotations" motions only the orientation of the pinna in space was altered. In "open–close motions" not only the orientation of the pinna was altered but also its geometry was changed [127].

The pinna movements are significant to the biosonar function of horseshoe bats and Old World leaf-nosed bats. The importance of pinna movement for the determination of target angle has been shown and partial immobilization or surgical removal of the pinna abolishes vertical and impairs horizontal localization of long CF signals [25]. The target angle can be represented by azimuth and elevation and can be localized in horizontal and vertical plane. Compared with the target localization in the horizontal plane, the pinna movements is more important in the vertical plane [65]. Bats with normal mobile pinnae scored between 70% and 90% successful flights both with vertical and horizontal wires [65]. After surgically immobilizing the pinnae by cutting motor nerves and ear muscles, avoidance performance with vertical wires (horizontal target localization) was unchanged but the percentage of successful flights with horizontal wires (vertical target localization) decreased significantly [65].

The pinna motions are correlated with the biosonar emission and reception and can change the acoustic characteristics of the biosonar reception [27, 95]. A close correlation between the alternating ear movements and the buzz (a sequence of short pulses prior to prey capture) were first found in horseshoe bats [27]. When a horseshoe bat has the greatest need for accurate information about some object at close range, it uses its shortest duration pulses and emits each of these while one ear is moving forward and the other backward [27]. Complete cycles of ear movement occur at half the pulse repetition-rate [27]. Similar to the situation in the horseshoe bats, the correlation between ear movement and ultrasound production was indicated for hipposiderid bats [95]. A movement that occurs just before the production of one pulse might well be synchronized to the arrival of echoes from the previous pulse [95].

A numerical analysis has shown that a nonrigid deformation in pinna shape could potentially alter the geometry of the beampattern [22]. For the upright position of the pinna, the side lobes of the beampattern were weak compared to the main lobe. During the deformation of the pinnae, the sensitivity in the side lobes increased significantly relative to the main lobe whereas the gain of the main lobe changed comparatively little [22]. When the pinnae returned from their bent state to their initial upright position, the beam patterns also reverted to their previous configuration [22]. Furthermore, the main lobes and the side lobes showed a different dependence on frequency. The main lobes changed comparatively little across frequency whereas the position and shape of the side lobes depended strongly on frequency for the majority of the side lobes [22, 67]. Thereby, nonrigid deformations of pinna provide additional degrees of freedom for encoding relevant information into the received signals [22].

All dynamic features of the bat pinna described above can be described by time-varying linear transfer function. In addition, recent work has shown that the bats are also capable of nonlinear changes. Hipposiderid and rhinolophid bats can actively add Doppler-shift signatures into echoes in echolocation sequences using their own fast pinna motions [126].

Doppler shifts do not only depend on the speeds involved by the pinna motions but also on the orientations of the velocity vectors [126]. Fast motion speeds with the orientations of the velocity vectors that are parallel to the orientations of the propagation vectors of the incoming echoes would cause large Doppler shifts [126]. Furthermore, the time-frequency Doppler signatures are direction-dependent [126]. It has been shown that the Doppler signatures would be appropriate to distinguish a large number of different target directions (up to about 1 million) [126]. Hence, it could be used to obtain information on the direction of a biosonar target [126]. Thereby, the nonlinear transformations due to the pinna-generated Doppler shifts add an additional characteristic to the pinna movements in bats [126].

2.3 Biomimetic reproductions

Biomimetic reproductions of bat biosonar have been undertaken for two different types of reasons: The first reason is as a model to understand bat biosonar better because it is difficult to measure the characteristics of a dynamic sonar system (e.g., direction represented by azimuth and elevation, frequency, as well as time) in a living animal which would require a large number of repetitions of exactly the same biosonar dynamics [67]. The second reason is as a stepping stone towards better sonar technology because bat biosonar is still more capable and efficient than technical sonar.

Large scale commercial use of in-air sonar, whether biomimetic or not, started with the Polaroid 600 Autofocus camera that was first released in 1981. It uses only one ultrasonic transducer to transmit the ultrasonic signals and receive the echoes reflected by the target. Using the time of flight and the velocity of the sound, the range to the target can be figured out. To improve from range estimation to include the ability to track an object in direction space, five identical transducers, which configured in the form of a cross, were used to build up

a sonar-driven robot [53]. An acoustic pulse is emitted by the transducer that locates in the center and the echoes are detected by two pairs of receivers that flank the center transmitter horizontally and vertically [53]. Using qualitative interpretation of the sonar signals, this robot can be implemented to track an object that moves in three dimensions [53]. In addition to the object detection, a sonar ring mounted on a mobile robot was designed to follow walls and avoid obstacles [14, 15]. The sonar ring consists of 48 ultrasonic transducers in 24 pairs [14, 15]. Each pair of transducers has a transmitter and a receiver and they are 15 degrees apart [14]. It is able to cover 360 degrees around robot with simultaneously emitting of all 24 transmitters [14].

Many of the subsequently designed sonar systems typically follow a biomimetic arrangement in which one center transmitter was flanked by two receivers [54, 55, 89, 91, 122]. In the earlier versions, each of the receivers only had one degree of freedom which is panning [54]. Later, one more degree of freedom which is tilting was added to the receivers [91, 122]. In addition to the mobility of the receivers, rotational degrees of freedom, which mimics the head motion of bat, were also added to the whole sonar systems [55, 89]. The rotational degrees of freedom were achieved either by a robot arm [55] or a mobile platform [89]. These sonar systems can be used to locate a small reflecting object and explore the environment [54, 55, 89].

Beside the biomimetic one transmitter and two receivers, the pinna shapes were first mounted on a sonar head named CIRCE [70, 74, 90]. The idealized pinna shapes were designed and fabricated which use the basic shape of an obliquely truncated horn and augments it with a flap modelling the tragus and a ripple pattern [90]. In order to add more shape features of the bat pinna, the obliquely truncated horn pinna shape was replaced by a 3D printed pinna shape which based on the 3D model of the scanned bat pinna [98]. In this new version, the ear canal was first added. At the end of the ear canal, the microphone was inserted to receive the ultrasonic signals reflected from the target [98].

Hipposiderid and rhinolophid bats have complicated pinna motions which include rotations and deformations. Therefore, pinna deformations have been implemented using an elastic rubber prototype. The prototype was dynamically deformed using a one-point actuation mechanism to produce a biomimetic bending of the prototype's tip [73, 75, 86]. In addition to the pinna motions, hipposiderid and rhinolophid bats also have dynamic noseleaves. In order to mimic the pulse-related motions of the anterior leaf of the horseshoe bat, a single actuator was used to continuously deforming the concave baffles [19]. In order to mimic the noseleaf movements observed in hipposiderid bats, a dynamic sonar emitter has been designed [125]. It consisted of a biomimetic baffle prototype, three stepper motors and two ultrasonic transducers [125]. The biomimetic baffle prototype was derived from the noseleaf geometry of Pratt's roundleaf bat [125]. Three stepper motors were used to mimic the noseleaf motion patterns which were closing motion and opening motion [125]. Two ultrasonic transducers were used to transmit ultrasonic output signals which mimicked the ultrasonic pulse emission by hipposiderid bats through two nostrils [125].

To mimic the dynamic emission and reception characteristics of horseshoe bats on a single sonar head, one dynamic sonar emitter which mimics the noseleaf deformation of horseshoe bat and two dynamic sonar receivers which mimic the pinna deformation of horseshoe bat were combined together [8]. Both artificial pinna and noseleaf were made of elastic rubber and actuated using one-point actuation mechanism to produce a biomimetic bending of the pinna and noseleaf [8]. Because of the low mold-ability of the rubber, the artificial pinna and noseleaf then were replaced by flexible silicone cast out based on the scanned model of horseshoe bat's pinna and noseleaf [9]. A three-point actuation mechanism was updated to actuate three surface elements of the noseleaf baffle to mimic anterior leaf and lancet motions observed in horseshoe bat noseleaves [9]. However, the pinna rotation has not been implemented on these two sonar heads. Currently, a next-generation prototype

of a biomimetic sonar head inspired by horseshoe bats is being developed [115]. Pneumatic actuator design is used to actuate the pinna and noseleaf deformation which allows for greater soft robotic pinna and noseleaf deformation [115].

Chapter 3

Variability in the rigid pinna motions

3.1 Title

Variability in the rigid pinna motions of hipposiderid bats and their impact on sensory information encoding (accepted)

3.2 Abstract

Many bat species, e.g., in the rhinolophid and hipposiderid families, have dynamic biosonar systems with highly mobile pinnae. Pinna motion patterns have been shown to fall into two distinct categories: rigid rotations and non-rigid motions (i.e., deformations). In the present work, two questions regarding the rigid rotations have been investigated: (i) what is the nature of the variability (e.g., discrete subgroups or continuous variation) within the rigid motions, (ii) what is its acoustic impact? To investigate the first question, rigid pinna motions in Pratt's leaf-nosed bats (*Hipposideros pratti*) have been tracked with stereo vision and a dense set of landmark points on the pinna surface. Axis-angle representations of the recorded rigid motions have shown a continuous variation in the rotation axes that covered a range of almost 180 degrees in azimuth and elevation. To investigate the second question, the observed range of rigid pinna motions has been reproduced with a biomimetic pinna. Normalized mutual information between acoustic inputs associated with every pair of the

rigid pinna motions showed that even small changes in the rotation axis resulted in more than 50% new sensory information encoding capacity (i.e., normalized mutual information less than 50%). This demonstrates a potential sensory benefit to the observed variability in the rigid pinna rotations.

3.3 Introduction

Many of the over 1,200 bat species worldwide [110] have evolved highly capable biosonar systems [31, 35, 79] that can detect, localize [80, 102], and classify [85, 121] prey targets. Bats could also use their biosonar systems to evaluate complex natural targets/textures, such as foliage, for navigation and spatial orientation [103]. It may be hypothesized that adaptations are critical to achieving these unusual sensory abilities based on ultrasonic echoes that can be described as a function of a single independent variable (time) when received at the bat's ear. In principle, such adaptations could happen at two levels, at the evolutionary level where species-specific traits are modified from generation to generation and at the level of behavioral plasticity where individual animals react to the situation they find themselves in. Furthermore, adaptions on both of these levels could effect all acoustical stages of the biosonar system: ultrasound generation, pulse emission into the free field, and echo reception [28].

An example of adaptations on the evolutionary level are the different time-frequency structures that can be found in bats' ultrasonic pulses [45, 102, 109]. Whereas the biosonar pulses of some bat species are frequency-modulated (FM) throughout their entire duration, the pulses of other species such as the Old World leaf-nosed bats (family Hipposideridae) and the horseshoe bats (family Rhinolophidae) contain a constant frequency (CF) portion. The CF portion is well-suited for the evaluation of Doppler-shifts that are produced by the

wingbeat of an insect prey and can hence distinguish prey among distracting targets (e.g., foliage). The FM component can support accurate target-range estimates and the evaluation of target spectral signatures [4, 41, 48, 77, 101, 102, 121].

Hipposiderid and rhinolophid bats emit their biosonar pulses through nostrils that are surrounded by noseleaves that function as megaphones. Intricate shape details found in these noseleaves contribute to the emission beampatterns [117, 118, 130, 131]. Similar to the situation on the emission side, hipposiderid and rhinolophid bats also have external ears (pinnae) that are characterized by geometric features such as the antitragus, horizontal ridges on the frontal pinna surface, and a vertical "spine" along the anterior pinna rim [59]. Biomimetic replicas of these static shape features have suggested an impact on the beampattern of at least some of these static features [86].

On the level of behavioral plasticity, bats are known to adjust their biosonar pulses and pulse trains according to the situation [17]. For example, when bats from certain families approach a prey target, they progressively decrease the intervals between their pulses [28, 102]. At the emission interface, hipposiderid and rhinolophid bats have muscular control over the shapes of their noseleaves and can deform them in ways that produce dynamic emission beampatterns [29]. On the reception side, these bats have intricate sets of pinna muscles [99, 100] that can support pinna motions. The patterns of these motions fall into two distinct categories: rigid motions, which change the orientation but do not alter the shape of the pinna substantially, and non-rigid motions, which change the geometry of the pinna [127]. Further research has shown that hipposiderid and rhinolophid bats can actively insert Doppler-shift signatures into echoes by virtue of their own fast pinna motions [126]. The Doppler signatures would be appropriate to distinguish a large number of different target directions (up to about 1 million) and it could be used to obtain information on the direction of a biosonar target [126].

Pinna motions are correlated with pulse emissions in a way that allows them to have an impact on the returning echoes [95, 126]. Hence, the motions could have a functional relevance for echo reception and biosonar-based navigation [65]. Nonrigid pinna deformations enhance encoding of sensory information by dynamically altering the geometry of the reception beampattern [22]. This time-variance provides additional degrees of freedom for encoding relevant information into the received signals [64]. This additional encoding capacity is useful for target direction finding by increasing the number of resolvable directions of sound incidence and improving the accuracy of direction finding [69]. Similarly, rigid rotations of the pinna are useful for rejection of background clutter [42, 119, 120] and target localization [119, 120, 122].

As of now, the nature of the pinna motions that fall within the non-rigid and rigid pinna motion categories has received little attention. Hence, it remains unknown whether the pinna motions in each category follow a stereotypical pattern or show a substantial amount of variability. In the latter case, the nature of the variability would also be of interest. It could be that this variability manifests itself in the form of distinct subcategories or it could take the form of a continuous variation. Regardless of the exact nature of the variation, presence of variability within the non-rigid or rigid motion could provide an additional substrate for behavioral-level plasticity in the biosonar system of hipposiderid and rhinolophid bats. To be suitable as a substrate for such adaptation, it would be necessary for this within-class variability to also have an acoustic impact. The research presented here has characterized the variability in the rigid pinna motions of hipposiderid bats. This was done by tracking dense grids of landmark points on the pinna with high-speed stereo vision to obtain the pinna motion characteristics across a large set of motions. To characterize the potential acoustic impact of the variability within the rigid pinna motions, these motions were reproduced with a movable biomimetic pinna shape that served as a microphone baffle.

3.4 Methods

3.4.1 Motion kinematics

Rigid pinna motions have been studied in a group of Pratt's leaf-nosed bats (*Hipposideros pratti*, [18]) that contained a total of five experimental subjects, three males and two females. The bats were obtained from caves in Fujian and Jiangxi provinces in south-eastern China. The pinna lengths of all experimental subjects were around 3 cm. The bats were housed in an indoor flight room (6 m long × 4 m wide × 3 m high) at Shandong University in Jinan, China. Inside this flight room, constant environmental conditions with a temperature of 23 °C and a humidity of 65 to 70% were maintained. The bats were kept under an equal light-and-dark cycle and the behavioral experiments took place during the dark phase of this cycle. The bats were fed on a diet of mealworms enriched with vitamin and mineral supplements; water was provided ad libitum.

Characterizations of the rigid pinna motions were obtained by virtue of reconstructions of the three-dimensional trajectories of landmark points that were placed on the pinna. The landmarks were dots (about 0.5 to 1.5 millimeters in diameter) that consisted of a white non-toxic dye. Between 50 and 130 such dots were distributed on the outer surface of one pinna including the rim (Fig. 3.2(a)). During the experiments, the bat was placed on a platform so that the pinnae with the landmarks was approximately positioned in the center of an array consisting of four high-speed video cameras (GigaView, Southern Vision Systems Inc., Huntsville, AL) with 50 mm lenses (Rodagon, Rodenstock, Feldkirchen, Germany) that were positioned along an arc with 55 cm radius (Fig. 3.1).

A small rotating propeller (9 mm diameter, operated at 10 to 80 revolutions per second) was used to mimic the Doppler shifts associated with the wing beat of a flying insect prey

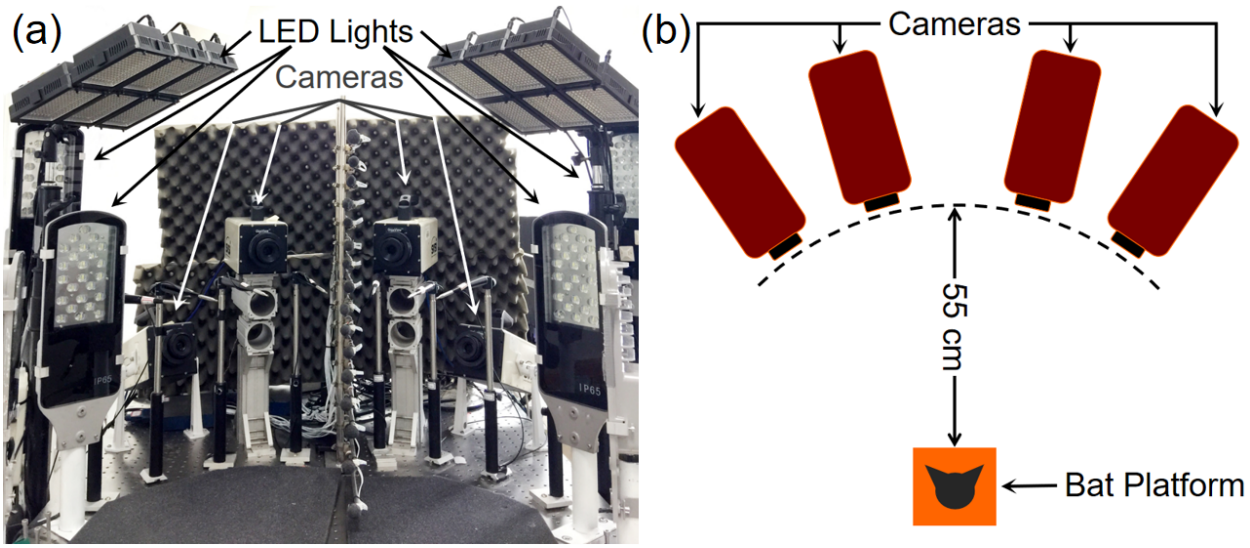

Figure 3.1: Experimental setup for collection of the pinna kinematics: a) frontal view of the setup with high-speed video cameras and lights, b) schematic top view of the setup including the bat platform.

in order to attract the attention of the bats in the experiments. The "artificial moth" was manually moved behind the high-speed video cameras. Six sets of light emitting diode (LED) lights were positioned around the high-speed cameras and the bat's platform to illuminate the pinna for the high-speed video recordings.

To record the high-speed video sequences, all four high-speed video cameras were focused on the position of the bat's pinna and all cameras were triggered simultaneously. The cameras were operated at a frame rate of 400 frames per second and a digital image resolution of 1280×1024 pixels. The high-speed video cameras were calibrated to obtain estimates of their intrinsic and extrinsic parameters using a checker-board target with 8×8 black-and-white square fields, each with an edge length of 5 mm. To create the calibration data set, the target was presented in different positions (Camera Calibration Toolbox for Matlab [5], Mathworks, Natick, MA).

The analysis presented here has been based on a total of 100 video sequences of rigid pinna

motions that were obtained across all five different individuals in the study group. A motion sequence was defined as a continuous segment of the recording over which the pinna was continuously in motion and that was free of reversals in the direction of the motion. Two of the experimental subjects were female and contributed a total of 27 (7+20) rigid pinna motion sequences. The remaining three bats were male and contributed 73 (24+29+20) sequences of rigid pinna motions. These sequences were selected for their quality (i.e., high-quality images of the pinna from at a minimum of two cameras) and the presence of rigid pinna motions. For each of the selected video sequences, the two-dimensional image coordinates of the landmark points were picked with a semi-automatic approach where the landmark points where manually identified in the first video frame of a sequence and then tracked across subsequent frames automatically using an optic flow algorithm [38]. The coordinates of the landmarks in the image plane were then used to reconstruct the three-dimension positions of the landmarks by means of stereo triangulation [5].

In order to verify that the pinna motions in the selected videos were rigid, the maximum change in the pairwise distances between the landmark points on the pinna rim across the motion was used as a criterion [127]. To this end, a matrix of the maximum changes across in the distances between all pairs of the landmark points along the pinna rim was constructed. The maximum distances were computed across all images in the sequence. If the largest value in this matrix was less than 1.5 mm, the motion was classified as rigid (Fig. 3.2).

To estimate the rigid pinna rotations in the recorded motion sequences, the landmark coordinates associated with each sequence were transformed into a common reference coordinate system to eliminate differences in the initial location and orientation of the pinna between different recordings. The coordinate system was defined based on three landmarks: the first on the pinna tip, the second near the center of the anterior rim, and the third near the center of the posterior rim (Fig. 3.3). All three of these points were used to define a plane. In this

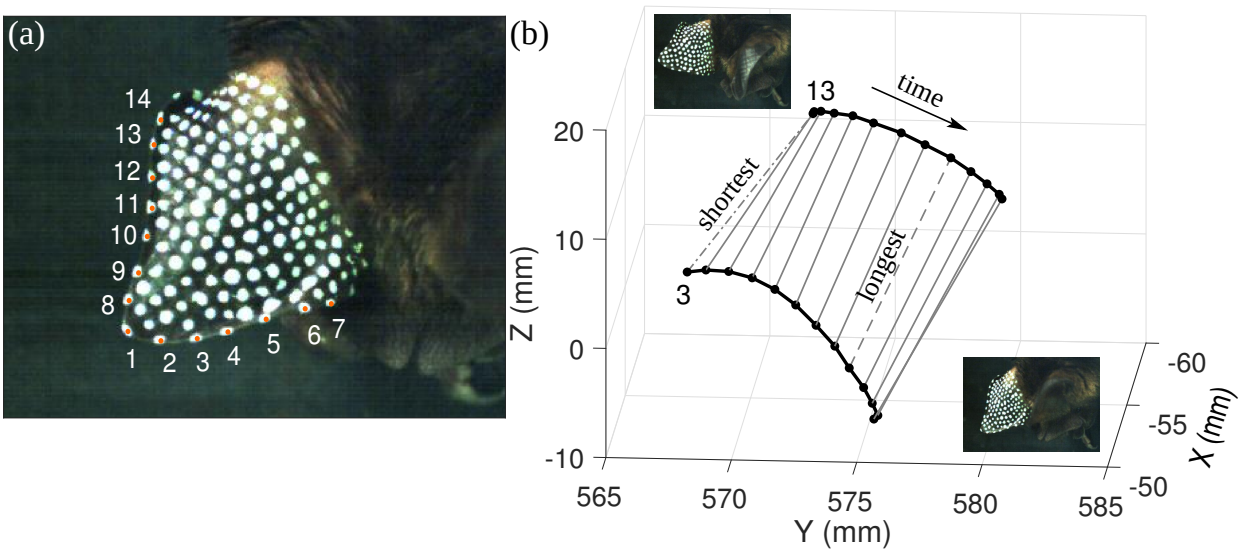

Figure 3.2: Example of verification of rigid motions: a) landmarks on the anterior rim and posterior rim of the pinna that were used to verify the rigid motion, b) trajectories of two points on the pinna rim, one on the anterior rim (point 3) and another on the posterior rim (point 13). The distances between the points at each time step (video frame) are indicated by gray lines. For each sequence, the shortest and the longest distances between the points were identified and the difference between them was used to verify the rigid motions.

plane, the vector between the points on the pinna tip and posterior rim was used to define the first axis of the new pinna-centered coordinate system. The second axis was defined by a vector that was orthogonal to the first axis and also fell into the plane. The final third axis was defined by the normal to the plane spanned by the first two axes.

To characterize the variability in the rigid pinna motions, each motion was represented by a set of parameters that specified a rotation axis and the rotation angle about this axis [37]. In order to obtain the rotation axis of a given rigid pinna motion sequence, the rotation center of each landmark point was estimated using the Taubin algorithm [116] that fits a circle to the three-dimensional landmark trajectories. The location of the center of this circle was used as the estimate for the rotation center for the respective landmark point. In a rigid rotation, the rotation centers of all landmark points should all fall onto the same straight line that marks the axis of the pinna rotation. To determine this axis, a liner fit to the rotation

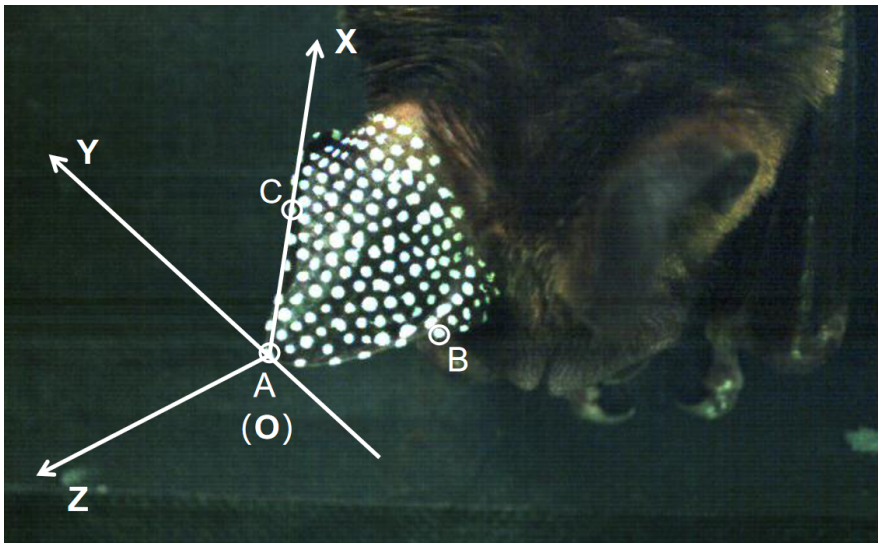

Figure 3.3: Pinna-centered coordinate system for determining rotation axis and angle: reference coordinate system derived from the landmark points on the pinna tip (A), and on the anterior (B) and posterior (C) rim of the pinna.

centers of all landmark points was obtained using singular value decomposition (SVD, [123]). The rotation angle for each landmark point was estimated from the point's initial and final position in the respective recording and the estimated rotation axis. The rotation angle for the entire pinna was estimated by virtue of the median of the individual rotation angles that were obtained for each landmark point. The median was used in this operation to prevent outliers in the individual angle estimates from influencing the final result.

In order to assess the accuracy of the employed method for determining the rotation parameters, artificial rigid pinna motion sequences were generated to serve as test data for which the true rotation value was known. For these artificial motion sequences, an artificial pinna shape was created as a triangular cut from the surface of a sphere. To realize this model, a genetic algorithm [124] was used to generate points that were evenly distributed on the surface of a sphere with a radius of 2 cm which was equal to the radius of a sphere that was fitted to the landmark points that had been placed on a bat's pinna using a least-squares method [92]. Ninety of these points were selected based on their positions within a trian-

gular region to form the model pinna representation (Fig. 3.4). The points on the model pinna were subjected to known rotations (45°rotation about an axis with an elevation of 0°and azimuth of -45°). The entire 45°rotation was conducted in 16 equal steps to create a sequence of pinna position equivalent to what would be in a sequence of high-speed video frames (Fig. 3.5). Identically independently distributed Gaussian noise samples with a standard deviation of 0.05 mm and different mean values (ranging from 0 mm to 0.2 mm in steps of 0.05 mm) were generated to serve as the amplitude values for the random displacement vectors that were added to each of the landmarks on the model pinna. The directions of the random displacement vectors were selected with uniform probability from a set of 3072 unit vectors that were generated using the HEALPix algorithm [26] (HEALPix Toolbox for Matlab, Mathworks Natick, MA). The unit vectors were scaled by the amplitude values drawn from the Gaussian distribution and then added to the positions of the landmarks in each orientation stage (i.e., equivalent to a video frame taken of a bat pinna) of the pinna model to create a randomly perturbed version of the model. For each mean amplitude of the perturbation vectors, 50 realizations of the respective noise-corrupted pinna models were generated. For each of these model realizations, the rotation axis and angle were estimated using the same algorithm that was also used for the digitized pinna-motion sequences recorded from the experimental subjects. The differences between the estimated axes and angles and their known true values were taken as a measure for the error of the method.

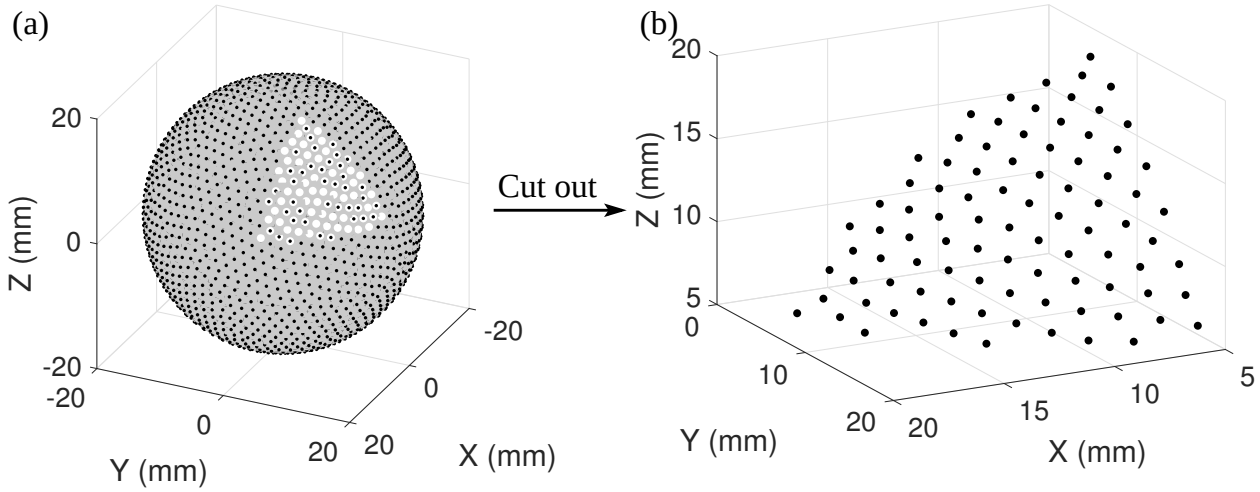

Figure 3.4: Rigid pinna rotation simulation: a) evenly distributed points on a sphere with a radius that matches that of a spherical fit to the landmark points on a real bat pinna, b) landmark points on the model pinna selected from the points in (a).

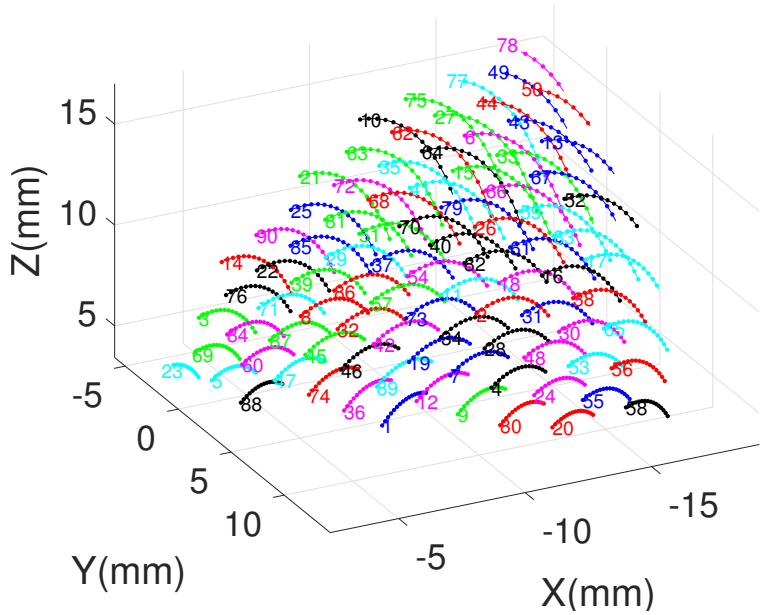

Figure 3.5: Rigid pinna rotation simulation: trajectories of the model landmark points that correspond to a total rotation of 45°.

The directions of the rotation axis estimates obtained for all 100 rigid pinna motion sequences were visualized on a map using a perspective projection. The rotation axis directions were also represented by a pair of angles, i.e., azimuth and elevation. The distributions of these angle values and the rotation angle magnitudes were estimated using histograms with the number of bins determined by Sturge's rule [106], and the normality of each distribution was tested using a Kolmogorov-Smirnov test [63].

In order to determine whether there was a continuous variation or distinct subgroups within the rigid pinna motions, the silhouette value [97] of the clustering results of the rigid pinna motions was computed. The silhouette value is a measure of how similar an object is to members of its own cluster (tightness) compared to members of other clusters (separation) [97]. The silhouette value ranges from -1 to $+1$, and a high silhouette value indicates that the object is well matched to its own cluster and poorly matched to its neighboring clusters [97]. If the rigid pinna motions belong to different distinct subgroups, they can be clustered to different clusters. The spectral clustering algorithm [81] was employed to investigate the presence of the distinct subgroups in the data. Using this method, hypothetical cluster numbers from two to 30 were tested and the mean silhouette value was computed for each number of clusters. If the data does contain clusters, it is expected that the silhouette value peaks for a tested cluster number that matches the true value. If there is continuous variation in the data, this should not happen.

3.4.2 Acoustic Impact of pinna motion variability

In order to investigate the acoustic impact of the variability in the rigid pinna rotations, a biomimetic rotating pinna was designed and implemented. The pinna model was created using 3d modeling software (Maya, Autodesk Corporation, San Rafael, California, United

States). The model pinna was scaled up relative to the size of the pinna in Pratt's leaf-nosed bats by a factor of two. The geometry of the pinna model was simplified to remove any shape irregularities but preserved all main shape features of the hipposiderid pinna: a pointed pinna tip, a set of horizontal ridges on the inner pinna surface, a vertical ridge along the anterior rim, and the antitragus (Fig. 3.6). A first physical realization of the pinna design was obtained as a 3d-print in polylactic acid (PLA). From this PLA-prototype, a mold was created that was used to cast the final artificial pinna model in a flexible silicone material (Dragonskin 30, Smooth-on, Macungie, Pennsylvania, United States) with a similar acoustic impedance as biological soft tissues [7].

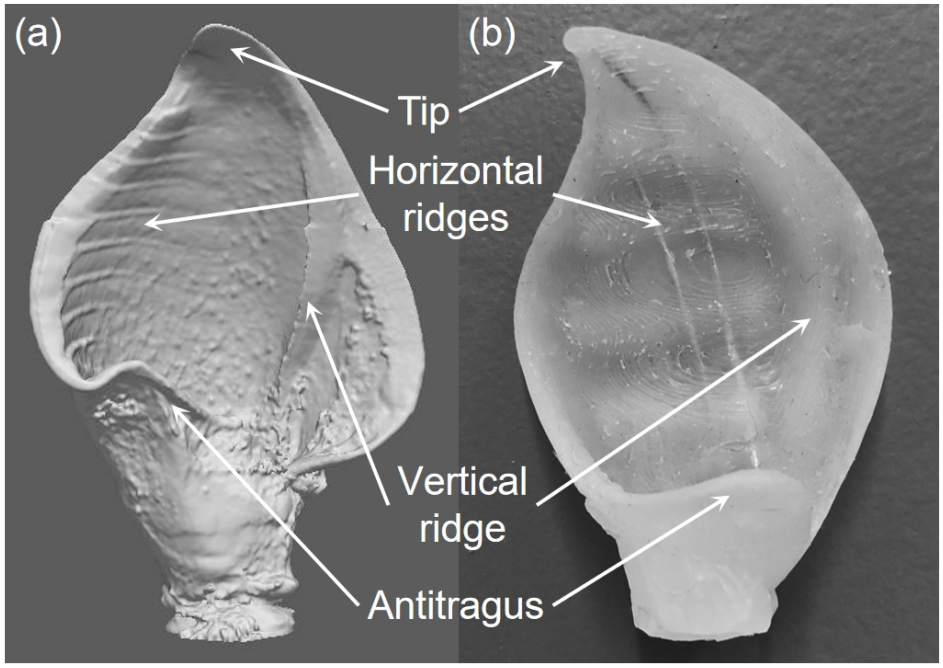

Figure 3.6: Pinna morphology of Pratt's leaf-nosed bat (*Hipposideros pratti*): a) bat pinna geometry reconstructed from a microCT scan, b) biomimetic pinna made of silicone.

The tested rigid pinna rotations were accomplished by a combination of two motion units (Fig. 3.7). The first was a pan-tilt unit (PTU-E46, FLIR, Burlington, ON, Canada) that was used to orient the rotation axis about which the pinna itself was rotated by virtue of an additional stepper motor (PKP Series, Oriental Motor, Japan with Easy Driver, Sparkfun,

Niwot, Colorado, United States) controlled via a microcontroller board (Arduino MEGA, Arduino, Ivrea, Italy). The stepper motor was mounted on the pan-tilt unit so that the vertical and horizontal rotation axes crossed at the bottom of the artificial pinna as is the case for the pinna rotations in the bats (Fig. 3.7). The coordinate system used for the rotation of the biomimetic pinna was hence not identical to the pinna-centric coordinates that were used to characterize the pinna rotations of the bats. Establishing the transform between rotations of the bat pinna and the biomimetic pinna was not necessary for the purpose of the current work since the goal was to establish whether pinna rotations in different directions are suitable for providing additional sensory information and not to analyze the signals associated with specific rotations. The pan-tilt unit was used to rotate the central axis of pinna over an angular range of 150°in azimuth. The stepper motor was used to cover an angular range of 45°in elevation. It was operated at a constant rotation speed of 10.5 $^{\mathrm{rad}}/_{\mathrm{s}}$ and caused a rigid pinna motion with a pinna tip speed of approximately 0.63 $^{\mathrm{m}}/_{\mathrm{s}}$.

An electrostatic ultrasonic transducer (diameter 38.43 mm, 600 series, SensComp, Livonia, Michigan, United States) driven by a high-voltage amplifier (A-301HS, AA Lab Systems, Israel) and a dedicated 200 V DC power supply (NCH6100HV Nixie Power Supply, Silicon Valley, CA, USA) was used to generate the ultrasonic pulse signals. The transducer was positioned 1 m away from the artificial pinna. A MEMS microphone (Monomic, Dodotronic, Rome, Italy) was mounted behind an artificial ear canal (length 3.5 mm) to capture the signals received by the pinna. The emitted test signals were acquired using a data acquisition card (NI SCB-68A, National Instruments, Austin, TX, USA) with a sampling rate of 500 kHz and a resolution of 16 bits (Fig. 3.8).

Since Pratt's leaf-nosed bat is a constant frequency-frequency modulated (CF-FM) bat with biosonar pulses that combine narrow-band, i.e. CF, and FM portions, the experiments were designed to test these two signal types separately and hence allow a comparison of the

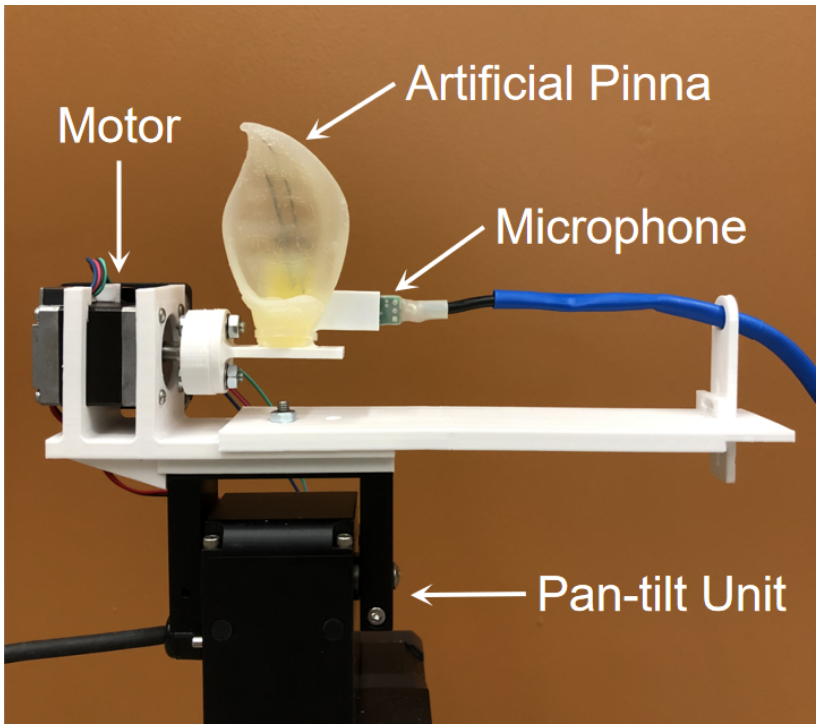

Figure 3.7: Experimental setup for acoustic characterization of the rigid pinna motions: A pan-tilt unit and an additional stepper motor were used to create vertical and horizontal rotation axes that intersect in the bottom of the pinna.

rotation effects on each signal type. To accomplish this, the experiments with the artificial pinna were carried out twice: one run with a constant-frequency pulse and the other with a frequency-modulated chirp signal.

In the biosonar pulses of Pratt's leaf-nosed bats, the second harmonic dominates in terms of signal energy [93]. The CF component is located at around 60 kHz and the lowest frequency of the FM component is 15%-20% lower than the CF part [20]. Since the artificial pinna used in the experiments were about twice as large as that of those of the bats, the frequencies of the ultrasonic signals used in the experiments were chosen to be about half of those found in the bats. Specifically, the CF signals were positioned at a frequency of 35 kHz and the FM signals were linear-frequency modulated that were swept downwards from 35 kHz to 30 kHz.

The orientation space for the rotation axes that was surveyed in the experiments covered

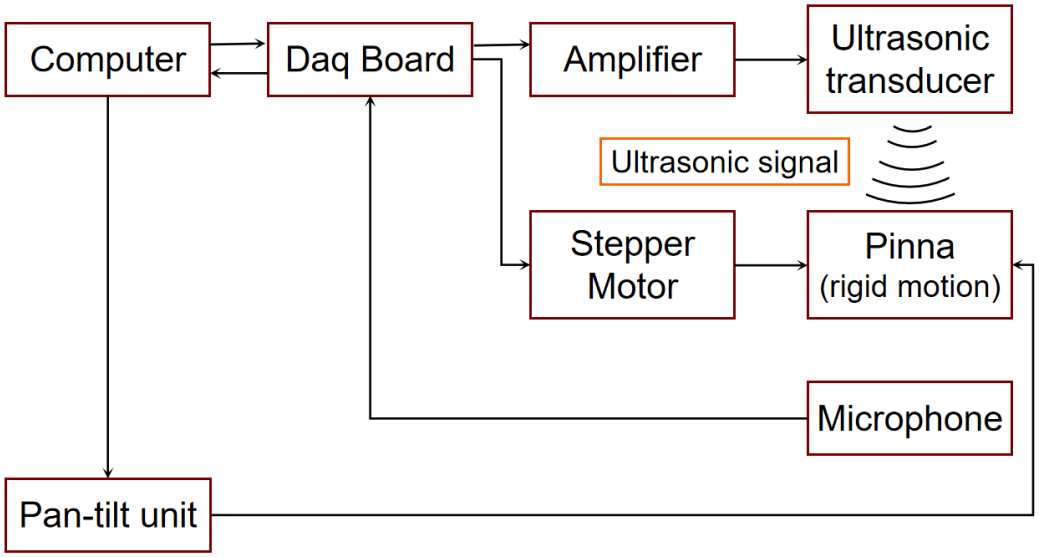

Figure 3.8: Block diagram of the experimental setup for acoustic characterization of the rigid pinna motions

a range of 150°(-75°to 75°) in azimuth and 135°(-60°to 75°) in elevation. Both ranges were scanned in steps of 15°. For each orientation of the rotation axes, 10 repetitions of the respective rotation were carried out. The timing of the motions and the pulse emissions were aligned so that the biomimetic pinna performed a continuous rotation while receiving the acoustic input signal. The rotation was carried out over a total time duration of 75 ms. Emission of the ultrasonic test pulse started 18 ms after the start of the rotation to ensure that any mechanical transients did not have an effect on the acoustic recordings. The acoustic pulses each had a duration of 40 ms which was hence approximately centered within the duration of the rotation. Since the biomimetic pinna moved about 3.5 times slower than bat pinna [126], the duration of the synthetic pulses corresponded to about 11 ms in the bats within the variation reported for individuals under laboratory conditions [20].

Normalized mutual information [11], which is a measure to quantify the statistical information shared between two variables, was used as a metric to assess the similarity between the sensory information that can be encoded in the course of different rigid rotations. Low values

of the (normalized) mutual information signify a weak dependence between sensory information in the signals associated with different rotations and hence indicate an opportunity for the bats to gain different sensory information by varying their ear motions. However, the mutual information neither specifies if the additional sensory information is useful to the bats, nor does it prove whether the animals use it. As a basis for carrying out this analysis, the signals recorded during the 10 repetitions of each experimental condition were averaged to reduce in-band noise. Furthermore, the signals were bandpass-filtered to reduce out-of-band noise (FIR filter, Hamming window design method, 513 taps, corner frequencies 33 and 37 kHz for experiments with CF signals and 28 and 37 kHz for experiments with FM signals). The envelopes of these cleaned-up signals were estimated as the magnitude of an analytic signal computed via the Hilbert transform [62]. Since all employed signals had a narrow-band carrier (constant or modulated), the envelope reflects all linear changes to the signals due to the ear rotations. Nonlinear changes, e.g., Doppler, were not considered, since the biomimetic pinna was rotated slowly. The envelope estimates were smoothed through a locally weighted linear regression filter (LOESS filter) that extends the concept of a moving average filter to local fitting of low-degree polynomials [10].

The normalized mutual information metric $\mathrm{NMI}(X, Y)$ between two different envelope signals X and Y is given by [114]

$$\mathrm{NMI}(X, Y) = \frac{I(X, Y)}{\sqrt{H(X)H(Y)}},$$

where $I(X, Y)$ is the mutual information between the envelope signals and $H(X)$ and $H(Y)$ are the respective Shannon entropies [107] of each signal. The mutual information was estimated using Kraskov continuous estimators that are based on evaluating a nearest-neighbor metric [52, 58].

3.5 Results

The error analysis of the estimation method for the pinna rotation axis and angle showed that the method was free of bias since the average error was zero for all three estimated quantities (rotation angle magnitude, azimuth and elevation of the axis orientation, Fig. 3.9). The variability in the estimates did increase with the level of the noise that was added to the point positions. However, even for a mean perturbation of 0.2 mm, the errors stayed below ±4°.

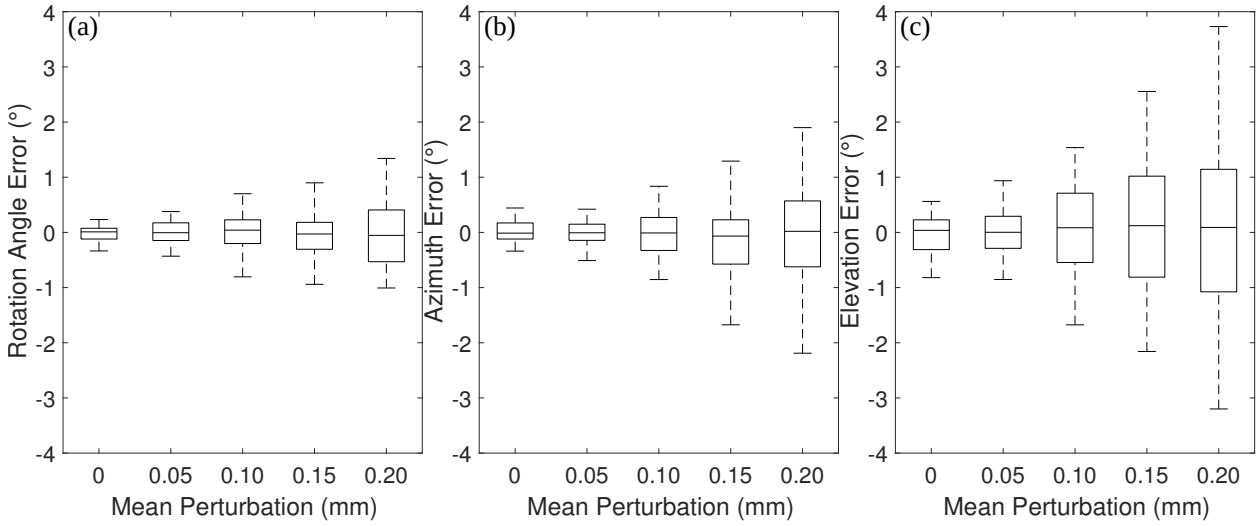

Figure 3.9: Estimation errors for the rotation parameters as a function of the level of perturbation noise that was added to the landmark positions: a) rotation angle magnitudes, b) azimuth values of the rotation axes, c) elevation values of the rotation axes. For each condition, 50 trials were evaluated. The boxes span the range between first and third quartile. The horizontal line within the box indicates the median and the whiskers indicate the minimum and maximum values.

For all of the 100 pinna motions analyzed, the maximum difference in the pairwise distances between the landmark points on the anterior and posterior rim (landmarks 1 to 7 and 8 to 14 in Fig. 3.10) never exceeded 1.5 mm. This establishes that all analyzed pinna motions can be thought of as rigid to a very good approximation (Fig. 3.11).

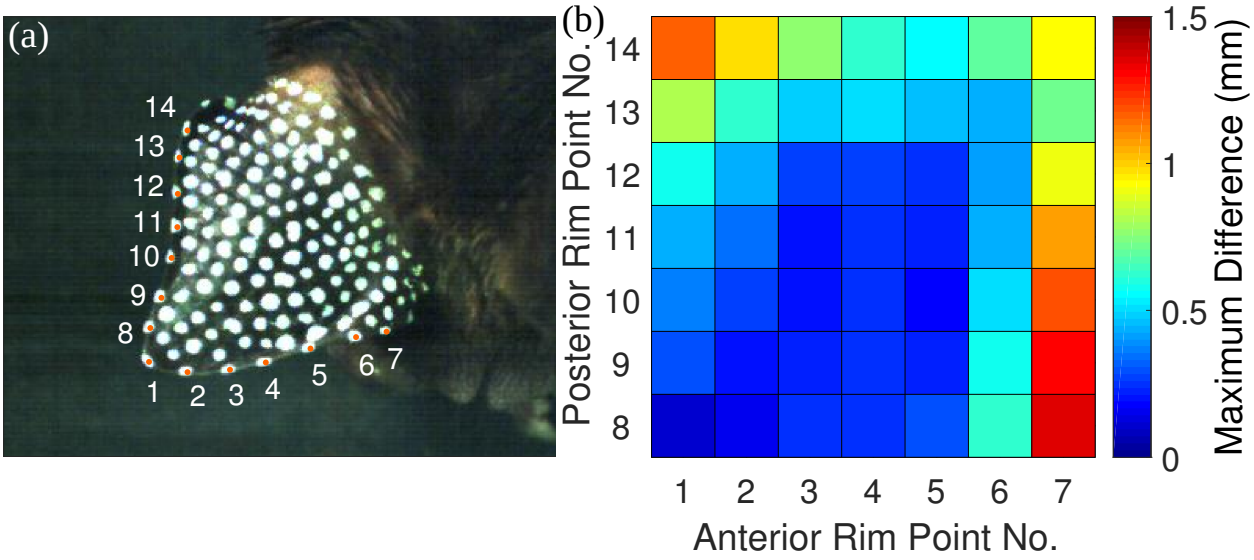

Figure 3.10: Verification of rigid motions: a) landmarks on the anterior rim and posterior rim of the pinna that were used to verify the rigid motion, b) matrix of maximum changes in the pairwise distances across all time steps between the pinna rim points shown in (a).

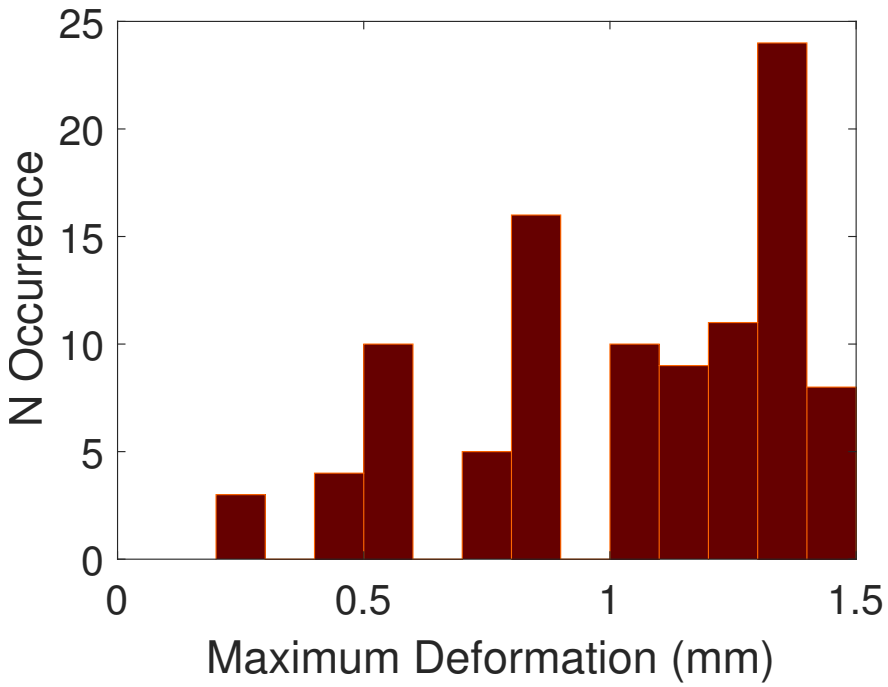

Figure 3.11: Verification of rigid motions: distribution of the maximum values in the matrix of maximum changes in the pairwise distances for 100 selected pinna motions.

The mean silhouette values obtained when clustering 100 rigid pinna motions into sets of two to 30 clusters ranged between -0.44 and zero. There was no peak in the silhouette value for any number of clusters (Table 3.1). Hence, these tests produced no evidence for the existence of distinct subgroups within rigid pinna motions and supported the hypothesis of a continuous variation.

Table 3.1: Mean silhouette value of the clustering results of 100 rigid rotation axes (azimuth [α], elevation [β]) and 100 rigid pinna motions (azimuth [α], elevation [β], angle [θ]).

# of clusters	2	3	4	5	6	7	8	9	10	20	30
(α, β)	0.03	-0.06	-0.07	-0.11	-0.16	-0.33	-0.19	-0.32	-0.30	-0.20	-0.06
(α, β, θ)	0.00	-0.07	-0.13	-0.21	-0.25	-0.29	-0.32	-0.34	-0.37	-0.46	-0.44

The distribution of the rotation angle magnitudes with standard deviation of 14.3°showed a substantial amount of continuous variability where 75% of the rigid pinna motions in the data set had rotation angles that fell into a range of 30°width (20 °to 50°, Fig. 3.12). Like the rotation angle magnitudes, the orientations of the rotation axes also showed a wide, continuous variation (Fig. 3.13). The azimuth values of the axis orientations covered a range of 180°with a standard deviation of 37.8°. For the elevation values of the axis orientations, the total range was also 180°and the standard deviation was 30.3°, i.e., somewhat smaller than for the azimuth component of the axis orientations (Table 3.2). The distributions of all rotation parameters (axis azimuth and elevation, rotation angles) were found not to differ significantly from normal distributions (p values 0.72, 0.57, and 0.26 respectively, Kolmogorov-Smirnov test [84], Table 3.2).

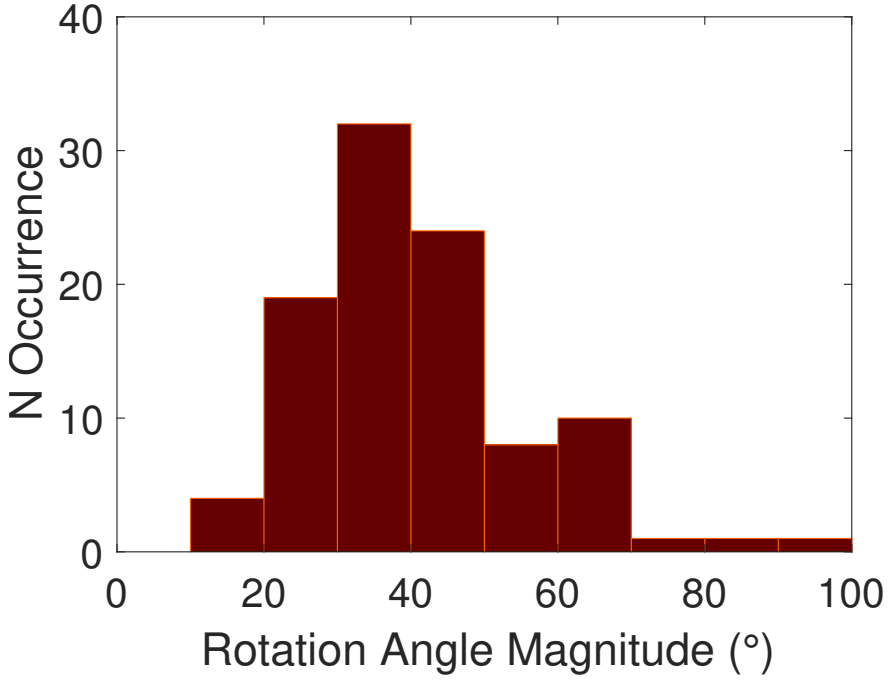

Figure 3.12: Variability in the rotation angle magnitudes across the analyzed set of rigid pinna motion sequences (n=100).

Table 3.2: Statistical characteristics of the distributions for the values of rotation angle magnitudes, azimuths and elevations of rotation axes over the 100 analyzed rigid pinna motions.

	mean	median	std	skewness	kurtosis	p-value (K-S test)
rotation angle magnitude	40.92	38.16	14.30	1.00	1.44	0.26
azimuth of rotation axis	-16.36	-14.34	37.85	0.36	-0.27	0.72
elevation of rotation axis	-1.82	-0.46	30.28	-0.31	0.80	0.57

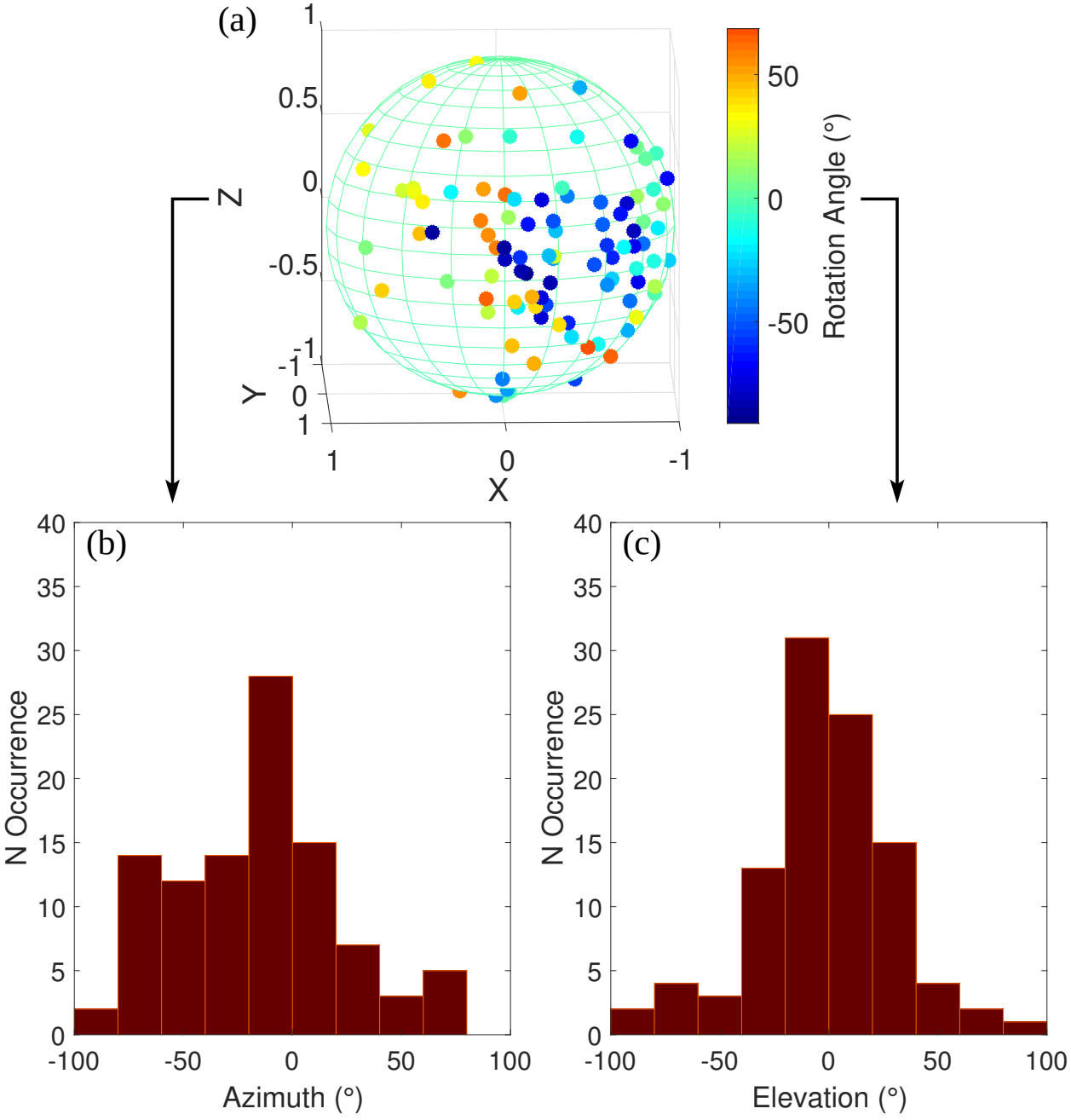

Figure 3.13: Variability in the orientations of the pinna rotation axes: a) map showing the axis orientations and the respective rotation angles (color scale), b) histogram estimate of the distribution of the azimuth values of the axis orientations, c) histogram estimate of the distribution of the elevation values of the axis orientations (n=100).

Qualitative examination of the echo envelopes recorded during the rotations of the biomimetic pinna showed a strong time-variance in the amplitudes, regardless of whether the signal's carrier was a constant-frequency sine or a chirp (Fig. 3.14).

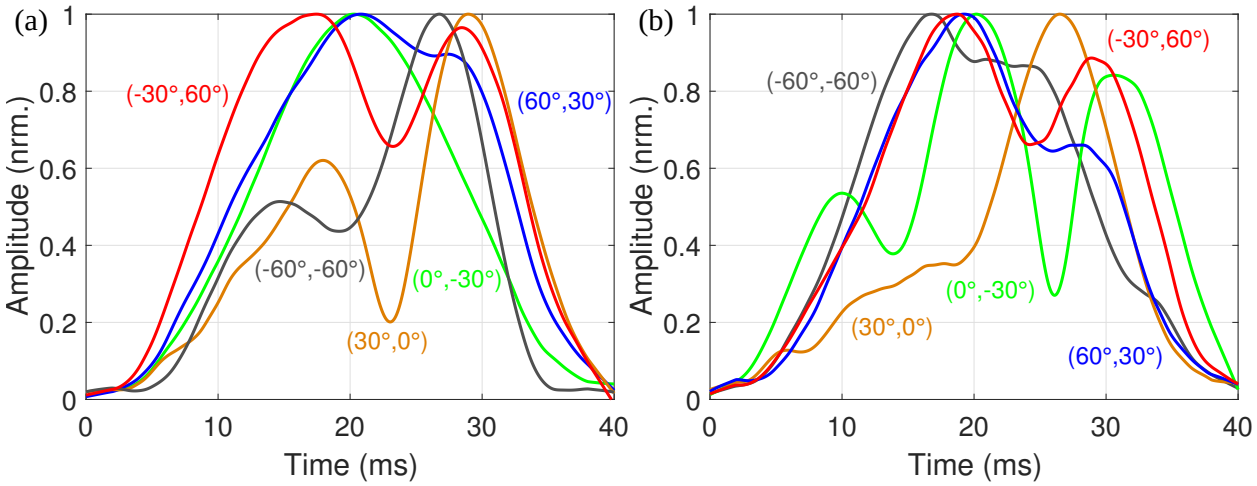

Figure 3.14: Example of pulse envelopes recorded during rigid pinna rotations with different rotation axes: a) for pulses with a single sine carrier. b) for pulses with a frequency-modulated carrier. Labels (M°,N°) denote azimuth and elevation of the respective rotation axis direction.

The normalized mutual information between pulse envelopes obtained for different rotation patterns was found to be less than 50% regardless of whether a constant-frequency sine or a chirp was used as the signal carrier (Fig. 3.15). For the pulses with a sine carrier, the normalized mutual information fell into the interval from 35.5 to 49.3% (mean 43.8%, standard deviation 2.42%). For the pulses with a chirp carrier, the respective interval was 34.7 to 48.4% (mean 42.4%, standard deviation 2.45%). Although the results for constant frequency and chirp carriers showed a statistically highly significant difference (p-value$<$0.0001, paired t-test), the value ranges overlap widely (by more about 94%).

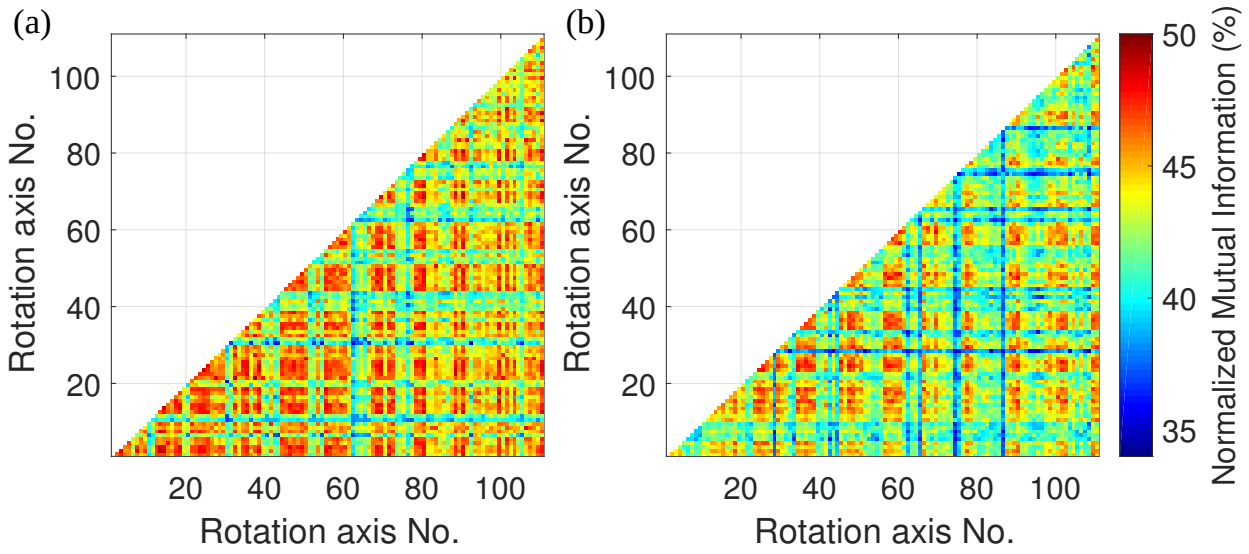

Figure 3.15: Normalized mutual information between the pulse envelopes collected with 110 different pinna rotation axes: a) for pulses with a sine carrier (CF), b) for pulses with a frequency-modulated carrier. For each graph, the different rotation axes positions studied are shown on both axes, so that each cell in the matrix shown represents the mutual information between the signals associated with the respective rotation axes orientations.

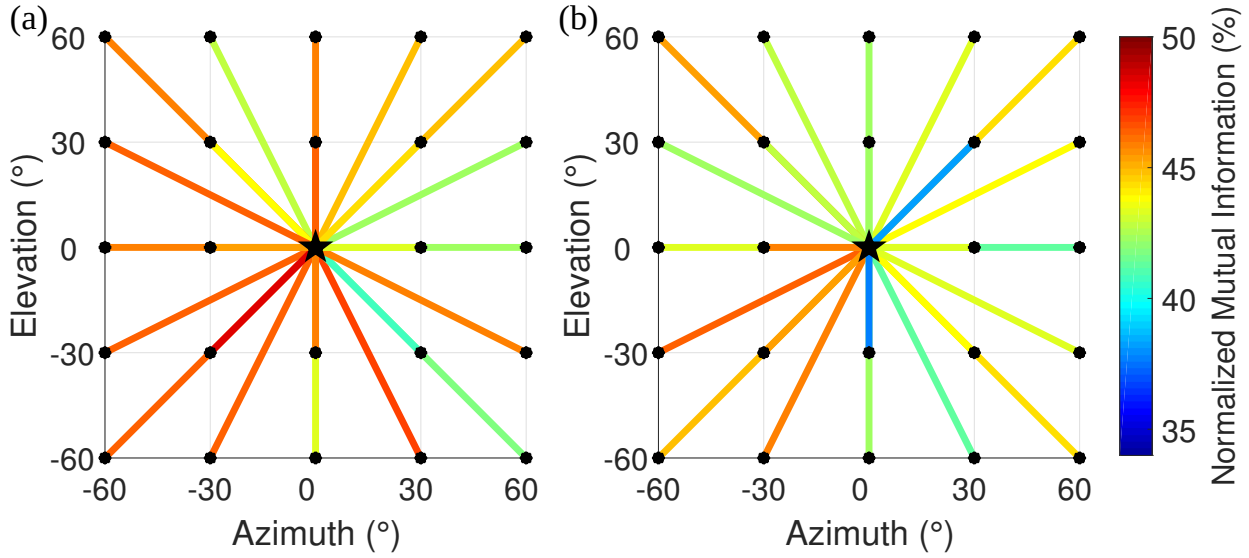

Figure 3.16: Example of normalized mutual information between the pulse envelopes of a reference rotation axis and all other rotation axes in sample: a) for pulses with a single sine carrier. b) for pulses with a frequency-modulated carrier. In each graph, the star marks the reference rotation axis and the dots mark the rotation axes that were used for comparison. The color value of the lines between the reference and the other rotation axes denotes the normalized mutual information between the pulse envelopes between these two orientations of the rotation axis.

Within the analyzed data set, there was no obvious dependence of the normalized mutual information between two pulse envelopes on how similar the orientations of the respective rotation axes were (Fig. 3.16), i.e., within the resolution of the selected sampling grid for the directional space, there was no indication that the normalized mutual information decreased with increasing distance between the orientations of the rotation axes.

3.6 Discussion

The presence of large, conspicuous pinna motions in hipposiderid bats has been known for almost 60 years [95, 99], but the exact nature of these motions and their variability (e.g., discrete subgroups, continuous variation) has received comparatively little attention so far. The work presented here has built on recent evidence that the pinna motions in hipposiderid bats fall into two distinct categories, rigid rotations and deformations [127] and has tried to examine what the pinna motions in the "rigid rotation" category look like. For the analyzed data set, it appears that no further discrete categories existed inside the rigid rotations. Instead, the rigid pinna rotations had a large amount of continuous variability in the orientations of the rotation axes as well as the angular distances over which they were rotated.

The numerical experiments with the simulated pinna rotation data make it unlikely that the observed variability in the results is due to large estimation errors. Even when an average error of 0.2 mm, about twice as large as the estimated stereo reconstruction error, was added to the landmark positions of the simulated pinna, the resulting errors in angle estimates were less than 4°or about one tenth of the observed variability in the data from the bat pinnae.

The pairwise comparisons of pulse envelopes associated with different rotation axes have shown that the normalized mutual information values always stayed below 50%. This means

that even moderate changes in the orientation of the pinna rotation (i.e., 30°or less) could result in substantial amounts of new sensory information since more than half of the variability of a signal that is received for a given pinna rotation axis is not explained by the signal associated with any of the other orientations.

Previous work has demonstrated that combining time-variant signals that had low mutual information due to different pinna shape configuration did enhance performance in sonar sensing tasks related to direction finding [69]. Different rotations of a constant shape could have a similar impact. It has already been demonstrated that a single rigid pinna rotation can provide information about target location, e.g., by changing the interaural intensity disparities over time [122] or using different harmonics in the pulse [120]. In the present work, the combined effects of changing carrier frequency and rigid rotation have been captured by use of the fm-signals, whereas the results for the cf-signals only capture the effect of pinna rotation at a fixed frequency. Although the difference in the normalized mutual information results for the cf- and fm-signal was found to be statistically highly significant, it remains to be investigated if there could be a functional difference between these signals given the large overlap between the value ranges.

We have used a biomimetic pinna prototype that was an approximation of an actual hipposiderid pinna in terms of geometry and size-to-frequency ratio. The finding that the mutual information between the signals of different rigid rotations was in a similar (low) range for the tested cf- and fm-signals suggests that a precise relationship between pinna size and wavelength is not a necessary condition for the effects we have encountered here.

The pinna motion data was obtained in behavioral experiments that contained some natural elements such as surveying the environment from a perch [87] or the use of an artificial moth to mimic a fluttering insect prey. Such experimental conditions have been previously shown to elicit pinna motions that coincide with the biosonar pulse trains [126, 128]. However,

it is unlikely that these elements were sufficient to recreate a complete natural context for the animals. Hence, the present results can only serve as an indication of capabilities that the animals have, but not as experimental proof that the animals use these capabilities. If the bats do use variable pinna rotations as part of their natural biosonar behaviors, it remains to be determined how this variability is integrated into the respective biosonar sensing paradigm. In the simplest case, the variability in the pinna rotations could be random and the bats would benefit from the additional sensory information that is collected across a random set of views. A more elaborate and potentially more powerful way to exploit the variability of the pinna rotations would be to control the parameters of the pinna rotations based on information from previous echoes or the context. Future research will be needed to explore these hypotheses. Finally, it should be investigated if the non-rigid pinna motions can be as variable as the rigid rotations and if so what the nature of this variability (e.g., discrete subgroups, continuous variation) is. This will, however, require the development of effective descriptions for the deformations that could take the place of the simple axis-angle representations of the rigid rotations used here.

3.7 Acknowledgements

The authors would like to thank Ruihao Wang for help with the realization of the biomimetic rotating pinna. This research was supported by the National Science Foundation (Award Id 1362886, data analysis), the Naval Engineering Education Center (contract number N00174-16-C-0026, biomimetic pinna), and the National Natural Science Foundation of China (grant numbers 11074149, 11574183, animal research).

Chapter 4

Variability in the non-rigid pinna motions

4.1 Introduction

The work described above has already shown that the rigid pinna motions exhibit a continuous variation that cover 180 degrees in azimuth and in elevation. However, it still remains unclear if further subdivisions of non-rigid pinna motions (e.g., different deformation patterns for non-rigid pinna motions) can be made. To characterize the variability in the non-rigid pinna motions, landmarks on the pinnae of Pratt's leaf-nosed bata (*Hipposideros pratti*) have been tracked using stereo vision. The resulting landmark trajectory data (positions as a function of time) was clustered to facilitate the detection of patterns.

4.2 Methods

Non-rigid pinna motions have been studied based on a pilot data set consisting of 10 video sequences in a group of Pratt's leaf-nosed bats (*Hipposideros pratti*, [18]) that contained three experimental subjects, one female and two males (Table 4.1). These sequences were selected from the videos recorded for rigid pinna motion analysis in Chapter 3 because

bats did rigid and non-rigid pinna motions randomly during the recording time. These sequences were selected for their quality and the presence of the non-rigid pinna motions. For each of the selected video sequences, the three-dimension landmark coordinates were reconstructed using stereo triangulation [5] with the two-dimensional image coordinates picked semi-automatically [38].

Table 4.1: Summary of the non-rigid pinna motion data set acquired from three different individuals of Pratt's leaf-nosed bat (*Hipposideros pratti*).

bat	No. 1	No. 2	No. 3	total
sex	female	male	male	
N sequences	3	2	5	10

In order to verify that each selected pinna motion sequence was non-rigid with large deformation (Fig. 4.1), the maximum difference between the maximum distance and the minimum distance of each set of pairwise landmarks on the pinna rim was used as a criterion [127]. For each pair of landmarks, one landmark was located on the anterior rim and another landmark was located on the posterior rim of the pinna. For each set of pairwise landmarks, the Euclidean distance was computed as a function of time over the entire duration of the pinna motion sequence. The difference between the maximum distance and the minimum distance over all time steps was computed and put into the maximum difference matrix, which represented the maximum deformation for that pairwise landmarks. If the largest value in this matrix was grater than or equal to 3 mm, the pinna motion was classified as non-rigid.

To characterize the variability in the non-rigid pinna motions, a spectral clustering algorithm was used to reveal the structure of coherent surface patches. The spectral clustering algorithm [81] is more powerful than the K-means algorithm (Fig. 4.2, [33]), and the difference between the K-means and the spectral clustering algorithms is that the spectral clustering

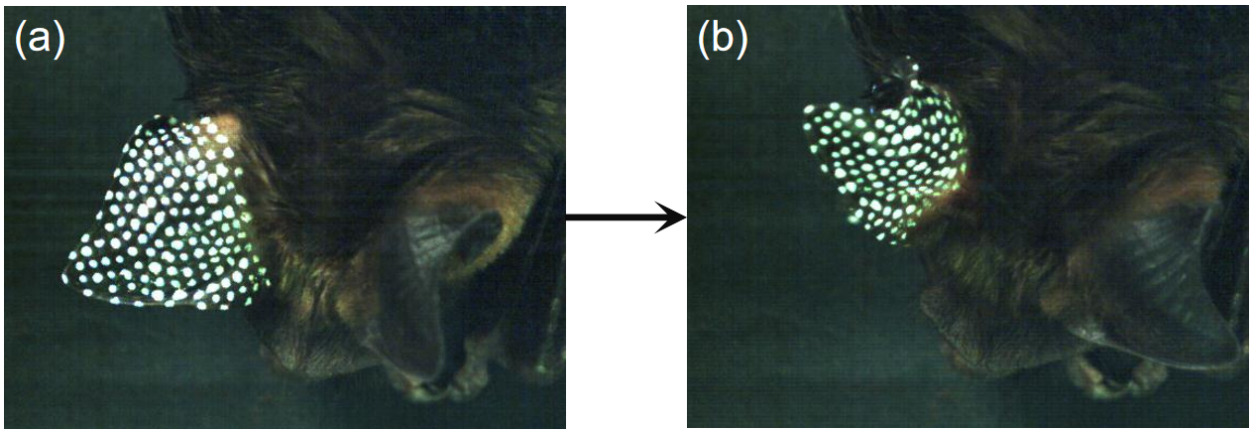

Figure 4.1: Example of a non-rigid motion sequence of a pinna (with landmarks on the surface): a) pinna geometry prior to the start of the non-rigid motion, b) pinna geometry after the non-rigid motion is complete.

uses K-means to cluster the object sets but the spectral clustering has three more steps before using K-means. The spectral clustering algorithm has four steps in total. The first step is to build a similarity matrix for representing object sets. The second step is to calculate the Laplacian matrix. The third step is to calculate the eigenvectors of the Laplacian matrix. The fourth step is to use K-means algorithm with first k eigenvectors to cluster the object sets. In the non-rigid pinna motion situation, the object sets are the landmarks on the pinna surface, and the displacement vectors of each landmark along motion time were inserted as one row of the input similarity matrix.

In order to show the differences between different clusters, the Euclidean distance [1] between every two landmark points during the motion pattern was computed for each non-rigid pinna motion sequence. The Euclidean distance per time step is defined by

$$\Delta_{ij} = \frac{1}{n_s}\sqrt{\sum_{k=1}^{n_s}(x_{ik}-x_{jk})^2+(y_{ik}-y_{jk})^2+(z_{ik}-z_{jk})^2}$$

where Δ_{ij} is the Euclidean distance per time step [$^{mm}/_{step}$], i is the reference landmark, j is the comparison landmark, n_s is the number of time steps which is equal to (n_f - 1), n_f is

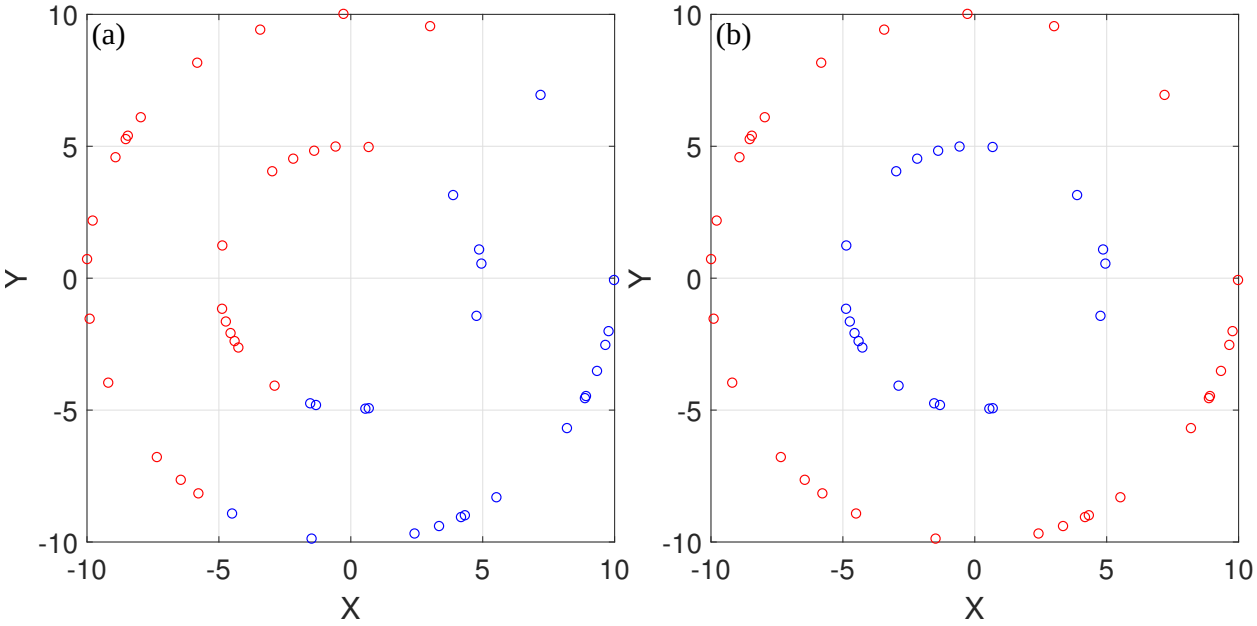

Figure 4.2: Comparison between K-means and spectral clustering algorithms using test data: a) for test data using K-means algorithm, b) for test data using spectral clustering algorithm.

the number of frames, x, y, z are the coordinates of the displacement vector of the landmark at each time step.

To learn the differences between different numbers of clusters, the normalized mean value of Euclidean distances within clusters for each number of clusters was computed. For each pair of two landmarks both located within the same cluster, the Euclidean distance between them was computed. Then, the mean value of all the computed Euclidean distances within clusters for each number of clusters was calculated. For each of the non-rigid pinna motions, the mean values of Euclidean distances within clusters for different numbers of clusters were normalized and compared.

4.3 Results

For all of the 10 analyzed pinna motion sequences in the pilot data set, the maximum difference in the pairwise distances between all pairs of the landmark points on the anterior and posterior rim exceeded 3 mm (Fig. 4.3). This establishes that there were big deformations of the pinna shapes during the pinna motions and hence these selected pinna motion sequences are non-rigid.

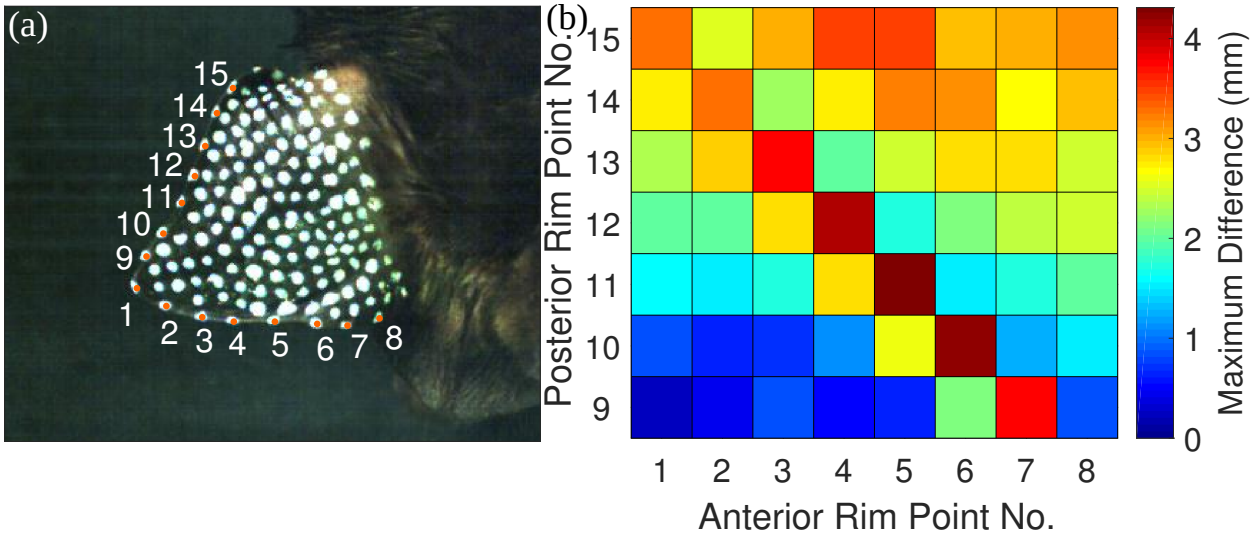

Figure 4.3: Verification of non-rigid motions: a) landmarks on the anterior rim and posterior rim of the pinna that were used to verify the non-rigid motion, b) matrix of maximum changes in the pairwise distances across all time steps between the pinna rim points shown in (a).

Different numbers of clusters were tested using spectral clustering algorithm and the normalized mean values of Euclidean distances within clusters were used to compare the differences between different numbers of clusters (Fig. 4.4). For 10 non-rigid pinna motion sequences, when the number of clusters is increased, the difference of the normalized mean values of Euclidean distances between the adjacent numbers of clusters becomes smaller. This indicates that the efficient clustering has a limited range of number of clusters.

There were similarities as well as pronounced differences among the pilot non-rigid pinna

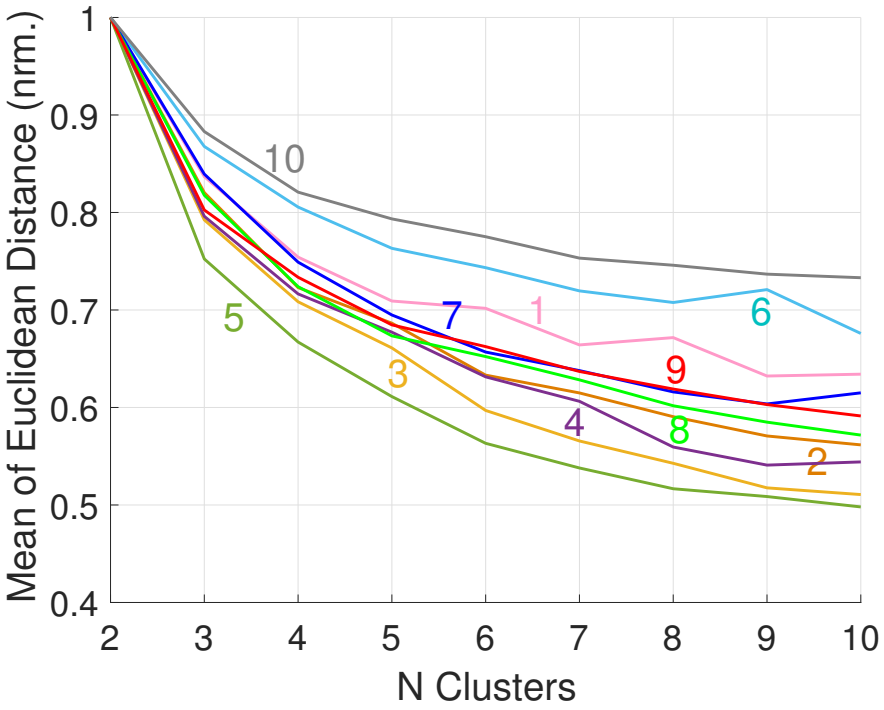

Figure 4.4: Normalized mean values of Euclidean distances within clusters of 10 non-rigid pinna motion sequences.

motion sequences. When the number of clusters is equal to or less than 5, the distributions of the clusters of the landmarks on the pinna surface of different samples are similar (Fig. 4.5). When the number of clusters is equal to or greater than 6, the distributions of the clusters of the landmarks on the pinna surface change a lot (Fig. 4.6). For example, when the number of cluster is 6, there are two different types of distributions of the clusters of the landmarks on the pinna surface based on the boundary lines between the clusters. For some non-rigid pinna motions, there is a closed boundary in the middle. However, other non-rigid pinna motions do not have such a closed boundary. This indicates that there are at least two subgroups within non-rigid pinna motions.

The Euclidean distances within clusters are smaller than that between clusters no matter how many clusters there are (Fig. 4.7, 4.8). This indicates that there are some differences between clusters and the clustering results are meaningful.

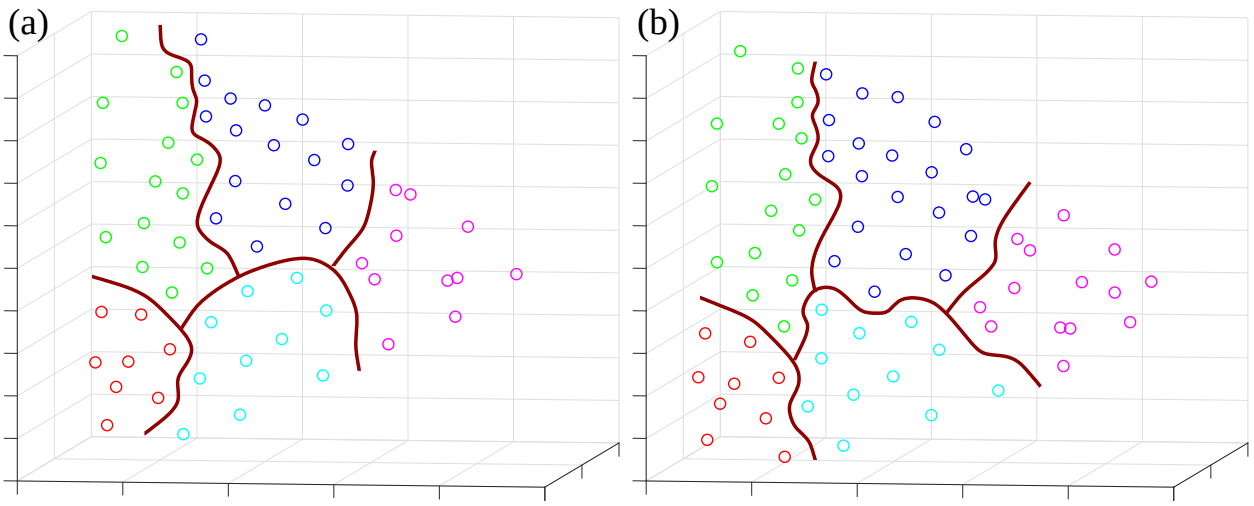

Figure 4.5: Example of spectral clustering results of non-rigid pinna motions with number of clusters equaling 5: a) for pinna motion sample 1, b) for pinna motion sample 2. Dots are the points marked on the pinna. Different colors denote different clusters. The maroon lines are the boundaries between the clusters. (a) and (b) are similar.

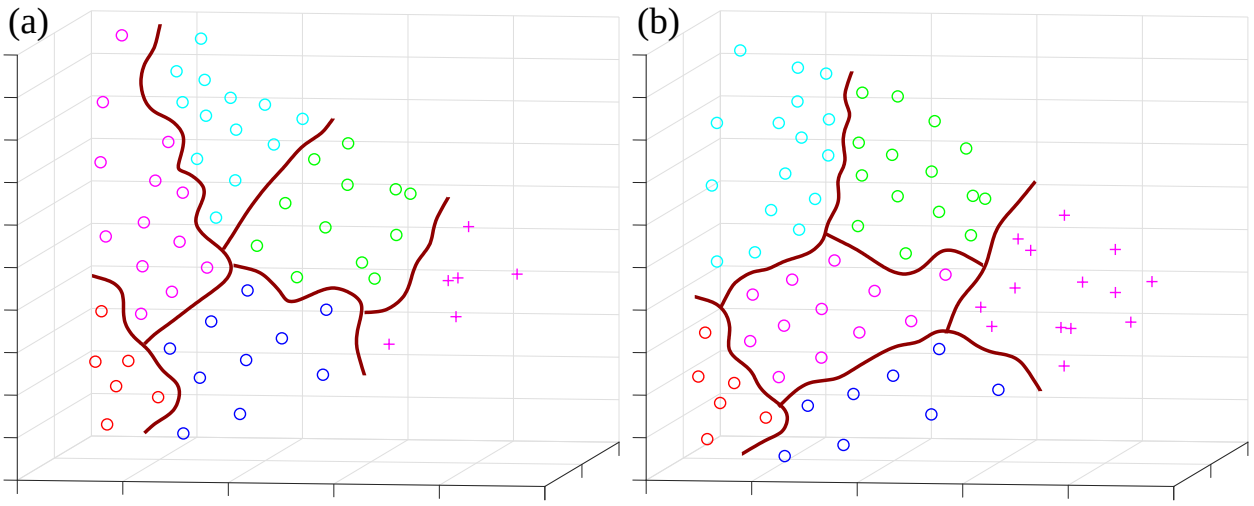

Figure 4.6: Example of spectral clustering results of non-rigid pinna motions with number of clusters equaling 6: a) for pinna motion sample 1, b) for pinna motion sample 2. Dots are the points marked on the pinna. Different colors denote different clusters. The maroon lines are the boundaries between the clusters. (a) and (b) are different.

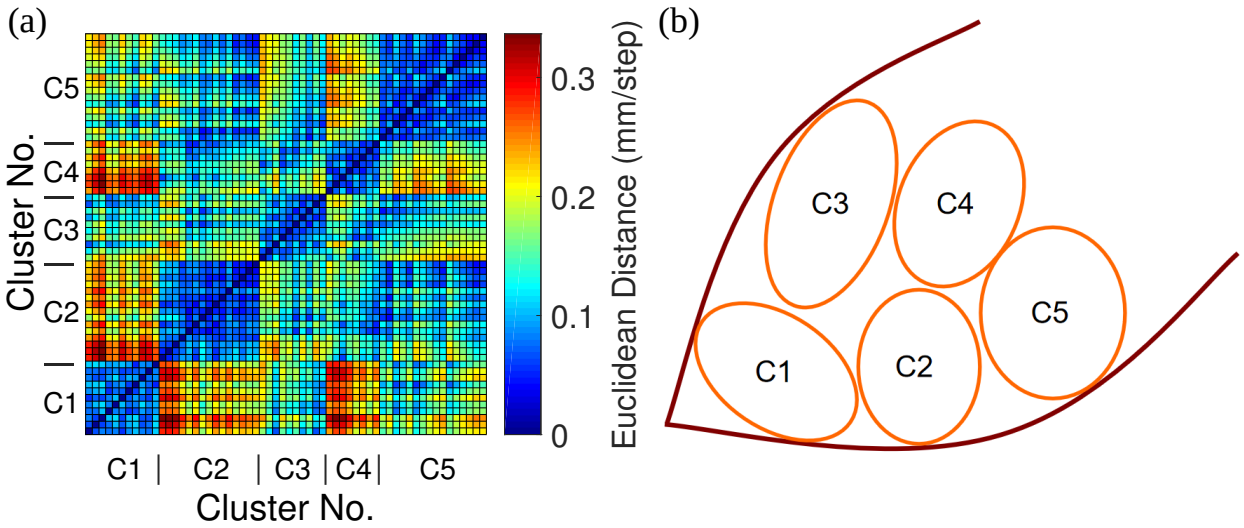

Figure 4.7: Example of matrix of Euclidean distances between clusters for non-rigid pinna motion with number of clusters equaling 5: a) matrix of Euclidean distance between clusters, b) distribution of different clusters on the pinna.

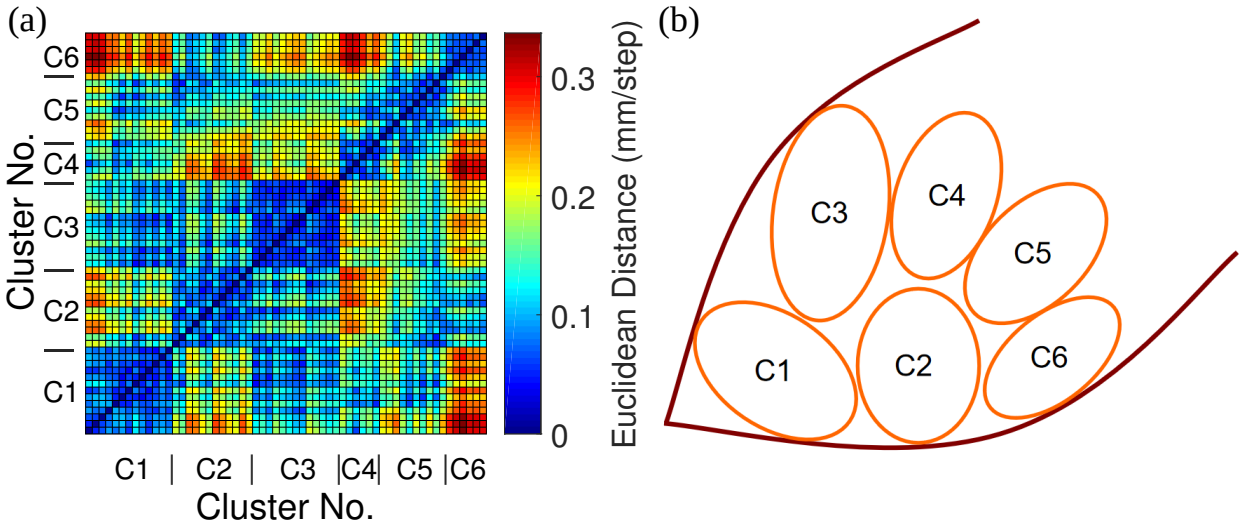

Figure 4.8: Example of matrix of Euclidean distances between clusters for non-rigid pinna motion with number of clusters equaling 6: a) matrix of Euclidean distance between clusters, b) distribution of different clusters on the pinna.

4.4 Discussion

The work presented in this chapter has investigated the potential variability within non-rigid pinna motions using a pilot data set consisting of 10 non-rigid motion sequences. In order to investigate how distinct the non-rigid motions are, different numbers of clusters were used to figure out the distribution of the clusters of the landmarks on the pinna surface. According to the boundary lines between the clusters of points on the pinna surface, it appears qualitatively as if there were at least two different motion patterns.

In order to figure out the exact number of subgroups within the non-rigid pinna motions, more future work needs to be done. More non-rigid pinna motion sequences need to be analyzed because only 10 non-rigid pinna motion sequences are not enough to reach a definitive conclusions. A suitable method needs to be worked out to determine the number of clusters because different numbers of clusters may cause different results. Besides, the differences between different subgroups (e.g., orientation, magnitude or deformation) need to be learned.

Chapter 5

Conclusions

5.1 Summary of research achievements

Bats have a recognized potential as model systems for developing sensing technologies. As mentioned in Chapter 2, bat's pinna, which can rotate and deform, works as a dynamic receiving baffle to enhance the hearing capacity. A dynamic sonar receiver inspired by bat's pinna has been designed while the full dynamic range of the pinna still has not been achieved. Hence, the primary purpose of this thesis is to investigate the variability in the rigid pinna motions and in the non-rigid pinna motions of bats in order to improve the dynamic sonar receiver. The major achievements in this thesis are as follows:

1. In order to characterize the variability in rigid pinna motions, 100 rigid motion sequences of Pratt's leaf-nosed bats were collected. Axis-angle representation was used to represent the rigid motions. It has been shown that the rigid pinna motions are highly variable with rotation axes covering 180 degrees in azimuth and in elevation, and the rigid pinna motions exhibit a continuous variation without any discernible groups.

2. To investigate the acoustic impact of the variability in the rigid pinna motions, a biomimetic rotating pinna was designed and implemented. The normalized mutual information between the pulse envelopes collected with different pinna rotation axes

showed that different rotation axes provide new sensory information and even small changes in axis can provide greater than 50% of new information.

3. In order to learn the variability in non-rigid pinna motions, a pilot data set consisting of 10 non-rigid pinna motion sequences of Pratt's leaf-nosed bats were collected. Distribution of the clusters of the points marked on the pinna surface generated by spectral clustering algorithm was used to represent the non-rigid pinna motions. It has been shown that the non-rigid pinna motions have at least two subgroups according to the boundary lines between the clusters of points on the pinna surface. Within each subgroup, it has the same large-scale patterns with some small-scale differences.

5.2 Significance

There are three principle possibilities for the variability in the pinna motions of bats. There could be (i) no variability at all, (ii) discrete subgroups, and (iii) continuous variation. Different possibilities of the variability could present different behaviours of bats. No variability of the pinna motions could either mean that the bats cannot make any changes to the pinna motions or mean that the bats can control their pinna movements precisely but the existed pinna motion is the best one. Discrete groups of the pinna motions could either mean that one group matches one task that the bats want to do or mean that they can only do several different ways of pinna motions (e.g. rotating or bending). Continuous variation of the pinna motions could either mean that the bats cannot control their pinna movements or mean that they could really benefit from having every ear motion going differently.

Previous work has shown that there are about 20 muscles on the bat's pinna and the pinna movements are enabled by specialized muscular actuation mechanisms [99, 100]. Hence, the bats could control their pinna movements by themselves. Besides, the evidence for

the existence of the variation has been found. There are two discrete categories of the pinna motions: rigid motion, which changes only the orientation of the pinna, and non-rigid motion, which changes also the shape of the pinna [127]. In addition to the variability in the pinna motions, there are variability within rigid pinna motions and within non-rigid pinna motions. The work presented in this thesis has found that the rigid pinna motions exhibit a continuous variation and are highly variable, and the non-rigid pinna motions have at least two subgroups.

Besides the variability, pinna motions are functionally relevant to the behaviours of bats. For the rigid pinna motions, the work presented in this thesis has found that different rotation axes have different acoustic influences and they provide new sensory information. Hence, the bats could gain from the rigid pinna motions. However, what the new information the rigid pinna motions encode and how the bats use these new information need to be further investigated. For the non-rigid pinna motions, the information-theoretic analysis shows that it is useful, e.g., increasing the number of resolvable directions of sound incidence and improving the accuracy of direction finding [69]. In addition, it has been shown that the non-rigid pinna motion changes the geometry of the beampattern and provides additional degrees of freedom for encoding relevant information into the received signals [22, 64, 86].

5.3 Suggestions for future work

The suggestions for future work can be concluded as follows:

1. Mutual information shows that different orientations of rigid pinna motions have acoustic impacts and can add new information to the signals received by the pinna. However, it is still not clear what the new information is about and what it encodes. Therefore,

the new information added by the rigid pinna motions and how the bats use this new information need to be further investigated.

2. The variability of the non-rigid pinna motions needs to be further characterized:

   (a) In this thesis, the variability of the non-rigid pinna motions was only studied based on a pilot data set consisting of 10 non-rigid pinna motion sequences. This pilot data set is too small to arrive at definitive conclusions. Therefore, more non-rigid pinna motion sequences need to be added.

   (b) Currently, the exact number of subgroups within the non-rigid pinna motions is still not known because the non-rigid pinna motions are higher dimensional and more complex than the rigid pinna motions and it is hard to describe them. Therefore, a low dimensional descriptor has to be addressed using possible nonlinear reduction methods such as isomap to represent the non-rigid pinna motions.

   (c) The work in this thesis has suggested that there are at least two subgroups in the non-rigid pinna motions. They could differ in the orientation, the magnitude or the deformation and it is still not known. Thus, the differences between different subgroups need to be learned.

3. The current study used a small rotating propeller to expose bats to novelty during the experiments. However, the bats were not asked to discriminate something or find a prey and it is unclear how pinna movements are correlated with behaviours of bats. Hence, more behaviour contexts need to be added to the experiments in order to integrate the variability of the pinna motions with the behaviors of the bats:

   (a) When the bats are placed on the platform, they need to be given some tasks. The pinna motion patterns with different tasks need to be observed.

(b) When the bats fly freely, they navigate through foliage, catch moths, and approach water surface for drinking accompanying with highly dynamic pinna movements. The pinna motion patterns during different behaviours of bats need to be observed.

4. Bat biosonar consists of one emitter (nose) and two receivers (left and right ears), and the motions of all these structures are highly variable. Therefore, the variability between them needs to be investigated:

   (a) It has already been shown that the left pinna and the right pinna moves oppositely for the rigid pinna motions. However, the correlation between the left pinna motions and the right pinna motions is still unknown. Therefore, the variability of the motions between left and right pinna needs to be investigated.

   (b) Similar to the situation in the dynamic pinna, bats have opening motions and closing motions for their noseleaves. However, the variability in the opening motions and in the closing motions of noseleaves needs to be further studied. Besides, the correlation between the noseleaf motions and the pinna motions needs to be investigated.

5. The acoustic impact of the rigid pinna motion variability was studied in the lab by a biomimetic reproduction of the bat's pinna and it has not been tested in the real environments at all. Therefore, the acoustic impact of the pinna motion variability using a sonar head needs to be tested in the nature.

Bibliography

[1] Anton, H. and Rorres, C. (2013). *Elementary Linear Algebra*. John Wiley & Sons.

[2] Arita, H. T. (1990). Noseleaf morphology and ecological correlates in phyllostomid bats. *Journal of Mammalogy*, 71(1):36–47.

[3] Atchison, D. A., Smith, G., and Smith, G. (2000). Optics of the human eye.

[4] Bell, G. P. and Fenton, M. B. (1984). The use of doppler-shifted echoes as a flutter detection and clutter rejection system: the echolocation and feeding behavior of hipposideros ruber (chiroptera: Hipposideridae). *Behavioral Ecology and Sociobiology*, 15(2):109–114.

[5] Bouguet, J.-Y. and Perona, P. (1998). Camera calibration from points and lines in dual-space geometry. In *Proc. 5th European Conf. on Computer Vision*, pages 2–6.

[6] Bruns, V. and Schmieszek, E. (1980). Cochlear innervation in the greater horseshoe bat: demonstration of an acoustic fovea. *Hearing research*, 3(1):27–43.

[7] Cafarelli, A., Miloro, P., Verbeni, A., Carbone, M., and Menciassi, A. (2016). Speed of sound in rubber-based materials for ultrasonic phantoms. *Journal of ultrasound*, 19(4):251–256.

[8] Caspers, P., Fu, Y., and Mueller, R. (2015). A design for a biomimetic dynamic sonar head. *The Journal of the Acoustical Society of America*, 137(4):2334–2334.

[9] Caspers, P. and Müller, R. (2018). A design for a dynamic biomimetic sonarhead inspired by horseshoe bats. *Bioinspiration & biomimetics*, 13(4):046011.

[10] Cleveland, W. S. and Devlin, S. J. (1988). Locally weighted regression: an approach to regression analysis by local fitting. *Journal of the American statistical association*, 83(403):596–610.

[11] Cover, T. M. and Thomas, J. A. (2012). *Elements of information theory*. John Wiley & Sons.

[12] D'Amico, A. and Pittenger, R. (2009). A brief history of active sonar. Technical report, SPACE AND NAVAL WARFARE SYSTEMS CENTER SAN DIEGO CA.

[13] Dickson, J. G. (1992). *The wild turkey: biology and management*. Stackpole Books.

[14] Fazli, S. and Kleeman, L. (2004). A real time advanced sonar ring with simultaneous firing. In *2004 IEEE/RSJ International Conference on Intelligent Robots and Systems (IROS)(IEEE Cat. No. 04CH37566)*, volume 2, pages 1872–1877. IEEE.

[15] Fazli, S. and Kleeman, L. (2005). Wall following and obstacle avoidance results from a multi-dsp sonar ring on a mobile robot. In *IEEE International Conference Mechatronics and Automation, 2005*, volume 1, pages 432–437. IEEE.

[16] Feng, L., Gao, L., Lu, H., and Müller, R. (2012). Noseleaf dynamics during pulse emission in horseshoe bats. *PloS one*, 7(5):e34685.

[17] Fenton, M. B. (2013). Evolution of echolocation. In Adams, R. A. and Pedersen, S. C., editors, *Bat evolution, ecology, and conservation*, pages 47–70. Springer.

[18] Francis, C. and Bates, P. (2008). Hipposideros pratti. In *The IUCN Red List of Threatened Species*, page e.T10155A3176469. 2015 International Union for Conservation of Nature and Natural Resources.

[19] Fu, Y., Caspers, P., and Müller, R. (2016). A dynamic ultrasonic emitter inspired by horseshoe bat noseleaves. *Bioinspiration & biomimetics*, 11(3):036007.

[20] Fu, Z., Dai, X., Xu, N., Shi, Q., Li, G., Li, B., Li, J., Li, J., Tang, J., Jen, P. H., and Chen, Q. (2015). Sexual dimorphism in echolocation pulse parameters of the cf-fm bat, hipposideros pratti. *Zoological Studies*, 54(1):44.

[21] Gageik, N., Müller, T., and Montenegro, S. (2012). Obstacle detection and collision avoidance using ultrasonic distance sensors for an autonomous quadrocopter. *University of Wurzburg, Aerospace information Technologhy (germany) Wurzburg*, pages 3–23.

[22] Gao, L., Balakrishnan, S., He, W., Yan, Z., and Müller, R. (2011). Ear deformations give bats a physical mechanism for fast adaptation of ultrasonic beam patterns. *Physical review letters*, 107(21):214301.

[23] Geva-Sagiv, M., Las, L., Yovel, Y., and Ulanovsky, N. (2015). Spatial cognition in bats and rats: from sensory acquisition to multiscale maps and navigation. *Nature Reviews Neuroscience*, 16(2):94.

[24] Göbbel, L. (2002). Morphology of the external nose in hipposideros diadema and lavia frons with comments on its diversity and evolution among leaf-nosed microchiroptera. *Cells Tissues Organs*, 170(1):39–60.

[25] Gorlinsky, I. A. and Konstantinov, A. I. (1978). Auditory localization of ultrasonic source by rhinolophus ferrumequinum. In *Proc. International Bat Research Conference, Nairobi.*, pages 145–153.

[26] Gorski, K. M., Hivon, E., Banday, A. J., Wandelt, B. D., Hansen, F. K., Reinecke, M., and Bartelmann, M. (2005). Healpix: a framework for high-resolution discretization and fast analysis of data distributed on the sphere. *The Astrophysical Journal*, 622(2):759.

[27] Griffin, D. R., Dunning, D. C., Cahlander, D. A., and Webster, F. A. (1962). Correlated orientation sounds and ear movements of horseshoe bats. *Nature*, 196(4860):1185.

[28] Gudra, T., Furmankiewicz, J., and Herman, K. (2011). Bats sonar calls and its application in sonar systems. In Prof. Kolev, N., editor, *Sonar Systems*, pages 209–234. IntechOpen.

[29] Gupta, A. K., Webster, D., and Müller, R. (2015a). Interplay of lancet furrows and shape change in the horseshoe bat noseleaf. *The Journal of the Acoustical Society of America*, 138(5):3188–3194.

[30] Gupta, N., Makkar, J. S., and Pandey, P. (2015b). Obstacle detection and collision avoidance using ultrasonic sensors for rc multirotors. In *2015 International Conference on Signal Processing and Communication (ICSC)*, pages 419–423. IEEE.

[31] Gustafson, Y. and Schnitzler, H.-U. (1979). Echolocation and obstacle avoidance in the hipposiderid batasellia tridens. *Journal of comparative physiology*, 131(2):161–167.

[32] Habersetzer, J., Schuller, G., and Neuweiler, G. (1984). Foraging behavior and doppler shift compensation in echolocating hipposiderid bats, hipposideros bicolor andhipposideros speoris. *Journal of Comparative Physiology A*, 155(4):559–567.

[33] Hartigan, J. A. and Wong, M. A. (1979). Algorithm as 136: A k-means clustering algorithm. *Journal of the Royal Statistical Society. Series C (Applied Statistics)*, 28(1):100–108.

[34] Hartley, D. J. and Suthers, R. A. (1987). The sound emission pattern and the acoustical role of the noseleaf in the echolocating bat, c arolliaperspicillata. *The Journal of the Acoustical Society of America*, 82(6):1892–1900.

[35] Hartridge, H. (1945). Acoustic control in the flight of bats. *Nature*, 156(3965):490.

[36] He, W., Pedersen, S. C., Gupta, A. K., Simmons, J. A., and Müller, R. (2015).

Lancet dynamics in greater horseshoe bats, rhinolophus ferrumequinum. *PLoS One*, 10(4):e0121700.

[37] Heard, W. B. (2006). Rotations specified by axis and angle. In *Rigid body mechanics*, pages 8–12. Wiley Online Library.

[38] Hedrick, T. L. (2008). Software techniques for two-and three-dimensional kinematic measurements of biological and biomimetic systems. *Bioinspiration & biomimetics*, 3(3):034001.

[39] Hill, J. E. and Smith, J. D. (1992). Bats: A natural history, reprint ed.

[40] Huihua, Z., Shuyi, Z., Mingxue, Z., and Jiang, Z. (2003). Correlations between call frequency and ear length in bats belonging to the families rhinolophidae and hipposideridae. *Journal of zoology*, 259(2):189–195.

[41] Jakobsen, L., Brinkløv, S., and Surlykke, A. (2013). Intensity and directionality of bat echolocation signals. *Frontiers in physiology*, 4:89.

[42] Jen, P. H.-S. (2010). Adaptive mechanisms underlying the bat biosonar behavior. *Frontiers in Biology*, 5(2):128–155.

[43] Jones, G. and Holderied, M. W. (2007). Bat echolocation calls: adaptation and convergent evolution. *Proceedings of the Royal Society B: Biological Sciences*, 274(1612):905–912.

[44] Jones, G. and Rayner, J. M. (1989). Foraging behavior and echolocation of wild horseshoe bats rhinolophus ferrumequinum and r. hipposideros (chiroptera, rhinolophidae). *Behavioral Ecology and Sociobiology*, 25(3):183–191.

[45] Jones, G. and Teeling, E. C. (2006). The evolution of echolocation in bats. *Trends in Ecology & Evolution*, 21(3):149–156.

[46] Jordan Price, J., P. Johnson, K., and H. Clayton, D. (2004). The evolution of echolocation in swiftlets. *Journal of Avian Biology*, 35(2):135–143.

[47] Knudsen, E. I. (1981). The hearing of the barn owl. *Scientific American*, 245(6):113–125.

[48] Kober, R. and Schnitzler, H.-U. (1990). Information in sonar echoes of fluttering insects available for echolocating bats. *The Journal of the Acoustical Society of America*, 87(2):882–896.

[49] Konishi, M. and Knudsen, E. I. (1979). The oilbird: hearing and echolocation. *Science*, 204(4391):425–427.

[50] Koopman, K. F. (1994). Chiroptera: systematics. *Handbook of zoology*, pages 1–217.

[51] Kössl, M. (1994). Otoacoustic emissions from the cochlea of the 'constant frequency'bats, pteronotus parnellii and rhinolophus rouxi. *Hearing research*, 72(1-2):59–72.

[52] Kraskov, A., Stögbauer, H., and Grassberger, P. (2004). Estimating mutual information. *Physical review E*, 69(6):066138.

[53] Kuc, R. (1993). Three-dimensional tracking using qualitative bionic sonar. *Robotics and Autonomous Systems*, 11(3-4):213–219.

[54] Kuc, R. (1996). Biologically motivated adaptive sonar system. *The Journal of the Acoustical Society of America*, 100(3):1849–1854.

[55] Kuc, R. (1997). Biomimetic sonar recognizes objects using binaural information. *The Journal of the Acoustical Society of America*, 102(2):689–696.

[56] Kuhn, B. and Vater, M. (1995). The arrangements of f-actin, tubulin and fodrin in the organ of corti of the horseshoe bat (rhinolophus rouxi) and the gerbil (meriones unguiculatus). *Hearing research*, 84(1-2):139–156.

[57] Ladegaard, M., Jensen, F. H., de Freitas, M., da Silva, V. M. F., and Madsen, P. T. (2015). Amazon river dolphins (inia geoffrensis) use a high-frequency short-range biosonar. *Journal of Experimental Biology*, 218(19):3091–3101.

[58] Lizier, J. T. (2014). Jidt: An information-theoretic toolkit for studying the dynamics of complex systems. *Frontiers in Robotics and AI*, 1:11.

[59] Ma, J. and Müller, R. (2011). A method for characterizing the biodiversity in bat pinnae as a basis for engineering analysis. *Bioinspiration & biomimetics*, 6(2):026008.

[60] Madsen, P. T., Johnson, M., De Soto, N. A., Zimmer, W. M. X., and Tyack, P. (2005). Biosonar performance of foraging beaked whales (mesoplodon densirostris). *Journal of Experimental Biology*, 208(2):181–194.

[61] Mann, D. A., Hawkins, A. D., and Jech, J. M. (2008). Active and passive acoustics to locate and study fish. In *Fish bioacoustics*, pages 279–309. Springer.

[62] Marple, L. (1999). Computing the discrete-time" analytic" signal via fft. *IEEE Transactions on signal processing*, 47(9):2600–2603.

[63] Massey Jr, F. J. (1951). The kolmogorov-smirnov test for goodness of fit. *Journal of the American statistical Association*, 46(253):68–78.

[64] Meymand, S. Z., Pannala, M., and Müller, R. (2013). Characterization of the time-variant behavior of a biomimetic beamforming baffle. *The Journal of the Acoustical Society of America*, 133(2):1141–1150.

[65] Mogdans, J., Ostwald, J., and Schnitzler, H.-U. (1988). The role of pinna movement for the localization of vertical and horizontal wire obstacles in the greater horseshoe bat, *Rhinolopus ferrumequinum*. *The Journal of the Acoustical Society of America*, 84(5):1676–1679.

[66] Moulton, D. G. (1977). Minimum odorant concentrations detectable by the dog and their implications for olfactory receptor sensitivity. In *Chemical signals in vertebrates*, pages 455–464. Springer.

[67] Müller, R. (2015). Dynamics of biosonar systems in horseshoe bats. *The European Physical Journal Special Topics*, 224(17-18):3393–3406.

[68] Müller, R. (2017). Quantitative approaches to sensory information encoding by bat noseleaves and pinnae. *Canadian Journal of Zoology*, 96(2):79–86.

[69] Müller, R., Gupta, A. K., Zhu, H., Pannala, M., Gillani, U. S., Fu, Y., Caspers, P., and Buck, J. R. (2017). Dynamic substrate for the physical encoding of sensory information in bat biosonar. *Physical review letters*, 118(15):158102.

[70] Müller, R. and Hallam, J. (2004). Biomimetic smart antenna shapes for ultrasonic sensors in robots. In *Proc. of the 35th International Symposium on Robotics ISR*.

[71] Müller, R. and Kuc, R. (2007). Biosonar-inspired technology: goals, challenges and insights. *Bioinspiration & biomimetics*, 2(4):S146.

[72] Müller, R., Lu, H., and Buck, J. R. (2008). Sound-diffracting flap in the ear of a bat generates spatial information. *Physical review letters*, 100(10):108701.

[73] Muller, R., Meymand, S. Z., Pannala, M., Reddy, O. P. K., and Gao, L. (2011). Design of a bio-inspired smart ear prototype. In *ASME 2011 Conference on Smart Materials, Adaptive Structures and Intelligent Systems*, pages 681–690. American Society of Mechanical Engineers.

[74] Müller, R., Mubeezi-Magoola, A. J., Peremans, H., Hallam, J., Jones, S., Flint, J., Reynaerts, D., Bruyninckx, H., Lerch, R., and Streicher, A. (2002). Chiroptera-inspired

robotic cephaloid (circe): A next generation biomimetic sonar head. *The Journal of the Acoustical Society of America*, 112(5):2335–2335.

[75] Müller, R., Pannala, M., Reddy, O. P. K., and Meymand, S. Z. (2012). Design of a dynamic sensor inspired by bat ears. *Smart Materials and Structures*, 21(9):094025.

[76] Munin, R. L., Fischer, E., and Gonçalves, F. (2012). Food habits and dietary overlap in a phyllostomid bat assemblage in the pantanal of brazil. *Acta Chiropterologica*, 14(1):195–204.

[77] Neuweiler, G. (1984). Foraging, echolocation and audition in bats. *Naturwissenschaften*, 71(9):446–455.

[78] Neuweiler, G. (1989). Foraging ecology and audition in echolocating bats. *Trends in ecology & evolution*, 4(6):160–166.

[79] Neuweiler, G., Bruns, V., and Schuller, G. (1980). Ears adapted for the detection of motion, or how echolocating bats have exploited the capacities of the mammalian auditory system. *The Journal of the Acoustical Society of America*, 68(3):741–753.

[80] Neuweiler, G., Metzner, W., Heilmann, U., Rübsamen, R., Eckrich, M., and Costa, H. H. (1987). Foraging behaviour and echolocation in the rufous horseshoe bat (rhinolophus rouxi) of sri lanka. *Behavioral ecology and sociobiology*, 20(1):53–67.

[81] Ng, A. Y., Jordan, M. I., and Weiss, Y. (2002). On spectral clustering: Analysis and an algorithm. In *Advances in neural information processing systems*, pages 849–856.

[82] Nowak, R. M. and Walker, E. P. (1999). *Walker's Mammals of the World*, volume 1. JHU press.

[83] Obrist, M. K., Fenton, M. B., Eger, J. L., and Schlegel, P. A. (1993). What ears do for bats: a comparative study of pinna sound pressure transformation in chiroptera. *Journal of Experimental Biology*, 180(1):119–152.

[84] Öner, M. and Deveci Kocakoç, İ. (2017). Jmasm 49: A compilation of some popular goodness of fit tests for normal distribution: Their algorithms and matlab codes (matlab). *Journal of Modern Applied Statistical Methods*, 16(2):30.

[85] Ostwald, J., Schnitzler, H.-U., and Schuller, G. (1988). Target discrimination and target classification in echolocating bats. In *Animal sonar*, pages 413–434. Springer.

[86] Pannala, M., Meymand, S. Z., and Müller, R. (2013). Interplay of static and dynamic features in biomimetic smart ears. *Bioinspiration & biomimetics*, 8(2):026008.

[87] Pavey, C. R. and Burwell, C. J. (2000). Foraging ecology of three species of hipposiderid bats in tropical rainforest in north-east australia. *Wildlife Research*, 27(3):283–287.

[88] Pedersen, S. C. (1993). Cephalometric correlates of echolocation in the chiroptera. *Journal of Morphology*, 218(1):85–98.

[89] Peremans, H., Mueller, R., Carmena, J. M., and Hallam, J. C. (2000). Biomimetic platform to study perception in bats. In *Sensor Fusion and Decentralized Control in Robotic Systems III*, volume 4196, pages 168–179. International Society for Optics and Photonics.

[90] Peremans, H. and Reijniers, J. (2005). The circe head: a biomimetic sonar system. In *International Conference on Artificial Neural Networks*, pages 283–288. Springer.

[91] Peremans, H., Walker, A., and Hallam, J. C. T. (1998). 3d object localisation with a binaural sonarhead, inspirations from biology. In *Proceedings. 1998 IEEE International*

Conference on Robotics and Automation (Cat. No. 98CH36146), volume 4, pages 2795–2800. IEEE.

[92] Pratt, V. (1987). Direct least-squares fitting of algebraic surfaces. In *ACM SIGGRAPH computer graphics*, volume 21, pages 145–152. ACM.

[93] Pye, J. D. (1980). Echolocation signals and echoes in air. In *Animal sonar systems*, pages 309–353. Springer.

[94] Pye, J. D., Flinn, M., and Pye, A. (1962). Correlated orientation sounds and ear movements of horseshoe bats. *Nature*, 196(4860):1186.

[95] Pye, J. D. and Roberts, L. H. (1970). Ear movements in a hipposiderid bat. *Nature*, 225(5229):285.

[96] Quazi, A. (1981). An overview on the time delay estimate in active and passive systems for target localization. *IEEE Transactions on Acoustics, Speech, and Signal Processing*, 29(3):527–533.

[97] Rousseeuw, P. J. (1987). Silhouettes: a graphical aid to the interpretation and validation of cluster analysis. *Journal of computational and applied mathematics*, 20:53–65.

[98] Schillebeeckx, F., De Mey, F., Vanderelst, D., and Peremans, H. (2011). Biomimetic sonar: Binaural 3d localization using artificial bat pinnae. *The International Journal of Robotics Research*, 30(8):975–987.

[99] Schneider, H. (1961). Die ohrmuskulatur von asellia tridens geoffr.(hipposideridae) und myotis myotis borkh.(vespertilionidae)(chiroptera). [the ear musculature of asellia tridens geoff. (hipposideridae) and myotis myotis borkh. (vespertilionidae) (chiroptera)]. *Zool. Jb., Abt. Anat. u. Ontog.*, 79:93–122.

[100] Schneider, H. and Möhres, F. P. (1960). Die ohrbewegungen der hufeisennasenflederm€ause (chiroptera, rhinolophidae) und der mechanismus des bildh€orens. [the ear motions of horseshoe bats (chiroptera, rhinolophidae) and the mechanism of image hearing]. *Z. Vergl. Physiol.*, 44(1):1–40.

[101] Schnitzler, H.-U. and Denzinger, A. (2011). Auditory fovea and doppler shift compensation: adaptations for flutter detection in echolocating bats using cf-fm signals. *Journal of Comparative Physiology A*, 197(5):541–559.

[102] Schnitzler, H.-U. and Kalko, E. K. (2001). Echolocation by insect-eating bats. *Bioscience*, 51(7):557–569.

[103] Schnitzler, H.-U., Moss, C. F., and Denzinger, A. (2003). From spatial orientation to food acquisition in echolocating bats. *Trends in Ecology & Evolution*, 18(8):386–394.

[104] Schoon, G. A. A. (1997). *The performance of dogs in identifying humans by scent*. PhD thesis.

[105] Schuller, G. and Pollak, G. (1979). Disproportionate frequency representation in the inferior colliculus of doppler-compensating greater horseshoe bats: evidence for an acoustic fovea. *Journal of Comparative Physiology*, 132(1):47–54.

[106] Scott, D. W. (2009). Sturges' rule. *Wiley Interdisciplinary Reviews: Computational Statistics*, 1(3):303–306.

[107] Shannon, C. E. (1948). A mathematical theory of communication. *Bell system technical journal*, 27(3):379–423.

[108] Simmons, J. A. (1969). Acoustic radiation patterns for the echolocating bats chilonycteris rubiginosa and eptesicus fuscus. *The Journal of the Acoustical Society of America*, 46(4B):1054–1056.

[109] Simmons, J. A. and Stein, R. A. (1980). Acoustic imaging in bat sonar: echolocation signals and the evolution of echolocation. *Journal of Comparative Physiology*, 135(1):61–84.

[110] Simmons, N. B. (2005). Order chiroptera. In Wilson, D. E. and Reeder, D. M., editors, *Mammal species of the world: a taxonomic and geographic reference*, volume 1, pages 312–529. Johns Hopkins University Press.

[111] Speakman, J. R. (2001). The evolution of flight and echolocation in bats: another leap in the dark. *Mammal Review*, 31(2):111–130.

[112] Springer, M. S., Murphy, W. J., Eizirik, E., and O'Brien, S. J. (2003). Placental mammal diversification and the cretaceous–tertiary boundary. *Proceedings of the National Academy of Sciences*, 100(3):1056–1061.

[113] Springer, M. S., Teeling, E. C., Madsen, O., Stanhope, M. J., and de Jong, W. W. (2001). Integrated fossil and molecular data reconstruct bat echolocation. *Proceedings of the National Academy of Sciences*, 98(11):6241–6246.

[114] Strehl, A. and Ghosh, J. (2002). Cluster ensembles—a knowledge reuse framework for combining multiple partitions. *Journal of machine learning research*, 3(Dec):583–617.

[115] Sullivan, K., Conk, M., Eckman, E., Lunsford, S., Martin, C., Singh, A., Wang, Y., Sutlive, J., and Müller, R. (2019). Design and manufacturing of a miniature pneumatic actuator for a bat robot. *The Journal of the Acoustical Society of America*, 145(3):1741–1741.

[116] Taubin, G. (1991). Estimation of planar curves, surfaces, and nonplanar space curves defined by implicit equations with applications to edge and range image segmentation. *IEEE Transactions on Pattern Analysis & Machine Intelligence*, (11):1115–1138.

[117] Vanderelst, D., Jonas, R., and Herbert, P. (2012). The furrows of rhinolophidae revisited. *Journal of the Royal Society Interface*, 9(70):1100–1103.

[118] Vanderelst, D., Lee, Y.-F., Geipel, I., Kalko, E., and Peremans, H. (2013). The noseleaf of rhinolophus formosae focuses the frequency modulated (fm) component of the calls. *Frontiers in physiology*, 4:191.

[119] Vanderelst, D., Reijniers, J., Firzlaff, U., and Peremans, H. (2011a). Dominant glint based prey localization in horseshoe bats: a possible strategy for noise rejection. *PLoS computational biology*, 7(12):e1002268.

[120] Vanderelst, D., Reijniers, J., Steckel, J., and Peremans, H. (2011b). Information generated by the moving pinnae of rhinolophus rouxi: tuning of the morphology at different harmonics. *PloS one*, 6(6):e20627.

[121] von der Emde, G. and Schnitzler, H.-U. (1986). Fluttering target detection in hipposiderid bats. *Journal of Comparative Physiology A*, 159(6):765–772.

[122] Walker, V. A., Peremans, H., and Hallam, J. C. T. (1998). One tone, two ears, three dimensions: A robotic investigation of pinnae movements used by rhinolophid and hipposiderid bats. *The Journal of the Acoustical Society of America*, 104(1):569–579.

[123] Wall, M. E., Rechtsteiner, A., and Rocha, L. M. (2003). Singular value decomposition and principal component analysis. In *A practical approach to microarray data analysis*, pages 91–109. Springer.

[124] Whitley, D. (1994). A genetic algorithm tutorial. *Statistics and computing*, 4(2):65–85.

[125] Yang, L., Yu, A., and Müller, R. (2018). Design of a dynamic sonar emitter inspired by hipposiderid bats. *Bioinspiration & biomimetics*, 13(5):056003.

[126] Yin, X. and Müller, R. (2019). Fast-moving bat ears create informative doppler shifts. *Proceedings of the National Academy of Sciences*, 116(25):12270–12274.

[127] Yin, X., Qiu, P., Yang, L., and Müller, R. (2017). Horseshoe bats and old world leaf-nosed bats have two discrete types of pinna motions. *The Journal of the Acoustical Society of America*, 141(5):3011–3017.

[128] Zhang, S., Liu, Y., Tang, J., Ying, L., and Müller, R. (2019). Dynamic relationship between noseleaf and pinnae in echolocating hipposiderid bats. *Journal of Experimental Biology*, 222(18):jeb210252.

[129] Zhang, S., Zhang, L., Zhang, R., and Müller, R. (2017). The relationship between pinna and noseleaf motions in hipposiderid bats. *The Journal of the Acoustical Society of America*, 141(5):3485–3485.

[130] Zhuang, Q. and Müller, R. (2006). Noseleaf furrows in a horseshoe bat act as resonance cavities shaping the biosonar beam. *Physical review letters*, 97(21):218701.

[131] Zhuang, Q. and Müller, R. (2007). Numerical study of the effect of the noseleaf on biosonar beamforming in a horseshoe bat. *Physical Review E*, 76(5):051902.

Appendices

Appendix A

Rigid pinna motion parameters

The following table shows a complete list of the parameters of all 100 analyzed rigid pinna motion sequences.

Table A.1: Parameters of the selected rigid pinna motion sequences of *Hipposideros pratti*. (Seq #: sequence number; NP: number of points marked on the pinna surface; T: motion time (ms); L: moving distance of pinna tip (mm); MD: maximum deformation (mm); θ: rotation angle (°); α: azimuth of rotation axis (°); β: elevation of rotation axis (°))

Seq #	NP	T (ms)	L (mm)	MD (mm)	θ (°)	α (°)	β (°)
Bat No. 1 (female)							
1	93	32.5	11.7	1.3	36.0	61.9	80.8
2	93	45	12.0	1.3	-44.4	-14.5	-18.1
3	85	40	15.2	1.5	38.3	-20.6	-26.4
4	87	30	11.0	1.5	-34.5	-27.3	-32.2
5	93	50	8.4	1.1	-25.9	-6.6	-68.0
6	87	62.5	18.8	1.5	-44.6	-76.0	-64.1
7	89	57.5	14.9	1.5	-60.0	-12.6	-15.3
Bat No. 2 (male)							
8	116	27.5	11.0	0.9	-46.1	-38.5	-3.1
9	111	20	12.4	1.1	-45.8	-36.3	1.4
10	115	32.5	14.1	1.1	-62.6	-48.7	4.8

(Continued on next page)

Table A.1 – Continued from previous page

Seq #	NP	T (ms)	L (mm)	MD (mm)	θ (°)	α (°)	β (°)
11	82	15	11.3	1.4	-26.3	-85.2	26.4
12	92	27.5	18.3	1.2	45.4	-11.9	61.2
13	80	15	12.2	1.5	-30.7	-61.2	-7.5
14	81	17.5	10.6	1.2	42.2	29.2	6.3
15	96	45	21.2	1	-48.9	-7.8	10.5
16	105	17.5	13.0	1.5	-52.7	-48.4	-0.4
17	103	27.5	15.2	0.8	46.0	7.6	22.5
18	104	17.5	9.6	1.2	36.4	29.4	17.1
19	104	25	10.9	1.2	-40.7	-34.9	8.6
20	100	30	17.6	1.3	-50.6	-43.2	11.2
21	100	30	16.2	1.3	-67.5	-15.4	-10.0
22	84	22.5	13.5	1.3	-33.4	-63.5	3.6
23	98	50	16.7	0.9	-45.8	-24.1	-25.9
24	98	47.5	15.7	1.1	53.9	-0.2	20.6
25	103	17.5	10.8	1.2	31.4	33.3	20.1
26	101	40	13.9	1	-43.5	-31.3	-4.8
27	109	40	17.6	1.2	-51.6	-64.2	34.6
28	82	37.5	18.7	0.9	46.4	59.0	-73.9
29	89	37.5	15.2	0.7	-37.0	-63.7	59.9
30	103	40	16.7	0.6	-38.0	12.3	-82.1
31	103	52.5	16.0	1.4	-36.8	-59.7	-33.6
Bat No. 3 (male)							

(Continued on next page)

Table A.1 – Continued from previous page

Seq #	NP	T (ms)	L (mm)	MD (mm)	θ (°)	α (°)	β (°)
32	56	32.5	12.0	1.2	38.8	-10.8	-18.6
33	57	22.5	18.9	1.4	68.6	-38.3	-38.3
34	69	27.5	13.2	1.3	22.7	-1.2	12.9
35	57	20	11.5	0.7	-34.8	-3.3	19.0
36	52	20	11.2	0.6	28.2	4.4	-7.2
37	50	32.5	13.7	0.4	31.1	73.8	37.7
38	50	32.5	14.2	0.6	49.5	2.9	2.6
39	51	25	14.0	0.4	45.1	-9.3	-14.9
40	49	25	15.5	0.9	-19.6	19.6	-9.6
41	48	35	19.4	0.3	32.9	-60.8	-28.3
42	50	30	14.7	0.9	-37.9	-3.6	-64.5
43	66	17.5	11.6	0.6	16.7	-70.5	10.6
44	61	22.5	14.1	0.4	28.5	5.9	-20.5
45	61	32.5	12.2	0.3	41.2	-3.3	-16.6
46	84	42.5	10.8	0.8	28.2	72.8	-31.9
47	51	15	8.4	0.5	-23.0	-54.3	7.1
48	55	27.5	11.5	0.3	29.3	38.3	20.1
49	55	22.5	7.6	0.6	-71.3	24.7	7.0
50	50	17.5	15.1	0.9	24.8	-66.8	-17.4
51	49	27.5	16.4	0.5	41.4	-3.1	-34.9
52	52	47.5	12.2	0.8	-32.9	19.2	21.1
53	44	20	12.0	0.4	-53.0	-52.9	-13.5

(Continued on next page)

Table A.1 – Continued from previous page

Seq #	NP	T (ms)	L (mm)	MD (mm)	θ (°)	α (°)	β (°)
54	50	47.5	14.5	0.6	44.9	-14.2	-44.6
55	56	22.5	8.3	0.5	-35.2	-39.2	-10.7
56	50	15	10.5	0.9	-34.0	-4.5	-18.7
57	49	15	9.7	0.6	29.8	34.0	21.4
58	62	22.5	10.8	0.7	28.9	-16.5	-0.8
59	70	20	11.3	1.1	19.7	17.0	41.5
60	70	7.5	5.0	1.4	13.1	52.2	-1.0
Bat No. 4 (male)							
61	87	37.5	13.7	1.4	-44.9	-5.0	-0.8
62	106	27.5	16.5	0.7	-60.5	-13.2	-22.9
63	121	30	12.5	1.3	-42.3	-35.3	16.2
64	102	40	15.7	1.4	-40.0	-51.0	-20.4
65	126	37.5	14.1	1.3	-40.1	-53.5	-0.3
66	110	22.5	13.9	1.4	-38.0	-37.5	-12.6
67	79	42.5	18.0	1.5	-51.4	-87.4	16.7
68	92	60	18.8	0.9	-38.8	0.4	-54.4
69	91	35	16.9	0.8	47.4	8.2	11.7
70	92	27.5	14.7	1.2	-32.2	-33.7	40.1
71	81	37.5	20.1	1	-91.2	-7.0	-6.4
72	81	30	19.8	1.2	-61.4	-47.1	14.3
73	79	40	24.0	1.4	67.7	-68.5	-47.7
74	101	42.5	16.4	1.4	61.6	6.4	-15.5

(Continued on next page)

Table A.1 – Continued from previous page

Seq #	NP	T (ms)	L (mm)	MD (mm)	θ (°)	α (°)	β (°)
75	116	42.5	18.1	0.8	-68.7	-5.3	-5.5
76	128	27.5	11.1	0.8	-29.0	-2.6	41.8
77	85	45	14.2	1.3	-67.3	0.0	-1.3
78	92	50	18.4	1.1	37.7	69.4	63.7
79	109	27.5	13.5	1	-55.3	-13.0	18.5
80	110	52.5	17.5	1.4	40.4	46.5	-15.4
Bat No. 5 (female)							
81	81	30	9.1	1.1	-28.6	-21.0	22.2
82	92	20	8.2	1.3	-38.9	-22.5	19.3
83	90	20	10.5	1	24.7	-53.1	16.0
84	90	20	7.8	1	-32.0	-50.7	-8.5
85	81	20	8.9	1	-36.3	-17.1	7.9
86	82	20	10.9	1	36.2	61.9	24.8
87	82	25	8.7	0.9	-37.8	-16.1	-1.6
88	80	22.5	8.8	0.9	-43.4	-16.5	11.2
89	81	30	9.2	1	-32.7	-43.5	-37.4
90	93	17.5	10.6	1.1	-35.2	-77.4	-9.9
91	93	30	10.8	1.2	-33.0	-43.7	-0.1
92	93	20	9.8	1.1	-25.4	-69.4	-20.4
93	92	32.5	10.1	1.4	47.2	5.6	6.9
94	90	42.5	12.9	1.2	-86.6	0.3	2.6
95	84	25	10.1	1.5	-36.4	-14.7	-0.5

(Continued on next page)

Table A.1 – Continued from previous page

Seq #	NP	T (ms)	L (mm)	MD (mm)	θ (°)	α (°)	β (°)
96	94	22.5	11.9	0.7	-24.9	-68.1	27.2
97	91	27.5	13.7	1.3	-24.7	-6.0	-82.7
98	97	27.5	10.8	1	-23.2	-65.6	32.0
99	91	42.5	12.1	1.4	-28.9	-64.9	16.6
100	94	62.5	14.7	1.4	51.6	26.4	39.3

Appendix B

Additional mutual information results

The following figures show the additional examples of normalized mutual information between the pulse envelopes of a reference rotation axis and all other rotation axes in sample.

For each example of normalized mutual information between the pulse envelopes of a reference rotation axis and all other rotation axes in sample: a) for pulses with a single sine carrier. b) for pulses with a frequency-modulated carrier. In each graph, the star marks the reference rotation axis and the dots mark the rotation axes that were used for comparison. The color value of the lines between the reference and the other rotation axes denotes the normalized mutual information between the pulse envelopes between these two orientations of the rotation axis.

B.1 Reference rotation axis (-60 °, -60 °)

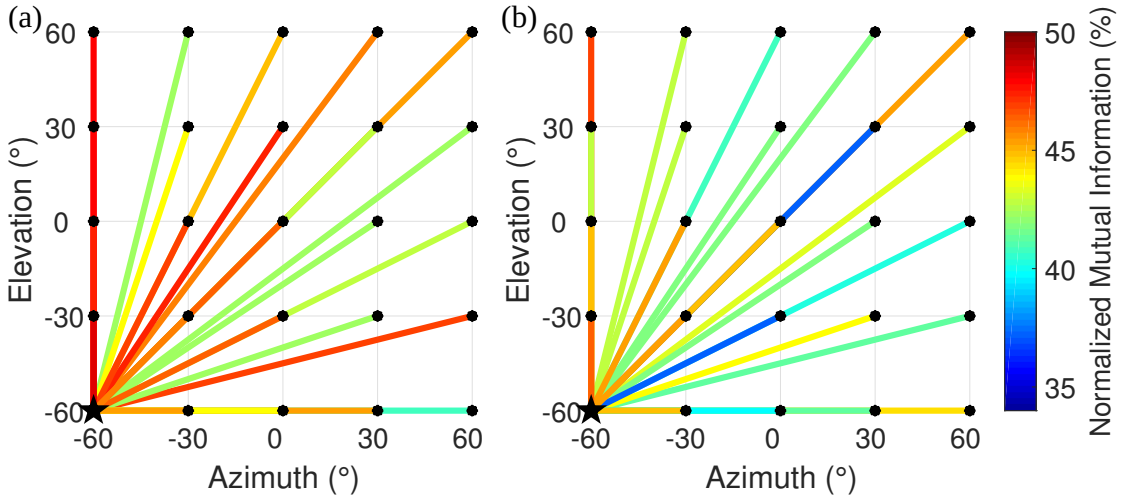

Figure B.1: Normalized mutual information between reference rotation axis (-60 °, -60 °) and all the other rotation axes

B.2 Reference rotation axis (-30 °, -60 °)

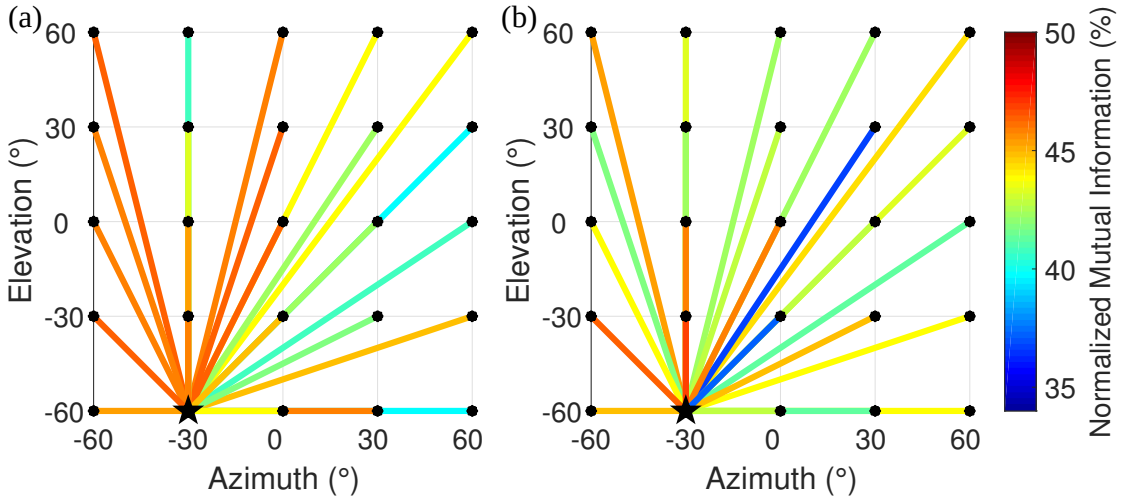

Figure B.2: Normalized mutual information between reference rotation axis (-30 °, -60 °) and all the other rotation axes

B.3 Reference rotation axis (0 °, -60 °)

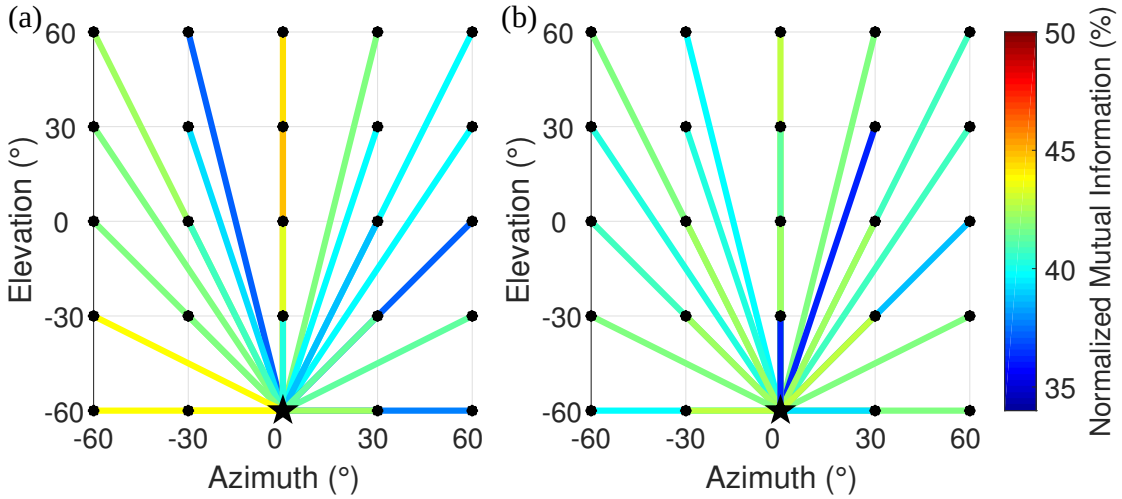

Figure B.3: Normalized mutual information between reference rotation axis (0 °, -60 °) and all the other rotation axes

B.4 Reference rotation axis (30 °, -60 °)

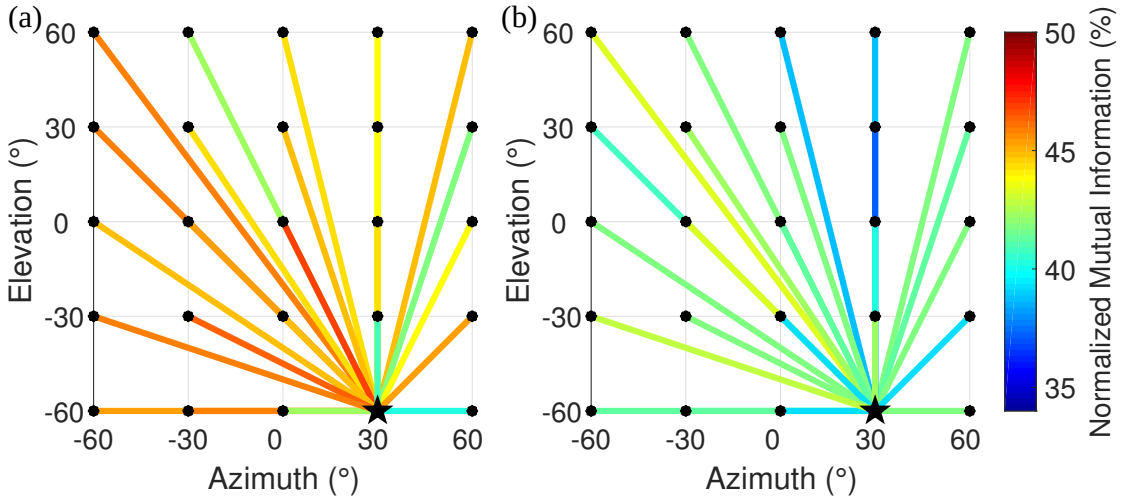

Figure B.4: Normalized mutual information between reference rotation axis (30 °, -60 °) and all the other rotation axes

B.5 Reference rotation axis (60 °, -60 °)

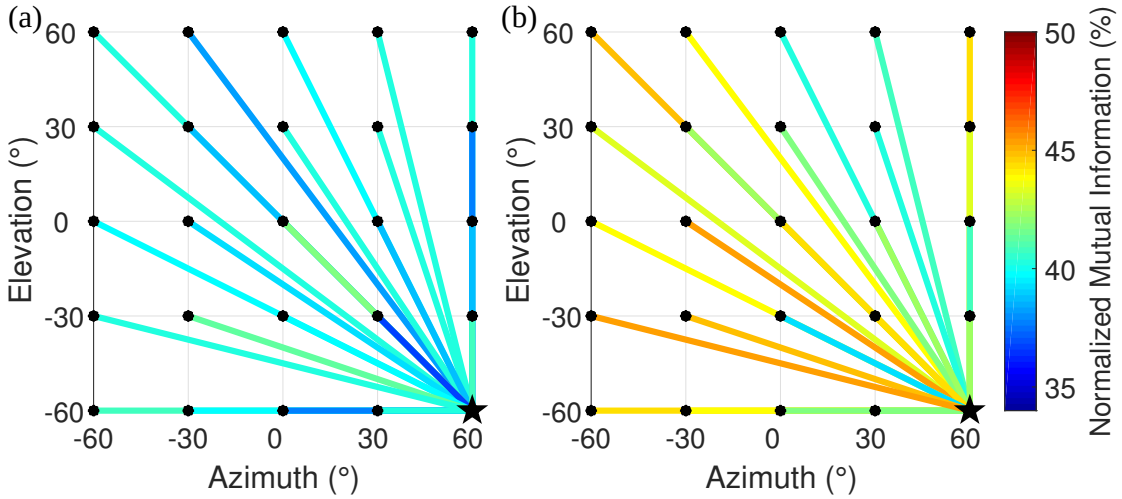

Figure B.5: Normalized mutual information between reference rotation axis (60 °, -60 °) and all the other rotation axes

B.6 Reference rotation axis (-60 °, -30 °)

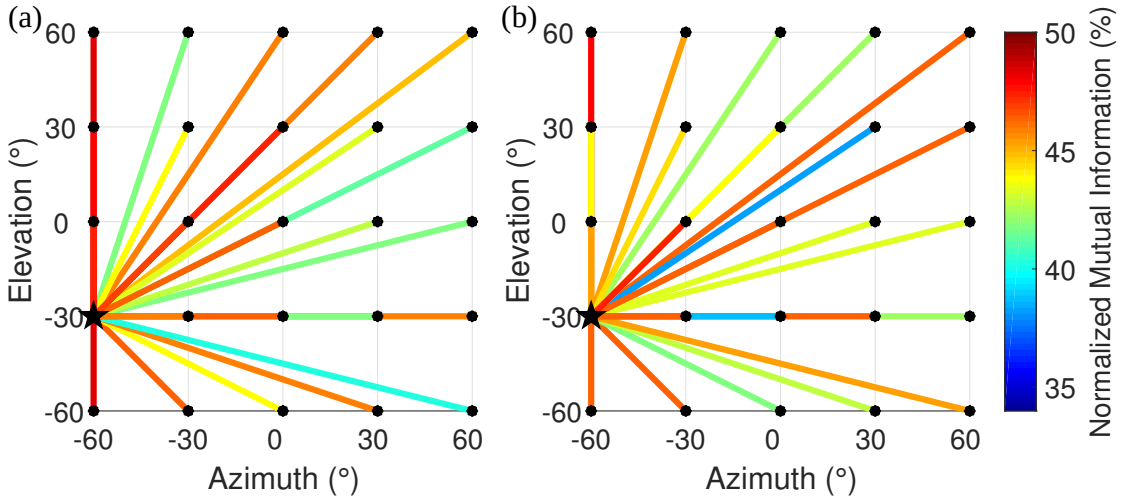

Figure B.6: Normalized mutual information between reference rotation axis (-60 °, -30 °) and all the other rotation axes

B.7 Reference rotation axis (-30 °, -30 °)

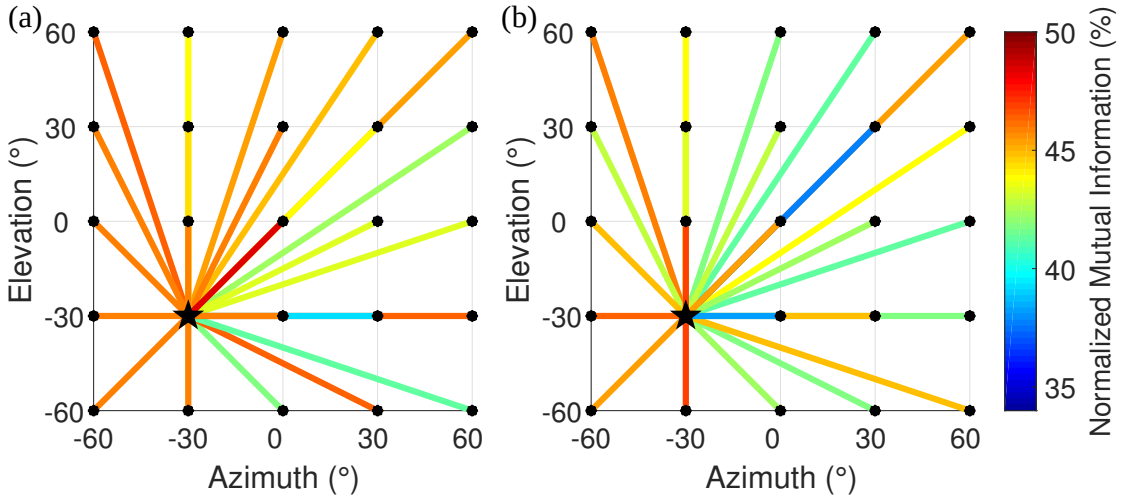

Figure B.7: Normalized mutual information between reference rotation axis (-30 °, -30 °) and all the other rotation axes

B.8 Reference rotation axis (0 °, -30 °)

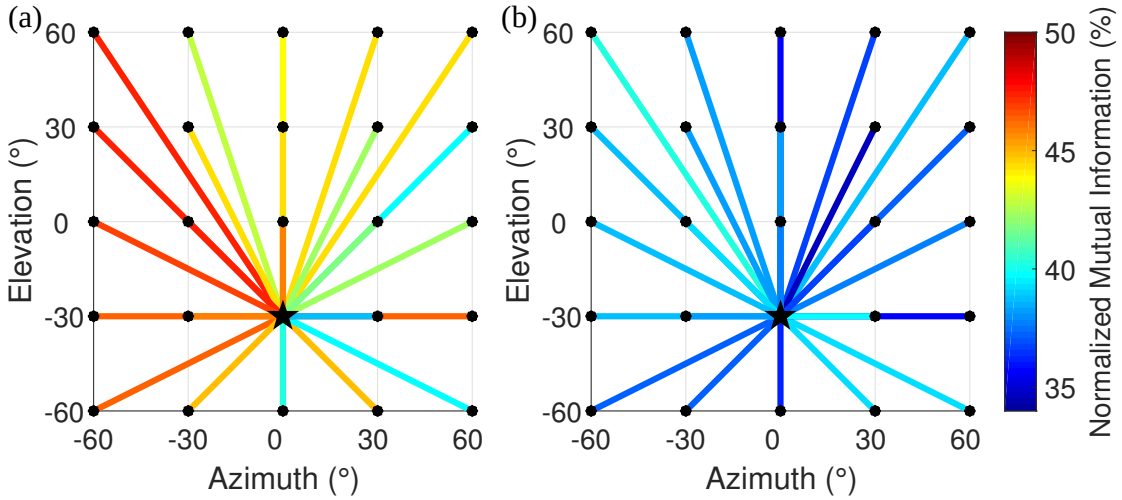

Figure B.8: Normalized mutual information between reference rotation axis (0 °, -30 °) and all the other rotation axes

B.9 Reference rotation axis (30 °, -30 °)

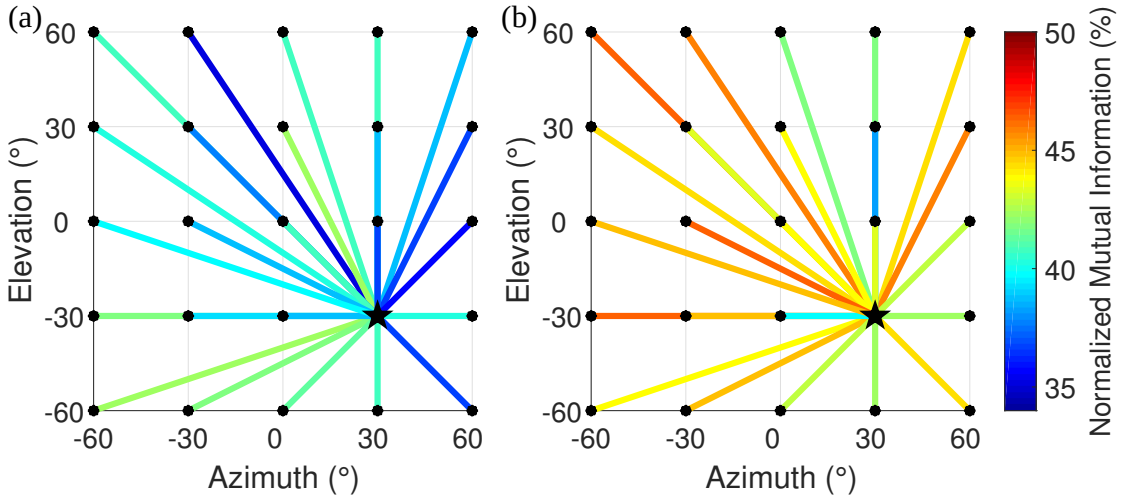

Figure B.9: Normalized mutual information between reference rotation axis (30 °, -30 °) and all the other rotation axes

B.10 Reference rotation axis (60 °, -30 °)

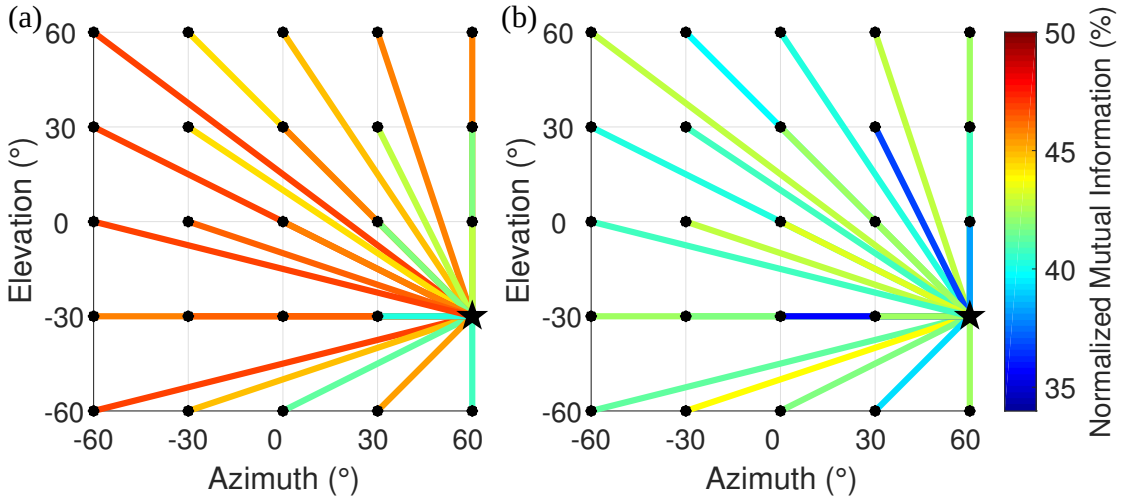

Figure B.10: Normalized mutual information between reference rotation axis (60 °, -30 °) and all the other rotation axes

B.11 Reference rotation axis (-60 °, 0 °)

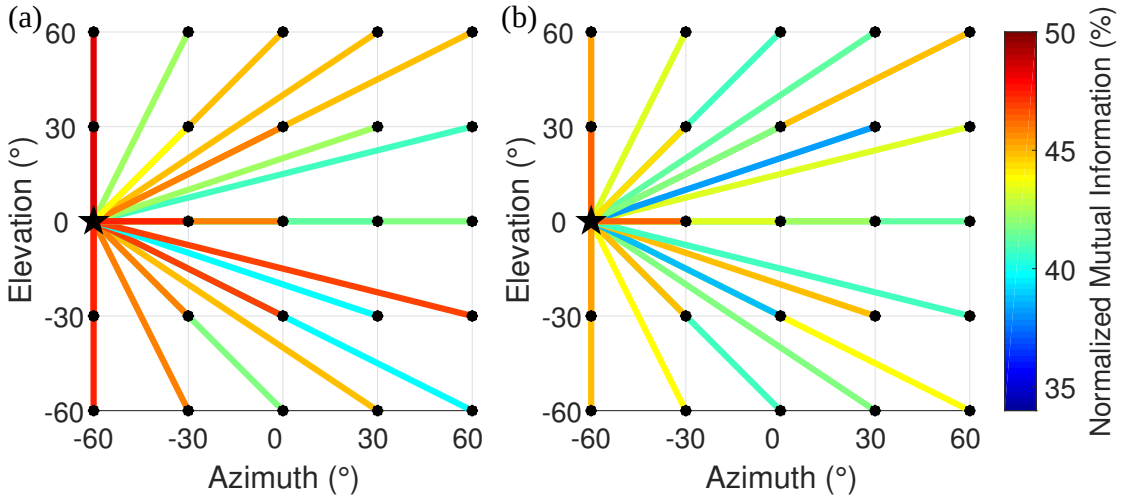

Figure B.11: Normalized mutual information between reference rotation axis (-60 °, 0 °) and all the other rotation axes

B.12 Reference rotation axis (-30 °, 0 °)

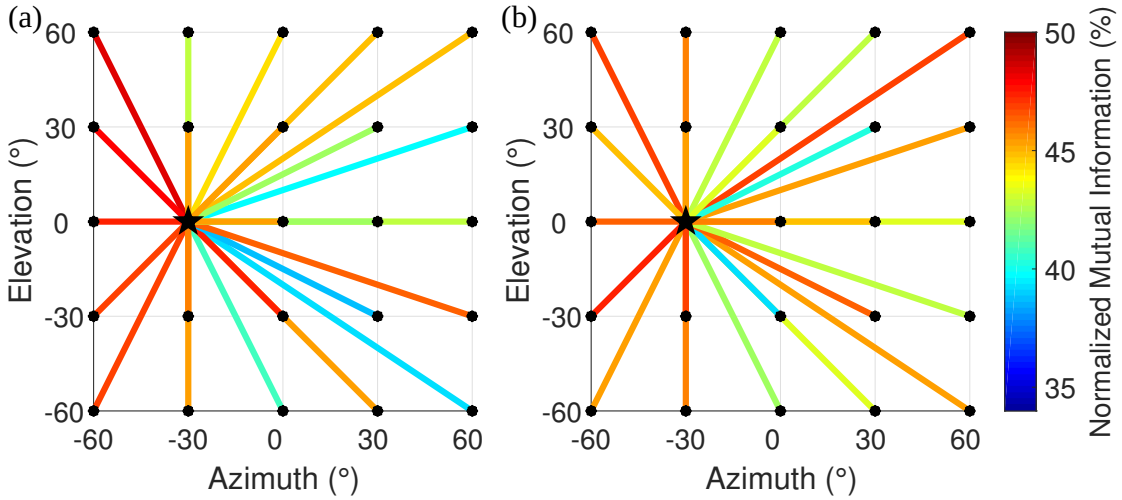

Figure B.12: Normalized mutual information between reference rotation axis (-30 °, 0 °) and all the other rotation axes

B.13 Reference rotation axis (30 °, 0 °)

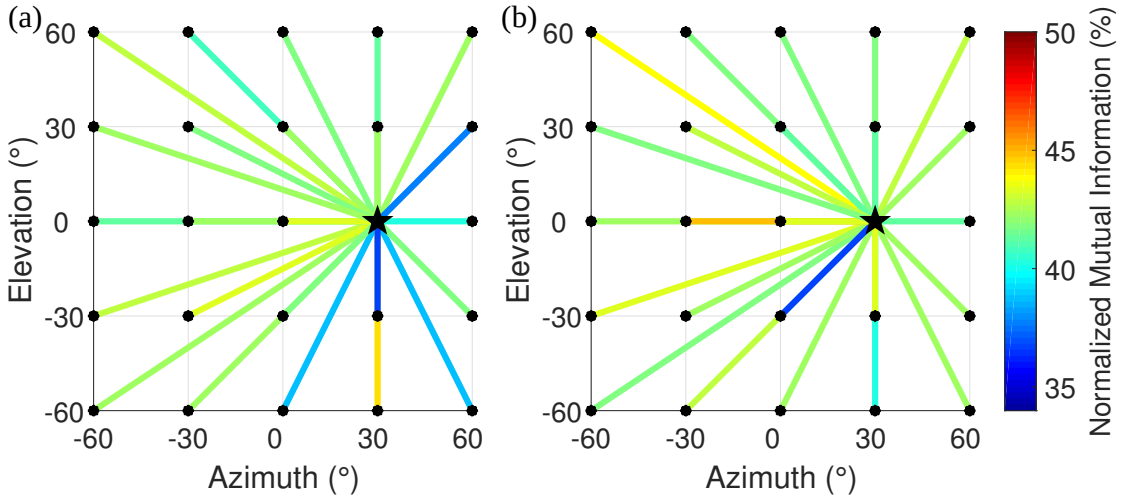

Figure B.13: Normalized mutual information between reference rotation axis (30 °, 0 °) and all the other rotation axes

B.14 Reference rotation axis (60 °, 0 °)

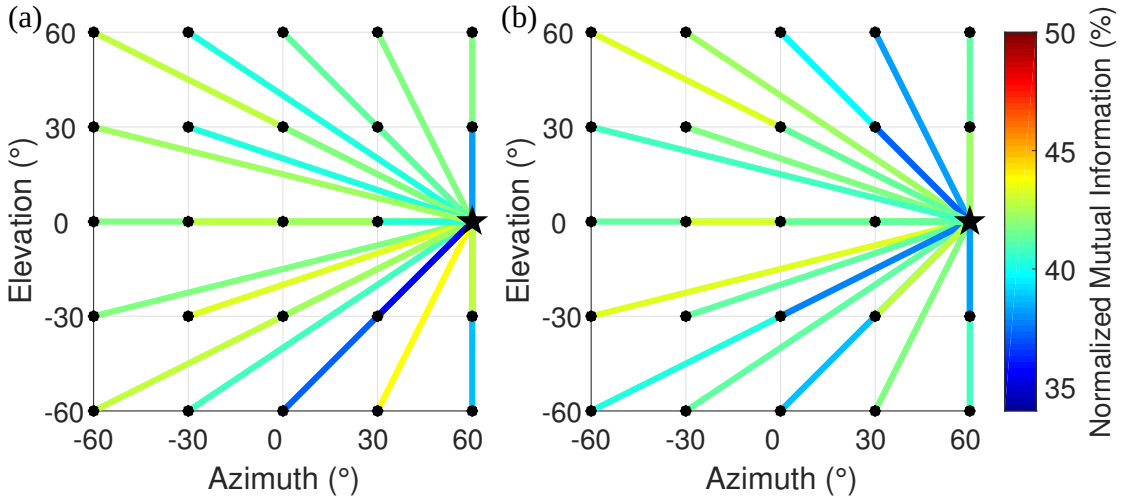

Figure B.14: Normalized mutual information between reference rotation axis (60 °, 0 °) and all the other rotation axes

B.15 Reference rotation axis (-60 °, 30 °)

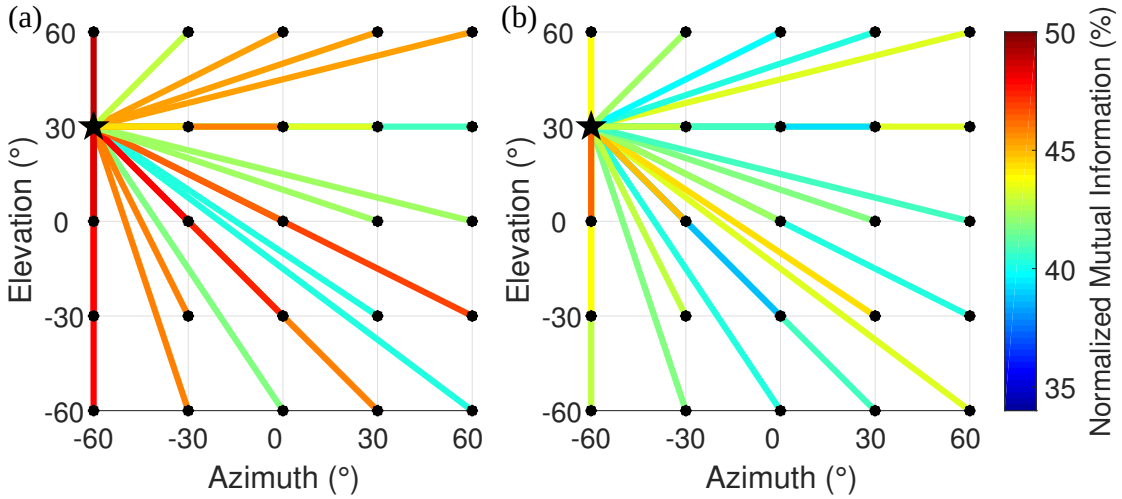

Figure B.15: Normalized mutual information between reference rotation axis (-60 °, 30 °) and all the other rotation axes

B.16 Reference rotation axis (-30 °, 30 °)

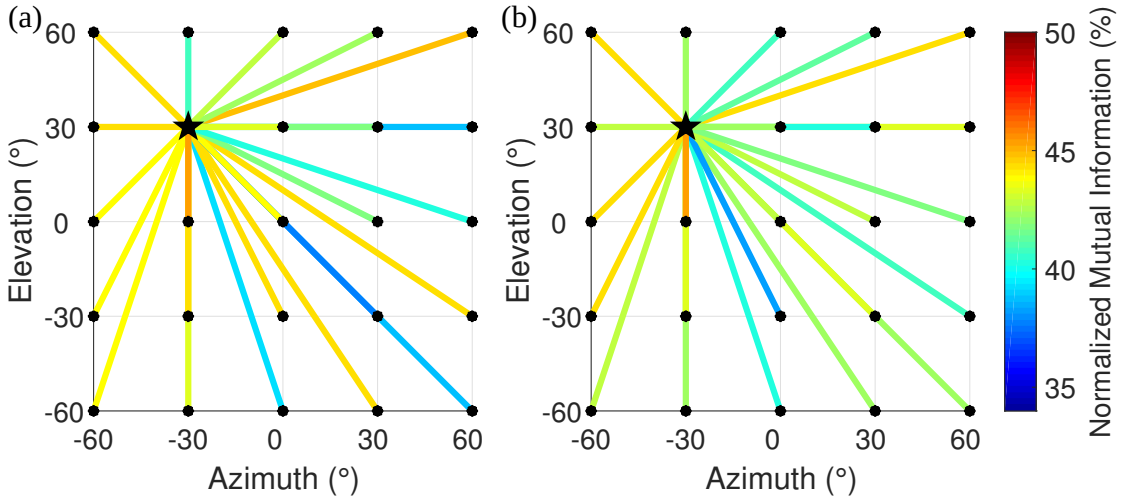

Figure B.16: Normalized mutual information between reference rotation axis (-30 °, 30 °) and all the other rotation axes

B.17 Reference rotation axis (0 °, 30 °)

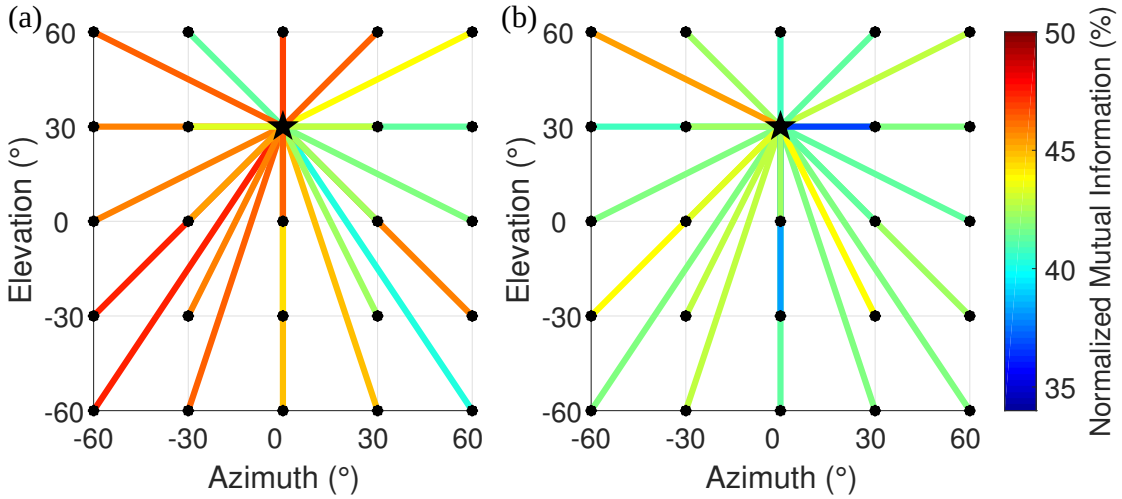

Figure B.17: Normalized mutual information between reference rotation axis (0 °, 30 °) and all the other rotation axes

B.18 Reference rotation axis (30 °, 30 °)

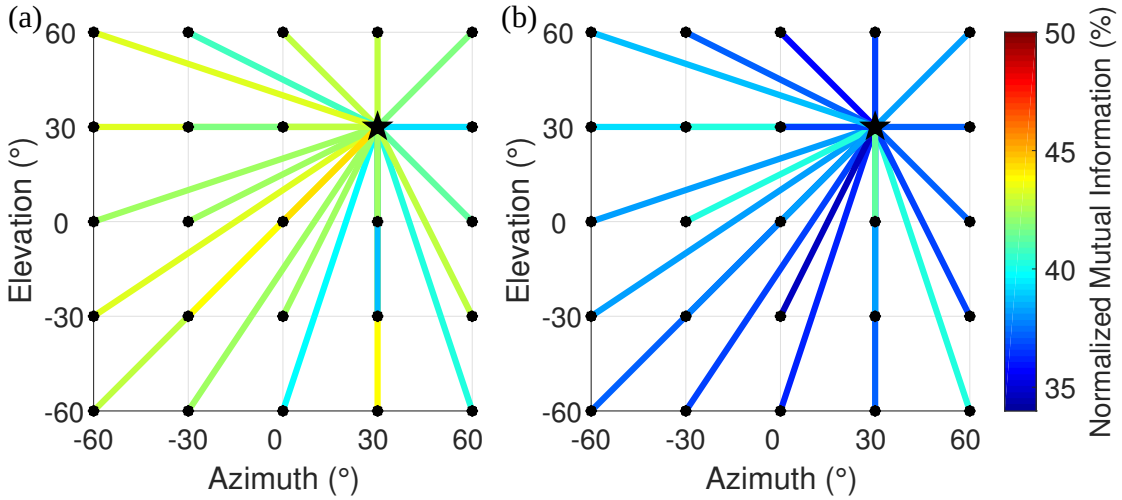

Figure B.18: Normalized mutual information between reference rotation axis (30 °, 30 °) and all the other rotation axes

B.19 Reference rotation axis (60 °, 30 °)

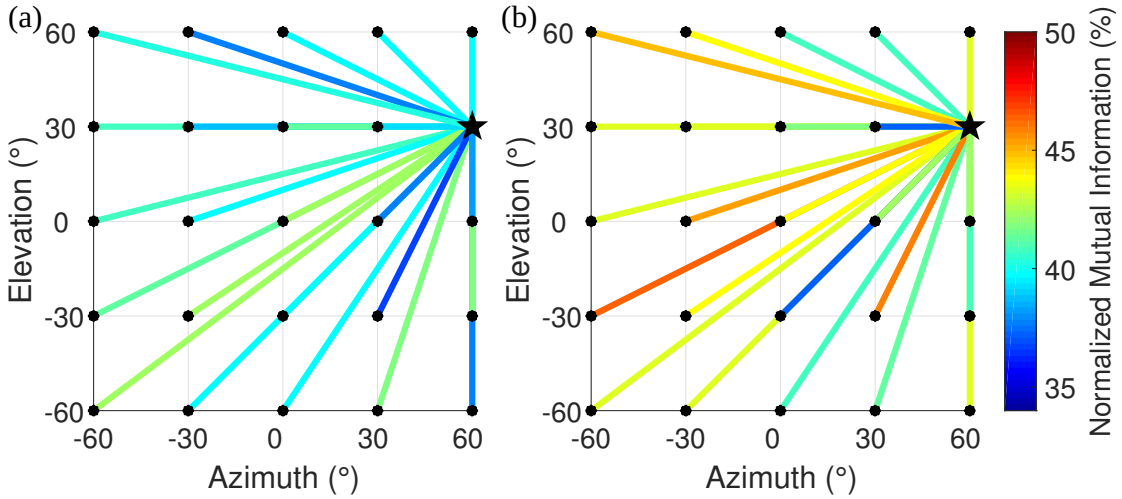

Figure B.19: Normalized mutual information between reference rotation axis (60 °, 30 °) and all the other rotation axes

B.20 Reference rotation axis (-60 °, 60 °)

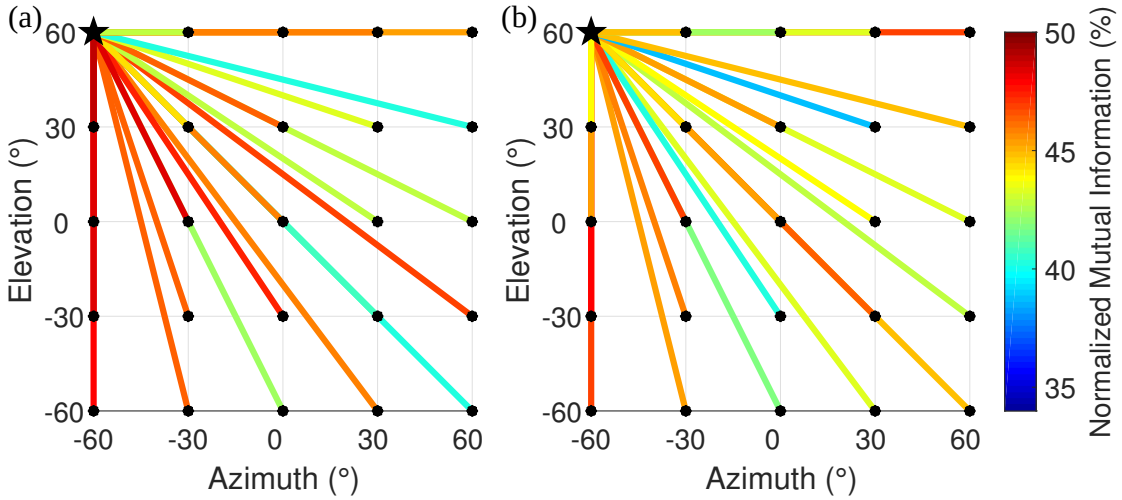

Figure B.20: Normalized mutual information between reference rotation axis (-60 °, 60 °) and all the other rotation axes

B.21 Reference rotation axis (-30 °, 60 °)

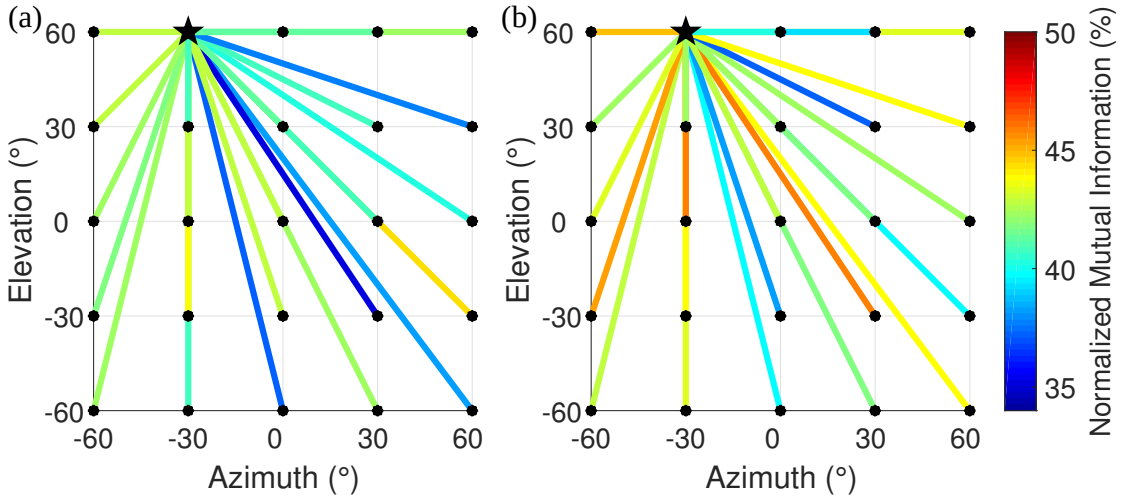

Figure B.21: Normalized mutual information between reference rotation axis (-30 °, 60 °) and all the other rotation axes

B.22 Reference rotation axis (0 °, 60 °)

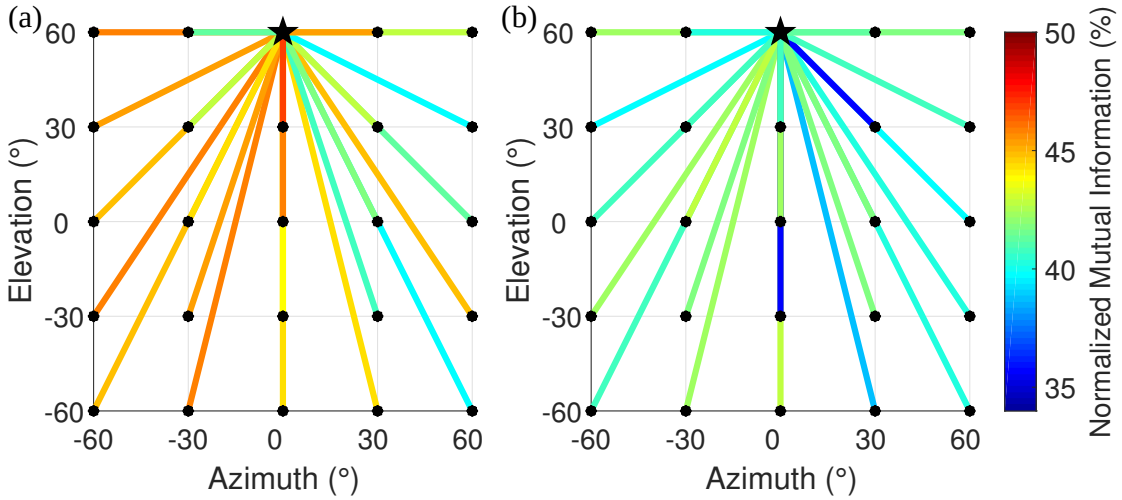

Figure B.22: Normalized mutual information between reference rotation axis (0 °, 60 °) and all the other rotation axes

B.23 Reference rotation axis (30 °, 60 °)

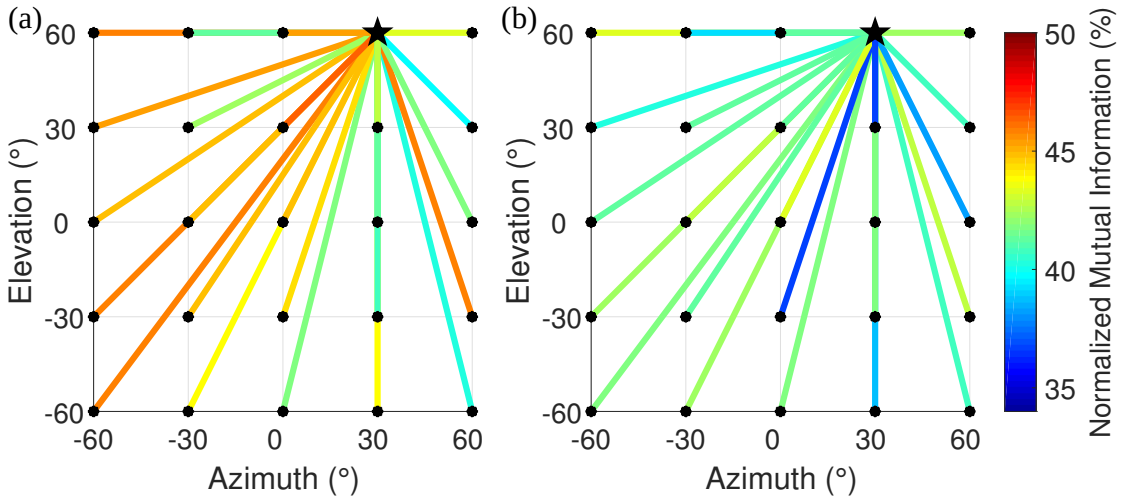

Figure B.23: Normalized mutual information between reference rotation axis (30 °, 60 °) and all the other rotation axes

B.24 Reference rotation axis (60 °, 60 °)

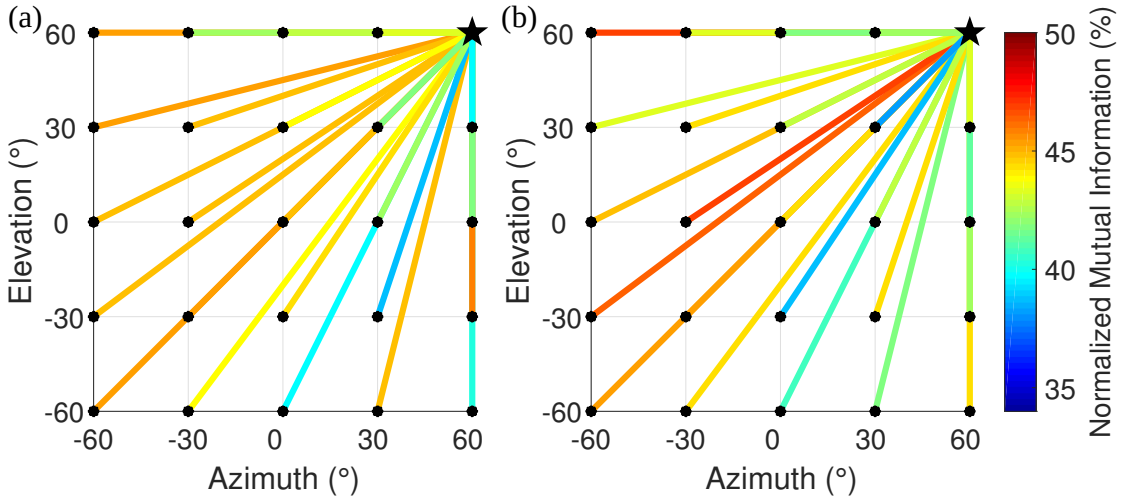

Figure B.24: Normalized mutual information between reference rotation axis (60 °, 60 °) and all the other rotation axes

Appendix C

Non-rigid pinna motion parameters

The following table shows a complete list of the parameters of the analyzed pilot data set consisting of 10 non-rigid pinna motion sequences.

Table C.1: Parameters of the selected non-rigid pinna motion sequences of *Hipposideros pratti*. (Seq #: sequence number; NP: number of points marked on the pinna surface; T: motion time (ms); L: moving distance of pinna tip (mm); MD: maximum deformation (mm))

Bat	Sex	Seq #	NP	T (ms)	L (mm)	MD (mm)
No.1	Female	1	82	75	22.8	3.8
		2	86	105	16.8	5.1
		3	89	65	17.4	4.5
No.2	Male	4	111	37.5	17.1	5
		5	107	125	25.5	4.3
No.3	Male	6	60	50	16.8	4
		7	60	47.5	24.1	4.1
		8	60	32.5	14.2	3
		9	71	42.5	13.9	3.9
		10	85	47.5	10.2	4.5

Appendix D

Additional clustering results

The following figures show the additional examples of the distribution of the clusters of the landmarks on the pinna surface using spectral clustering algorithm of non-rigid pinna motion sequences.

D.1 Pinna motion sample 1

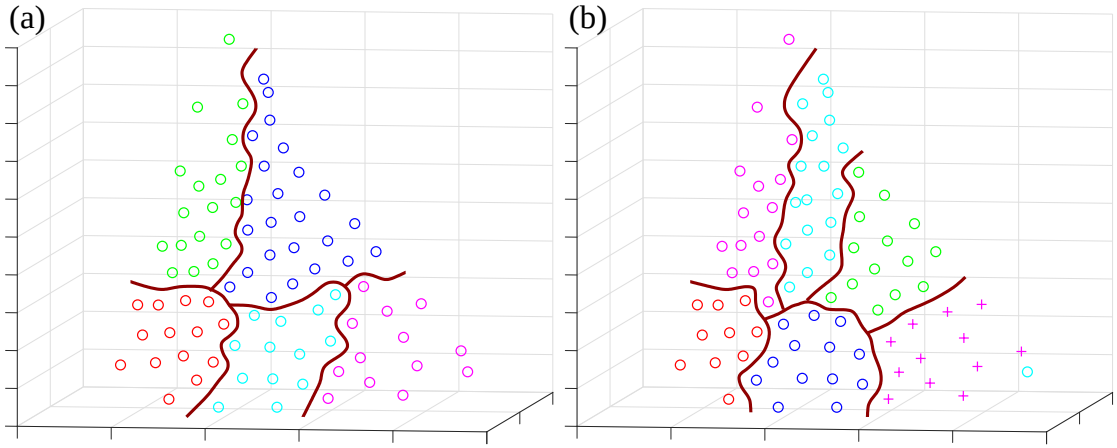

Figure D.1: Spectral clustering results of pinna motion sample 1: a) number of clusters is 5, b) number of clusters is 6. Dots are the points marked on the pinna. Different colors denote different clusters. The maroon lines are the boundaries between the clusters.

D.2 Pinna motion sample 2

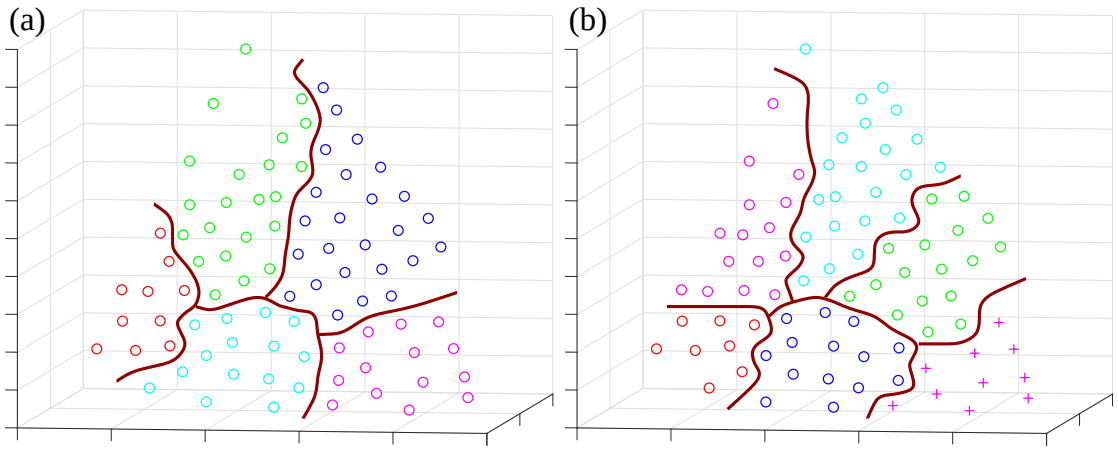

Figure D.2: Spectral clustering results of pinna motion sample 2: a) number of clusters is 5, b) number of clusters is 6. Dots are the points marked on the pinna. Different colors denote different clusters. The maroon lines are the boundaries between the clusters.

D.3 Pinna motion sample 3

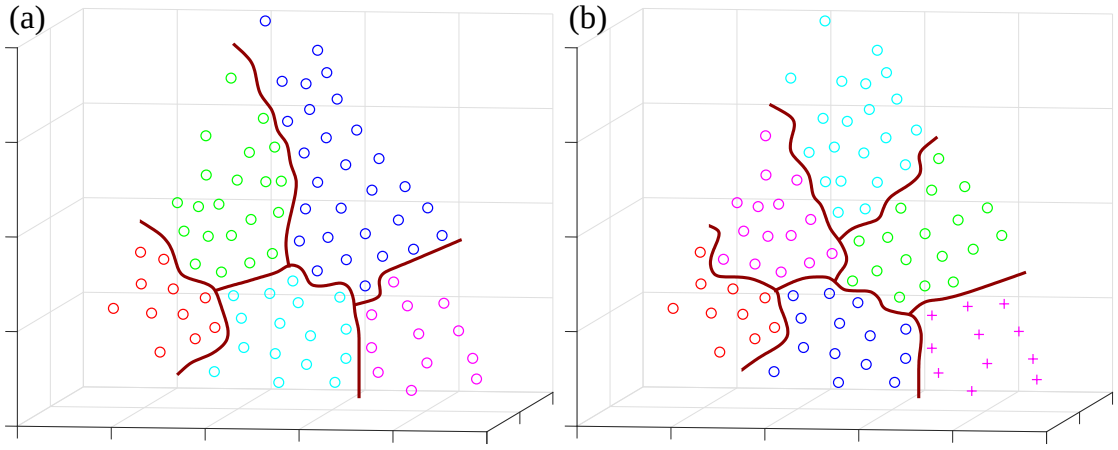

Figure D.3: Spectral clustering results of pinna motion sample 3: a) number of clusters is 5, b) number of clusters is 6. Dots are the points marked on the pinna. Different colors denote different clusters. The maroon lines are the boundaries between the clusters.

D.4 Pinna motion sample 4

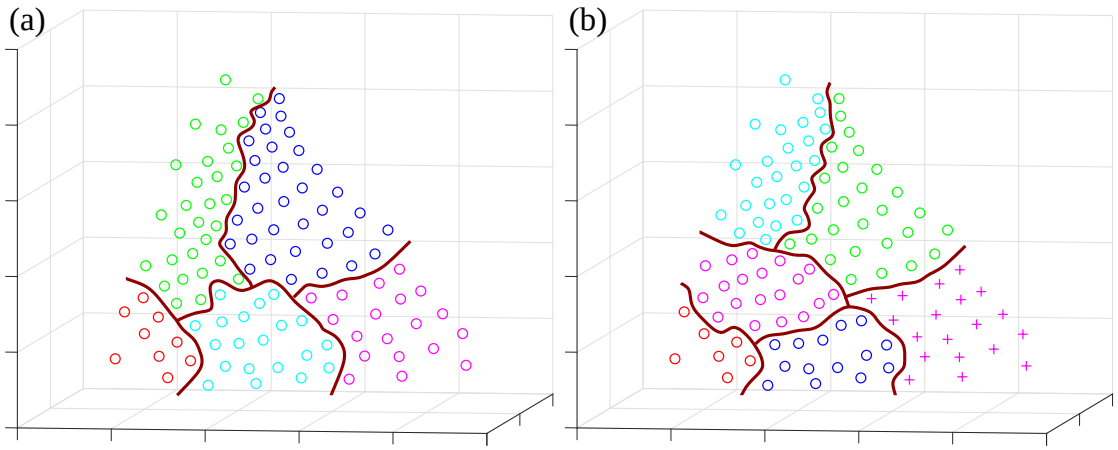

Figure D.4: Spectral clustering results of pinna motion sample 4: a) number of clusters is 5, b) number of clusters is 6. Dots are the points marked on the pinna. Different colors denote different clusters. The maroon lines are the boundaries between the clusters.

D.5 Pinna motion sample 5

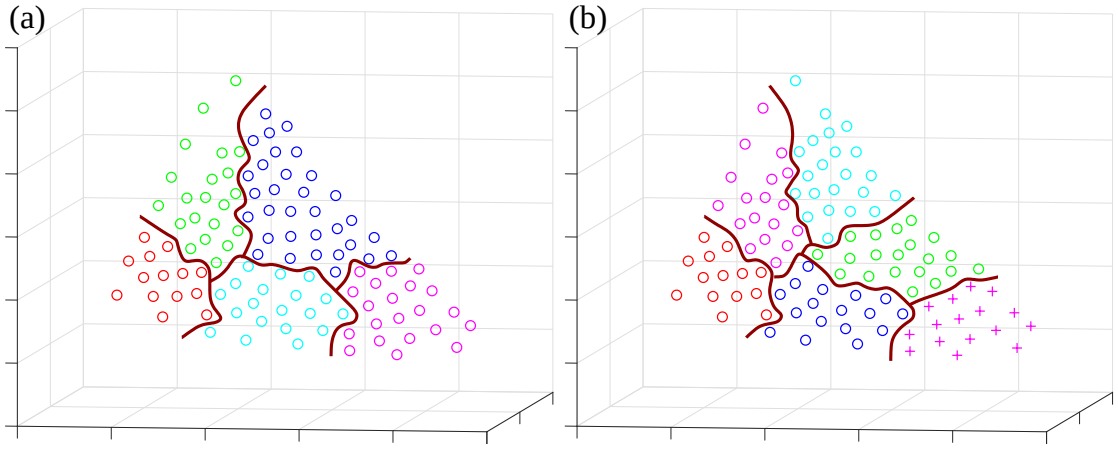

Figure D.5: Spectral clustering results of pinna motion sample 5: a) number of clusters is 5, b) number of clusters is 6. Dots are the points marked on the pinna. Different colors denote different clusters. The maroon lines are the boundaries between the clusters.

D.6 Pinna motion sample 6

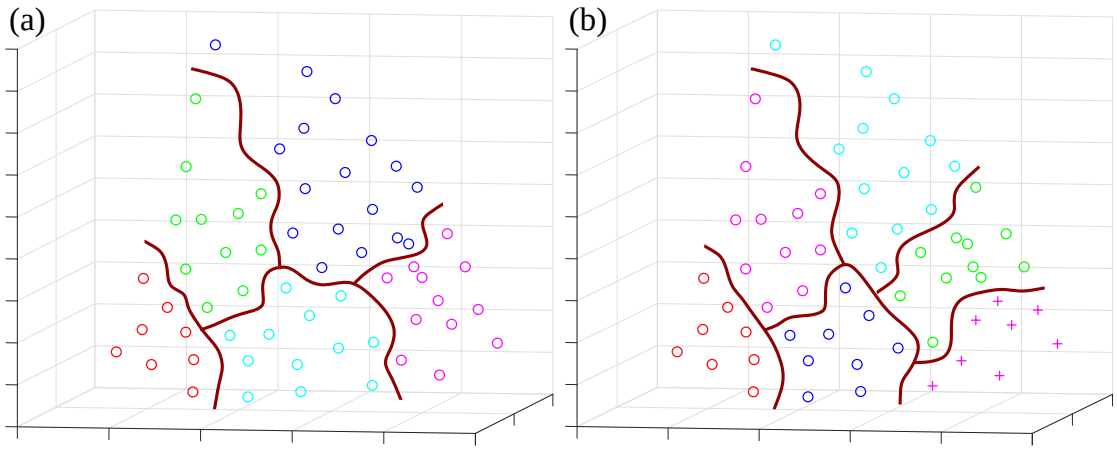

Figure D.6: Spectral clustering results of pinna motion sample 6: a) number of clusters is 5, b) number of clusters is 6. Dots are the points marked on the pinna. Different colors denote different clusters. The maroon lines are the boundaries between the clusters.

D.7 Pinna motion sample 7

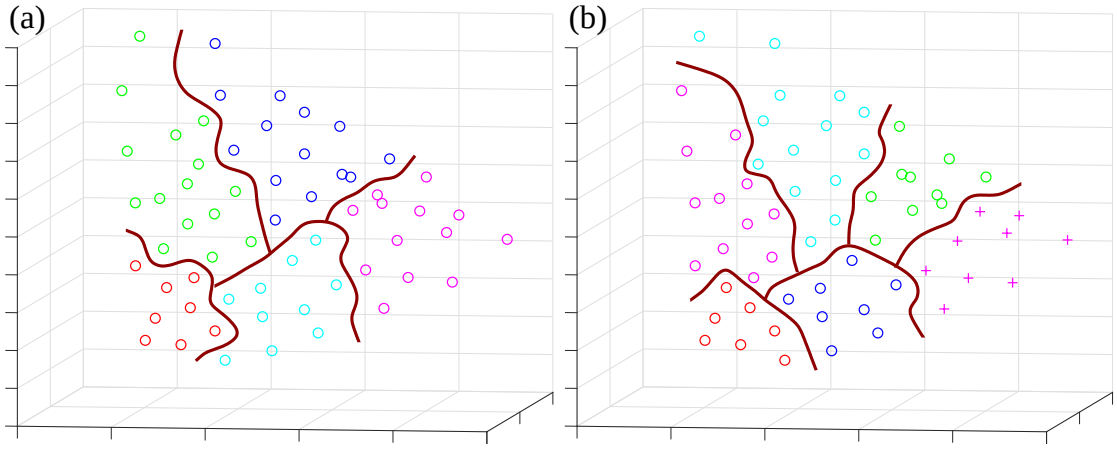

Figure D.7: Spectral clustering results of pinna motion sample 7: a) number of clusters is 5, b) number of clusters is 6. Dots are the points marked on the pinna. Different colors denote different clusters. The maroon lines are the boundaries between the clusters.

D.8 Pinna motion sample 8

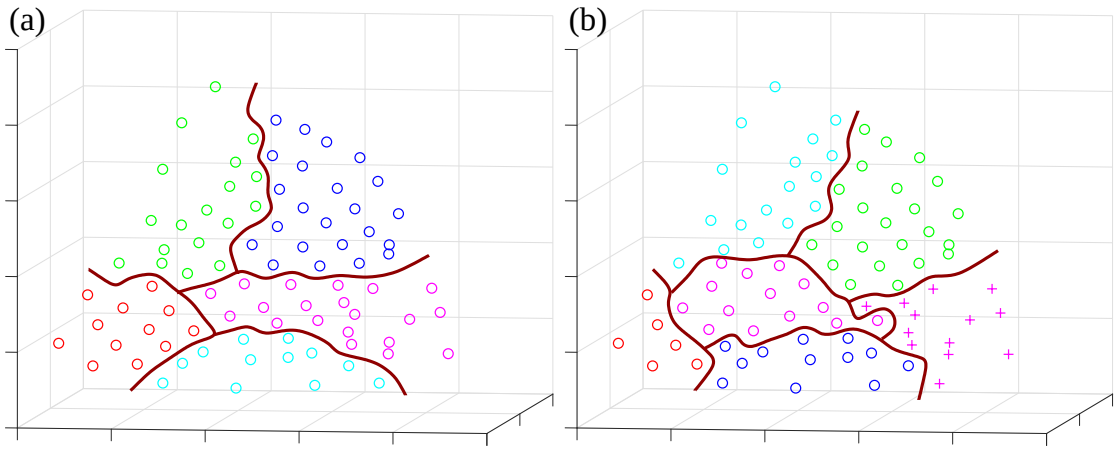

Figure D.8: Spectral clustering results of pinna motion sample 8: a) number of clusters is 5, b) number of clusters is 6. Dots are the points marked on the pinna. Different colors denote different clusters. The maroon lines are the boundaries between the clusters.

Appendix E

Additional distances between clusters results

The following figures show the additional results of the Euclidean distances between the clusters in the non-rigid pinna motion sequences.

E.1 Distribution of clusters for non-rigid pinna motion samples from 1 to 7

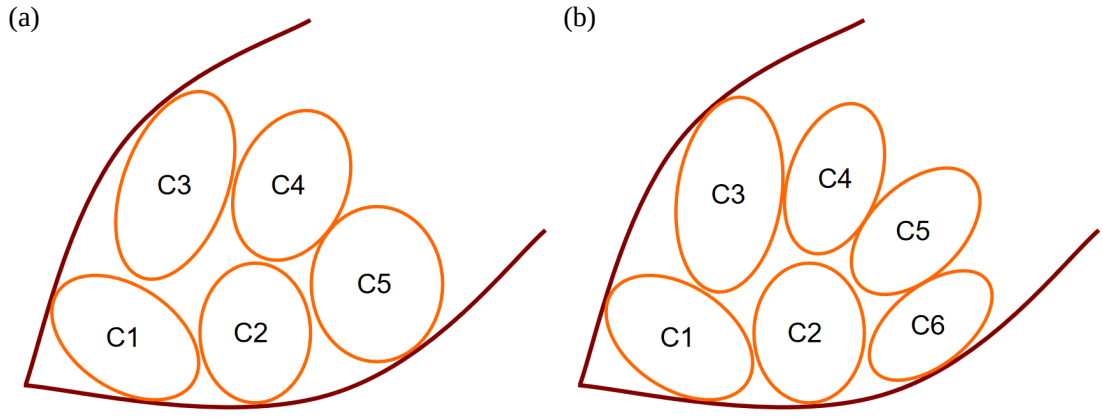

Figure E.1: Distribution of clusters on the pinna surface for non-rigid pinna motion samples from 1 to 7: a) number of clusters is 5, b) number of clusters is 6.

E.2 Pinna motion sample 1

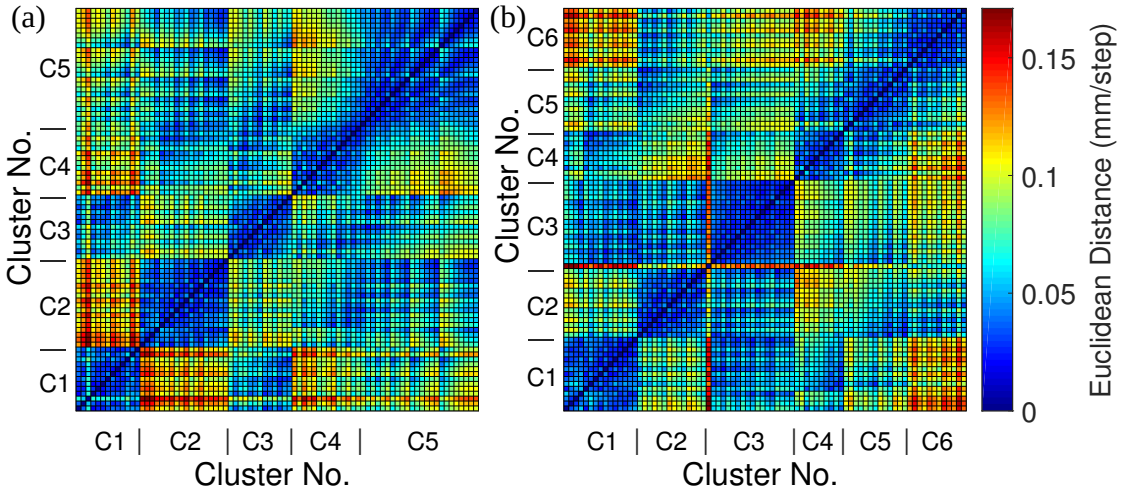

Figure E.2: Matrix of Euclidean distances between clusters for non-rigid pinna motion sample 1: a) number of clusters is 5, b) number of clusters is 6.

E.3 Pinna motion sample 2

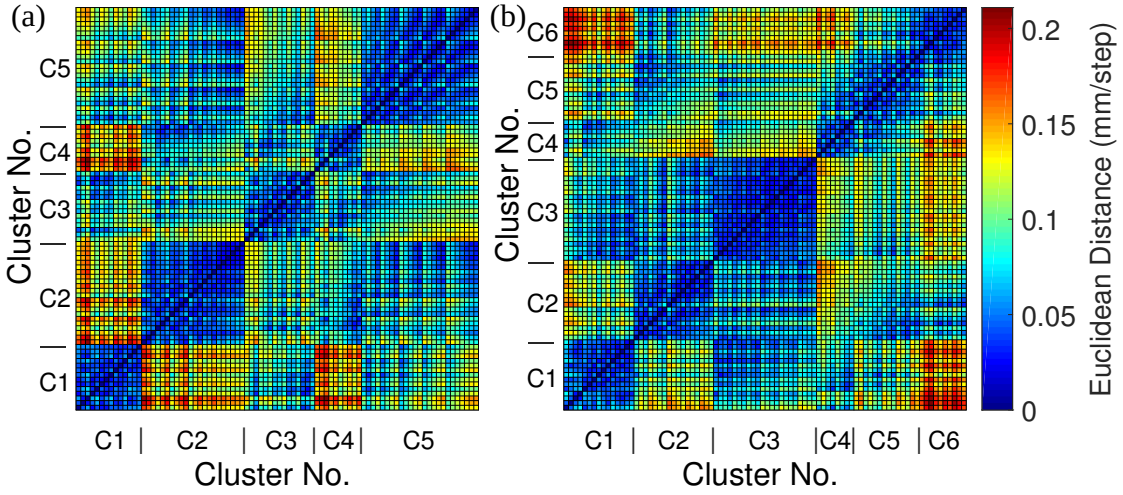

Figure E.3: Matrix of Euclidean distances between clusters for non-rigid pinna motion sample 2: a) number of clusters is 5, b) number of clusters is 6.

E.4 Pinna motion sample 3

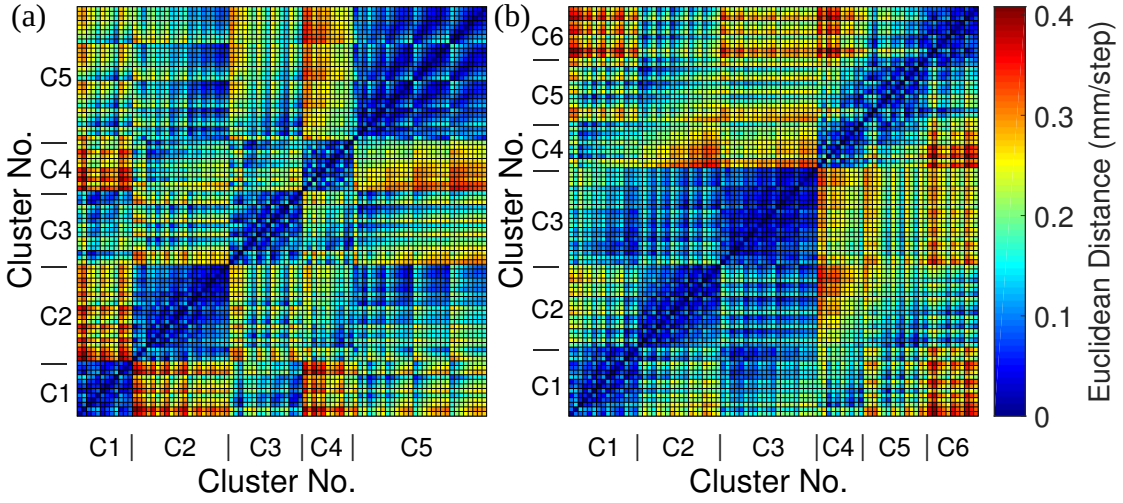

Figure E.4: Matrix of Euclidean distances between clusters for non-rigid pinna motion sample 3: a) number of clusters is 5, b) number of clusters is 6.

E.5 Pinna motion sample 4

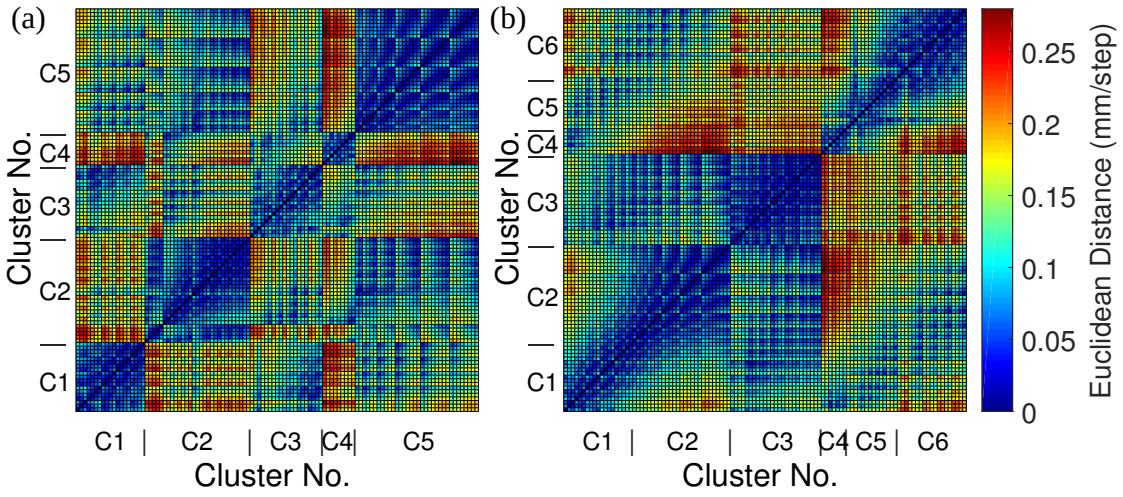

Figure E.5: Matrix of Euclidean distances between clusters for non-rigid pinna motion sample 4: a) number of clusters is 5, b) number of clusters is 6.

E.6 Pinna motion sample 5

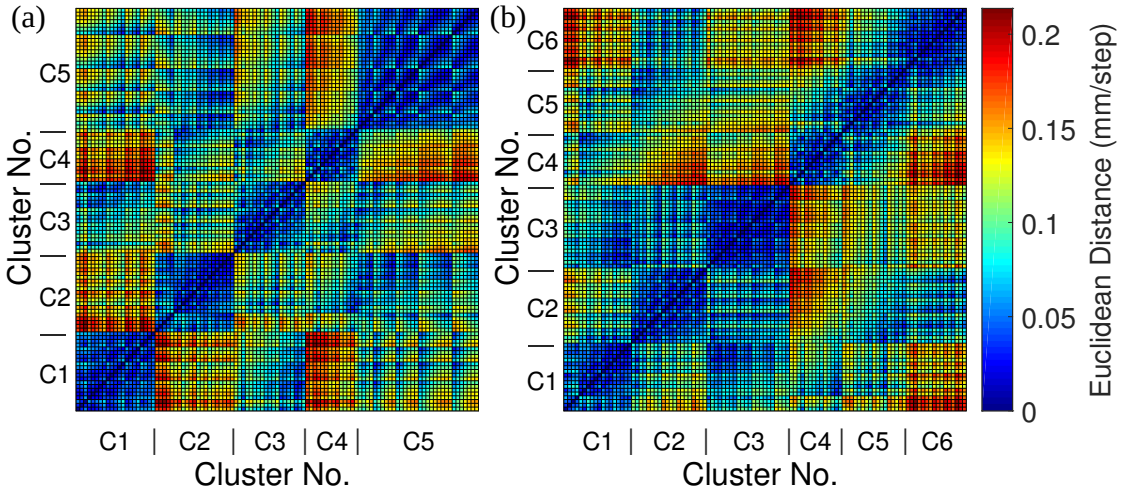

Figure E.6: Matrix of Euclidean distances between clusters for non-rigid pinna motion sample 5: a) number of clusters is 5, b) number of clusters is 6.

E.7 Pinna motion sample 6

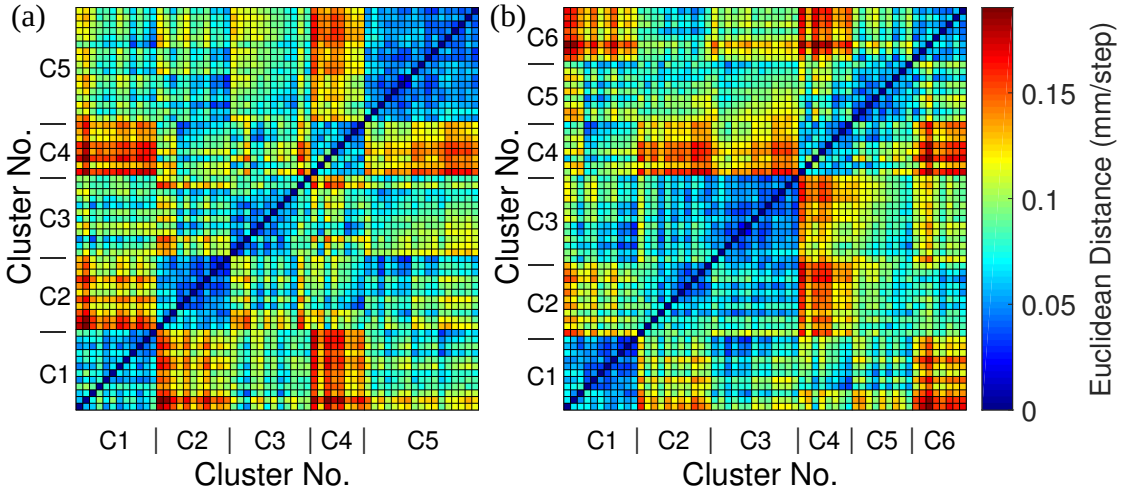

Figure E.7: Matrix of Euclidean distances between clusters for non-rigid pinna motion sample 6: a) number of clusters is 5, b) number of clusters is 6.

E.8 Pinna motion sample 7

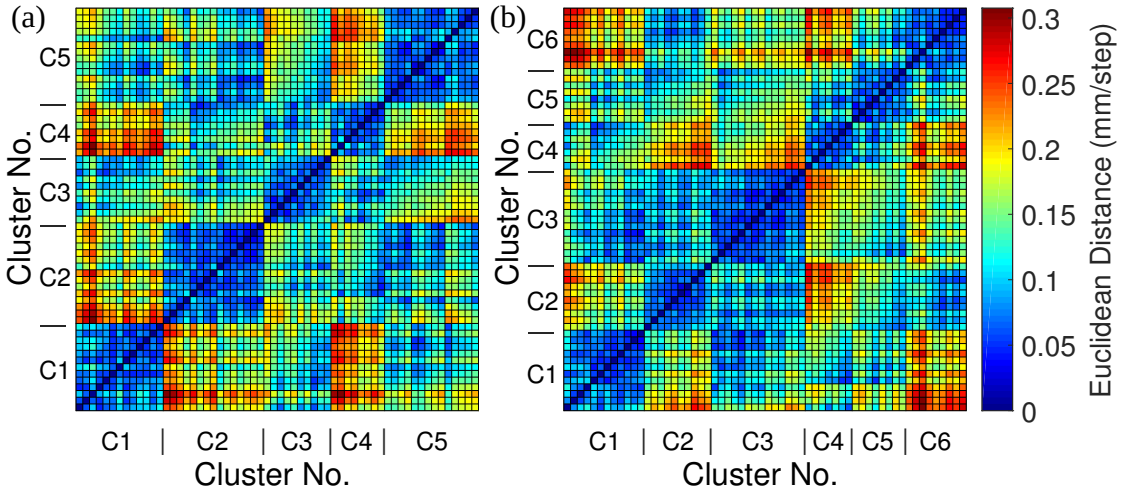

Figure E.8: Matrix of Euclidean distances between clusters for non-rigid pinna motion sample 7: a) number of clusters is 5, b) number of clusters is 6.

E.9 Distribution of clusters for non-rigid pinna motion samples from 8 to 9

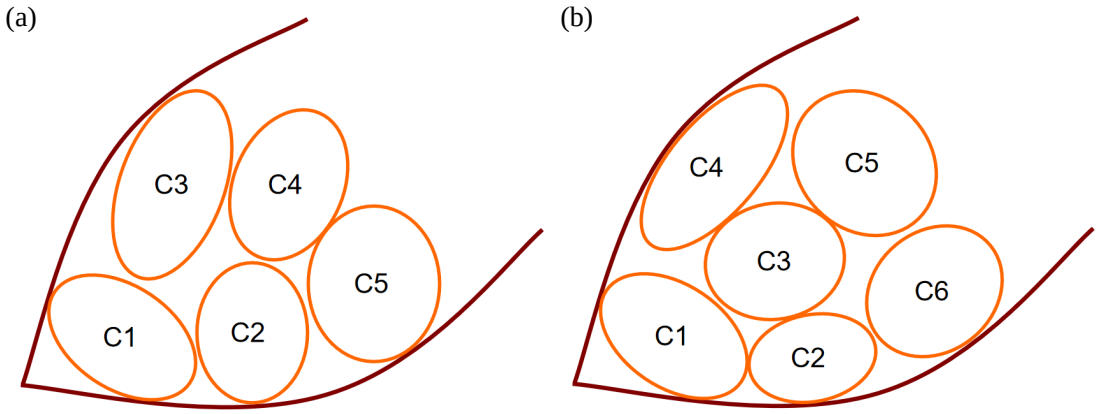

Figure E.9: Distribution of clusters on the pinna surface for non-rigid pinna motion samples from 8 to 9: a) number of clusters is 5, b) number of clusters is 6.

E.10 Pinna motion sample 8

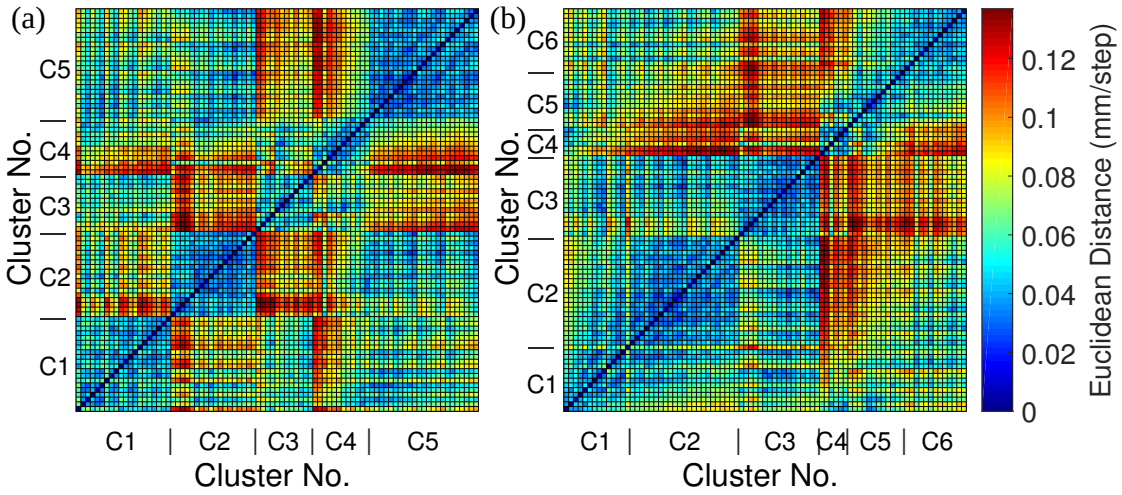

Figure E.10: Matrix of Euclidean distances between clusters for non-rigid pinna motion sample 8: a) number of clusters is 5, b) number of clusters is 6.

E.11 Pinna motion sample 9

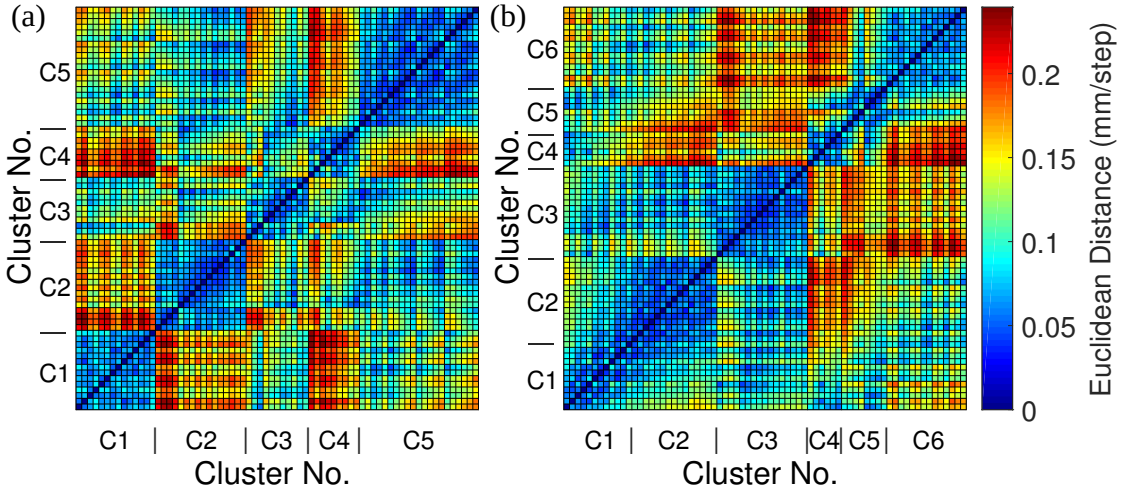

Figure E.11: Matrix of Euclidean distances between clusters for non-rigid pinna motion sample 9: a) number of clusters is 5, b) number of clusters is 6.

Appendix F

Program sources

F.1 Rigid pinna motion analysis

F.1.1 Axis-angle representation

This program can be used to represent the rigid pinna motion sequence with axis and angle.

```
clc;
clear all;
close all;

%% find the file location of the data sets
cd('E:\Peiwen_Qiu\Research in VT\Motion Profile Data New')
Folder = cd;
FileList = dir(fullfile(Folder, '**', '3D.mat'))
file = {FileList.folder};

for k=1:100            % 100 rigid pinna motion sequences in total
    % load data automatically
    cd_name=char(file(1,k))
    cd(cd_name)
    load('coordinates.mat');
```

```
16      load('3D.mat');
17
18      %% Calculate the transfer & rotation matrix from old coordinate to ...
            new coordinate
19      eval(['PB=PT_' num2str(s) ';']);
20      eval(['PC=PT_' num2str(e) ';']);
21      A=PT_1(:,1)
22      B=PB(:,1)
23      C=PC(:,1)
24
25      syms x y z
26      [x,y,z]=solve('(A(1,1)-B(1,1))*x+(A(2,1)-B(2,1))*y+(A(3,1)-B(3,1))*z=0',
27      '(A(1,1)-C(1,1))*x+(A(2,1)-C(2,1))*y+(A(3,1)-C(3,1))*z=0','x=A(1,1)',
28      'x','y','z');
29      x=eval([x']);
30      y=eval([y']);
31      z=eval([z']);
32      Z=-[x;y;z];
33      eZ=Z./(norm(Z));
34
35      syms x y z
36      [x,y,z]=solve('(A(1,1)-C(1,1))*x+(A(2,1)-C(2,1))*y+(A(3,1)-C(3,1))*z=0',
37      'Z(1,1)*x+Z(2,1)*y+Z(3,1)*z=0','x=A(1,1)','x','y','z');
38      x=eval([x']);
39      y=eval([y']);
40      z=eval([z']);
41      X=-[x;y;z];
42      eX=X./(norm(X));
43
44      syms x y z
45      [x,y,z]=solve('Z(1,1)*x+Z(2,1)*y+Z(3,1)*z=0','X(1,1)*x+X(2,1)*y+
```

```
46      X(3,1)*z=0','x=A(1,1)','x','y','z');
47      x=eval([x']);
48      y=eval([y']);
49      z=eval([z']);
50      Y=-[x;y;z];
51      eY=Y./(norm(Y));
52
53      % transfer matrix
54      T=[1 0 0 0;0 1 0 0;0 0 1 0;-A(1,1) -A(2,1) -A(3,1) 1];
55      % rotation matrix
56      R=[eX(1,1) eY(1,1) eZ(1,1) 0;eX(2,1) eY(2,1) eZ(2,1) 0;eX(3,1) ...
            eY(3,1) eZ(3,1) 0;0 0 0 1];
57
58      %% find the new coorodinates in every frame
59      for i=1:Fn;
60          FnPT=[];
61          for j=1:PTn-Hpn,
62              pt=[];
63              eval(['pt=PT_' num2str(j) ';']);
64              New=[pt(:,i)' 1]*T*R;
65              fnpt=New(:,1:3)';  % calculate the point-coordinates in the ...
                    new coordinate system
66              FnPT=[FnPT fnpt];
67          end
68          eval(['FnPT_' num2str(i) '=FnPT' ';']);
69      end
70
71      %% transfer the coorodinates from every frame to every points
72      for i=1:PTn-Hpn;
73          PTFn=[];
74          for j=1:Fn,
```

```
75              pt=[];
76              eval(['pt=FnPT_' num2str(j) ';']);
77              ptfn=pt(:,i);
78              PTFn=[PTFn ptfn];
79          end
80          eval(['PTFn_' num2str(i) '=PTFn' ';']);
81      end
82
83      %% Calculate Rotation Center & Angle
84      center=[];
85      angle=[];
86      for i=1:PTn-Hpn;
87          PTFn=[];
88          eval(['PTFn=PTFn_' num2str(i) ';']);
89          PTFn=PTFn';
90          [rotation_center,rotation_angle]=SimplifiedRotationCalculate(PTFn,Fn);
91          center=[center rotation_center];
92          angle=[angle rotation_angle];
93      end
94
95      %% Calculate the mean & median of the rotation angle
96      angle_mean=mean(angle);
97      angle_median=median(angle);
98
99      %% 3D Line Fitting of the rotation centers to get the rotation axis
100     data=center';
101     [direction,p0]=SVD_line(data);
102     eDirection=direction/norm(direction);
103     xx=eDirection(1)*angle_mean;
104     yy=eDirection(2)*angle_mean;
105     zz=eDirection(3)*angle_mean;
```

```
106       axis_angle=[xx yy zz]';
107
108       % save data
109       axis_angle=[axis_angle;angle_mean;angle_median];
110       save('SVD.mat','axis_angle')
111   end
112
113   %%
114   clc;
115   clear all;
116   close all;
117
118   %% find the file location of the data sets
119   cd('E:\Peiwen_Qiu\Research in VT\Motion Profile Data New')
120   Folder = cd;
121   FileList = dir(fullfile(Folder, '**', 'SVD.mat'));
122   file = {FileList.folder};
123
124   %% get the rotation axes of all the rigid motions
125   vector=[];
126   norm_vector=[];
127   pts_num=[];
128   for k=1:100          % 100 rigid pinna motion sequences in total
129       % load data automatically
130       cd_name=char(file(1,k));
131       cd(cd_name);
132       load('SVD.mat');
133       [num,¬]=size(error_points);
134       axis=axis_angle(1:3,:);
135       angle=axis_angle(5,:)';
136       vector=[vector axis];
```

```
137         norm_vector=[norm_vector angle];
138         pts_num=[pts_num num];
139     end
140
141     %% normalized rotation axes
142     [a,b] = size(vector);
143     motion=[];
144     Normalized_motion=[];
145     for i=1:b
146         X=vector(:,i)./norm(vector(:,i)).*norm_vector(1,i);
147         Y=vector(:,i)./norm(vector(:,i));
148         motion=[motion X];
149         Normalized_motion=[Normalized_motion Y];
150     end
151     AxisAngleData=[Normalized_motion;norm_vector];
152
153     for i=1:b
154         if AxisAngleData(2,i)<0
155             AxisAngleData(:,i)=-AxisAngleData(:,i);
156         end
157     end
158     angle=AxisAngleData(4,:);
159     normalized_axis=AxisAngleData(1:3,:);
160
161     %% plot the rotation axes on the map
162     figure(1)
163     R=1;
164     [x,y,z]=sphere(20);
165     mesh(R*x,R*y,R*z)
166     [B,I]=sort(angle);
167     % J =jet;
```

```
168 J =gray;
169 for i=1:b
170     f=floor(i/2);
171     if B(1,i)<0
172     figure(1)
173     hold on;
174     plot3(normalized_axis(1,I(i)),normalized_axis(2,I(i)),normalized_axis(3,I(i)),
175     '*','linewidth',8,'color',J(f+1,:));
176     else
177     figure(1)
178     hold on;
179     plot3(normalized_axis(1,I(i)),normalized_axis(2,I(i)),normalized_axis(3,I(i)),
180     '*','linewidth',8,'color',J(f+1,:));
181     end
182 end
183 xlabel('X','Fontsize',15);
184 ylabel('Y','Fontsize',15);
185 zlabel('Z','Fontsize',15);
186 colormap(J(1:f+1,:));
187 caxis([min(B),max(B)]);
188 colorbar
189 % saveas(figure(1),'mapping')
190
191 %% plot the histogram of the magnitudes of the rotation angles
192 figure(2)
193 histogram(norm_vector,'BinMethod','sturges','FaceColor','k','EdgeColor','k')
194 xlabel('Absolute Value of Rotation Angle (degree)','Fontsize',15);
195 ylabel('Number','Fontsize',15);
196 % saveas(figure(2),'Absolute Value of Rotation Angle')
197
198 %% get the azimuth of the rotation axes
```

```
199 Azimuth=[];
200 for i=1:b
201     sin_azi=normalized_axis(1,i)/sqrt(normalized_axis(1,i)^2+normalized_axis(2,i)^2);
202     azi=rad2deg(asin(sin_azi));
203     Azimuth=[Azimuth azi];
204 end
205
206 %% plot the histogram of the azimuth of the rotation axes
207 figure(3)
208 histogram(Azimuth,'BinMethod','sturges','FaceColor','k','EdgeColor','k')
209 xlabel('Azimuth (degree)','Fontsize',15);
210 ylabel('Number','Fontsize',15);
211 % saveas(figure(3),'Azimuth')
212
213 %% get the elevation of the rotation axes
214 Elevation=[];
215 for i=1:b
216     sin_ele=normalized_axis(3,i)/sqrt(normalized_axis(1,i)^2+normalized_axis(2,i)^2
217     +normalized_axis(3,i)^2);
218     ele=rad2deg(asin(sin_ele));
219     Elevation=[Elevation ele];
220 end
221
222 %% plot the histogram of the elevation of the rotation axes
223 figure(4)
224 histogram(Elevation,'BinMethod','sturges','FaceColor','k','EdgeColor','k')
225 xlabel('Elevation (degree)','Fontsize',15);
226 ylabel('Number','Fontsize',15);
227 % saveas(figure(4),'Elevation')
```

F.1.2 Normalized mutual information

This program can be used to calculate the normalized mutual information between the pulse envelopes collected with 110 different pinna rotation axes.

```
clc;
close all;
clear all;

Fs = 500E3;      % sample rate
tacq = 70E-3;       % data acquisition time
t = single(0:1/Fs:tacq);

%% Bandpass filter design
fd = fdesign.bandpass('N,Fc1,Fc2',512,(33E3/250E3),(37E3/250E3));
ff = design(fd);

%% Load pulse data collected during pinna moving
cd('E:\Peiwen_Qiu\Research in VT\Experiments_Final\Data_35kHz\CF\DOWN');
data_mean=[];
for i = -60:15:75
    for j= -75:15:75
        filename = sprintf('CFDOWN_%d_%d.mat',i,j);
        load(filename);
        data=sonarTest.data.xdata;
        data_mean=[data_mean mean(data,2)];
    end
end
[~,Size]=size(data_mean);

```

```
26 %% Normalized the pulse data
27 data_normalized=[];
28 for i=1:Size
29     filter_data=ff.filter(data_mean(10000:30000,i));
30     data_normalized(:,i) = filter_data./max(filter_data); % normalized
31 end
32
33 %% Get the envelope of the pulse data
34 envelope_data=[];
35 for i=1:Size
36     filter_data=ff.filter(data_mean(10000:30000,i));
37     Envelope=abs(hilbert( filter_data));
38     Envelope_smooth=smooth(Envelope,0.1,'lowess');
39     envelope_data=[envelope_data Envelope_smooth];
40 end
41
42 % Normalized the pulse envelope
43 envelope_data_normalized=[];
44 for i=1:Size
45     envelope_data_normalized(:,i) = ...
          envelope_data(:,i)./max(envelope_data(:,i)); % normalized
46 end
47
48 %% Mutual Information
49 % Path
50 addpath('E:\Peiwen_Qiu\Research in VT\Mutual ...
      Information\infodynamics-dist-1.5\demos\octave');
51 javaaddpath('E:\Peiwen_Qiu\Research in VT\Mutual ...
      Information\infodynamics-dist-1.5/infodynamics.jar');
52
53 % The name of the concrete implementation of the interface ...
```

```
    infodynamics.measures.continuous.MutualInfoCalculatorMultiVariate ...
    which we wish to use for the calculation.
implementingClass =
'infodynamics.measures.continuous.kraskov.MutualInfoCalculatorMultiVariateKraskov1';

miUnivariateValue=zeros(Size,Size);
% Pull out the columns from the data set for a univariate MI calculation:
for i=1:Size
    univariateSeries1 = envelope_data_normalized(:,i);
    for j=(i+1):Size
        univariateSeries2 = envelope_data_normalized(:,j);
        % Dynamically instantiate an object of the given class:
        miCalc = javaObject(implementingClass);
        % Start using the MI calculator:
        % a. Initialise the calculator for a univariate calculation:
        miCalc.initialise(1, 1);
        % b. Supply the observations to compute the PDFs from:
        miCalc.setObservations(octaveToJavaDoubleArray(univariateSeries1),
        octaveToJavaDoubleArray(univariateSeries2));
        % c. Make the MI calculation:
        miUnivariateValue(i,j) = ...
            miCalc.computeAverageLocalOfObservations();
        % Compute normalized mutual information
        Normalized_MI(i,j)=miUnivariateValue(i,j)
        /sqrt(entropy3(envelope_data_normalized(:,i))
        *entropy3(envelope_data_normalized(:,j)));
    end
end
Normalized_MI=Normalized_MI.*100;

%% get the pcolor fig of the normalized mutual information
```

```
82 for i=1:Size
83     for j=1:i
84         Normalized_MI(i,j) =NaN;
85     end
86 end
87 [m,n] = size(Normalized_MI);
88 Normalized_MI(m+1,:)=[0];
89 Normalized_MI(:,n+1)=[0];
90
91 figure
92 colormap(gray);
93 pcolor(Normalized_MI);
94 caxis([34,50]);
95 colorbar;
96 xlabel('Rotation axis No.');
97 ylabel('Rotation axis No.');
98 set(gca,'fontsize',12 );
```

F.2 Non-rigid pinna motion analysis

F.2.1 Spectral clustering

This program can be used to figure out the distribution of the clusters of the landmarks on the pinna surface using spectral clustering algorithm.

```
clc; clear all; close all;

%% Load coordinates of the landmarks on the pinna surface
cd('C:\Users\Peiwen Qiu\Desktop\Peiwen_Qiu\Research in VT\Motion Profile ...
    Data New\Nonrigid Motion\King\12-29-2017\2\12\results');
load('coordinate.mat');

%% Calculate the distance between two frames(vectors)
ALLPT=[];
for i=1:PTn-Hpn;
    eval(['YY=PT_' num2str(i) ';']);
    DisPT=[];
    for j=1:Fn-1,
        dispt=[];
        A1=YY(:,j);
        A2=YY(:,j+1);
        dispt=A2-A1;
        DisPT=[DisPT dispt'];
    end
    ALLPT=[ALLPT;DisPT];
end

```

```
22 %% Cluster the landmarks on the pinna using spectral clustering algorithm
23 data=ALLPT;
24 k=5;
25 U=NJW(data,k);
26 [IDX,C] = kmeans(U,k,'Start','plus','MaxIter',10000,'Replicates',200);
27
28 % plot the clustering result
29 figure,
30 hold on;
31 for i=1:size(IDX,1)
32     if IDX(i,1) == 1
33         eval(['point=PT_' num2str(i) ';']);
34         plot3(point(1,Fn),point(3,Fn),-point(2,Fn),'mo');hold on;
35         text(point(1,Fn),point(3,Fn),-point(2,Fn),strcat(num2str(i)),'fontsize',7);
36     elseif IDX(i,1) == 2
37         eval(['point=PT_' num2str(i) ';']);
38         plot3(point(1,Fn),point(3,Fn),-point(2,Fn),'go');hold on;
39         text(point(1,Fn),point(3,Fn),-point(2,Fn),strcat(num2str(i)),'fontsize',7);
40     elseif IDX(i,1) == 3
41         eval(['point=PT_' num2str(i) ';']);
42         plot3(point(1,Fn),point(3,Fn),-point(2,Fn),'co');hold on;
43         text(point(1,Fn),point(3,Fn),-point(2,Fn),strcat(num2str(i)),'fontsize',7);
44     elseif IDX(i,1) == 4
45         eval(['point=PT_' num2str(i) ';']);
46         plot3(point(1,Fn),point(3,Fn),-point(2,Fn),'ro');hold on;
47         text(point(1,Fn),point(3,Fn),-point(2,Fn),strcat(num2str(i)),'fontsize',7);
48     elseif IDX(i,1) == 5
49         eval(['point=PT_' num2str(i) ';']);
50         plot3(point(1,Fn),point(3,Fn),-point(2,Fn),'bo');hold on;
51         text(point(1,Fn),point(3,Fn),-point(2,Fn),strcat(num2str(i)),'fontsize',7);
52     elseif IDX(i,1) == 6
```

```
53          eval(['point=PT_' num2str(i) ';']);
54          plot3(point(1,Fn),point(3,Fn),-point(2,Fn),'m+');hold on;
55          text(point(1,Fn),point(3,Fn),-point(2,Fn),strcat(num2str(i)),'fontsize',7);
56      elseif IDX(i,1) == 7
57          eval(['point=PT_' num2str(i) ';']);
58          plot3(point(1,Fn),point(3,Fn),-point(2,Fn),'g+');hold on;
59          text(point(1,Fn),point(3,Fn),-point(2,Fn),strcat(num2str(i)),'fontsize',7);
60      elseif IDX(i,1) == 8
61          eval(['point=PT_' num2str(i) ';']);
62          plot3(point(1,Fn),point(3,Fn),-point(2,Fn),'c+');hold on;
63          text(point(1,Fn),point(3,Fn),-point(2,Fn),strcat(num2str(i)),'fontsize',7);
64      elseif IDX(i,1) == 9
65          eval(['point=PT_' num2str(i) ';']);
66          plot3(point(1,Fn),point(3,Fn),-point(2,Fn),'r+');hold on;
67          text(point(1,Fn),point(3,Fn),-point(2,Fn),strcat(num2str(i)),'fontsize',7);
68      else
69          eval(['point=PT_' num2str(i) ';']);
70          plot3(point(1,Fn),point(3,Fn),-point(2,Fn),'b+');hold on;
71          text(point(1,Fn),point(3,Fn),-point(2,Fn),strcat(num2str(i)),'fontsize',7);
72      end
73  end
74  hold off;
75  % title('Spectral Clustering with 5 clusters');
76  xlabel('X');
77  ylabel('Y');
78  zlabel('Z');
79  grid on;
80  % saveas(figure (1),'Spectral Clustering with 5 clusters');
81
82  save('sc 5.mat');
```

F.2.2 Euclidean distance

This program can be used to compute the Euclidean distances between the clusters of the landmarks on the pinna surface.

```
clc;
clear all;
close all;

%% load clustering data
cd('E:\Peiwen_Qiu\Research in VT\Motion Profile Data New\Nonrigid ...
    Motion\Bat_3\7-25-2017\2\1\results');
load('sc 6.mat');

%% Calculate Euclidean distance per step
ED=[];
for i=1:PTn-Hpn,
    DPV1=ALLPT(i,:);
    for j=1:PTn-Hpn,
        DPV2=ALLPT(j,:);
        ed=sqrt((sum((DPV1-DPV2).^2)));        % Euclidean distance
        ED(i,j)=ed;
    end
end
ED=ED./(Fn-1);    % Euclidean distance Per Step

%% Calculate Euclidean distance within clusters
for i=1:k
    eval(['CPnum_' num2str(i) '=[]' ';']);
end
```

```
25
26 % find point numbers of different clusters
27 for i=1:size(IDX,1)
28     if IDX(i,1) == 1
29         CPnum_1=[CPnum_1 i];
30     elseif IDX(i,1) == 2
31         CPnum_2=[CPnum_2 i];
32     elseif IDX(i,1) == 3
33         CPnum_3=[CPnum_3 i];
34     elseif IDX(i,1) == 4
35         CPnum_4=[CPnum_4 i];
36     elseif IDX(i,1) == 5
37         CPnum_5=[CPnum_5 i];
38     elseif IDX(i,1) == 6
39         CPnum_6=[CPnum_6 i];
40     elseif IDX(i,1) == 7
41         CPnum_7=[CPnum_7 i];
42     elseif IDX(i,1) == 8
43         CPnum_8=[CPnum_8 i];
44     elseif IDX(i,1) == 9
45         CPnum_9=[CPnum_9 i];
46     else
47         CPnum_10=[CPnum_10 i];
48     end
49 end
50
51 % Re-arrange point numbers according to the clustering results
52 point_list=[];
53 num_label=[0];
54 for i=1:k
55     eval(['CPnum=CPnum_' num2str(i) ';']);
```

```
56      [a,b] = size(CPnum);
57      point_list=[point_list CPnum];
58      num_label=[num_label b+num_label(1,i)];
59  end
60  [a,b] = size(num_label);
61  num_label_end=num_label(1,2:b-1);
62  num_label_text=num_label(1,1:b-1);
63  label=[num_label_end+1];
64  label=sort(label);
65
66  % Re-arrange the Euclidean distances according to the new point numbers
67  ED_List=[];
68  for i=1:PTn-Hpn,
69      m=point_list(1,i);
70      for j=1:PTn-Hpn,
71          n=point_list(1,j);
72          ED_List(i,j)=ED(m,n);
73      end
74  end
75
76  %% get the pcolor fig of Euclidean distances between clusters
77  [m,n] = size(ED_List);
78  ED_List(m+1,:)=[0];
79  ED_List(:,n+1)=[0];
80
81  figure,
82  colormap(jet);
83  pcolor(ED_List)
84  % caxis([0,6]);
85  set(gca, 'Xtick', ...
        label,'XtickLabel',{'|','|','|','|','|','|','|','|','|','|'});
```

```
86 set(gca, 'Ytick', label,'YtickLabel',{'—','—','—','—','—','—','—','—
    ','—','—'});
87 pbaspect([1 1 1]);
88 colorbar;
89 saveas(figure (1),'Euclidean Distance with 6 clusters');
90
91 %% find Euclidean distances of different clusters
92 for i=1:k
93     eval(['CPnum=CPnum_' num2str(i) ';']);
94     [a,b] = size(CPnum);
95     EDC=[];
96     for j=1:b
97         m=CPnum(1,j);
98         for z=1:b
99             n=CPnum(1,z);
100            edc=ED(m,n);
101            EDC(j,z)=edc;
102        end
103        eval(['EDC_' num2str(i) '=EDC' ';']);
104    end
105 end
106
107 %% Calculate mean Euclidean distance of different clusters (within & ...
    between clusters)
108 ED_Single_within=[];
109 for i=1:k
110     eval(['EDC=EDC_' num2str(i) ';']);
111     [a,b] = size(EDC);
112     for j=1:(b-1)
113         for z=(j+1):b
114             ed_single_within=EDC(j,z);
```

```
115                 ED_Single_within=[ED_Single_within ed_single_within];
116             end
117         end
118     end
119     [m,n] = size(ED_Single_within);
120     ed_mean_within=sum(ED_Single_within)/n
121     min_ED_Within=min(ED_Single_within);
122     std_within=std(ED_Single_within);
123     max_ED_Within=max(ED_Single_within);
124
125     %% Find min Euclidean distance between clusters & max Euclidean distance ...
            within clusters
126     ED_Between=[];
127     [m,n] = size(point_list);
128     b_all=0;
129     for i=1:(k-1)
130         eval(['CPnum=CPnum_' num2str(i) ';']);
131         [a,b] = size(CPnum);
132         b_all=b_all+b;
133         for j=(b_all-b+1):b_all
134             g=point_list(1,j);
135             for z=(b_all+1):n
136                 h=point_list(1,z);
137                 edb=ED(g,h);
138                 ED_Between=[ED_Between edb];
139             end
140         end
141     end
142     max_ED_Between=max(ED_Between);
143     min_ED_Between=min(ED_Between);
144     std_between=std(ED_Between);
```

```
145  [m,n] = size(ED_Between);
146  ed_mean_between=sum(ED_Between)/n;
147  % save('ed 6.mat');
```